

Engineering Journal



American Institute of Steel Construction

First Quarter 2012 Volume 49, No. 1

- 1 Applications of Pretensioned Anchor
Rods in Industrial Facilities
Shu-Jin Fang
- 11 Recommendations for Shear Lag Factors for
Longitudinally Welded Tension Members
Patrick J. Fortney and William A. Thornton
- 33 Mechanical Properties of ASTM A992 Steel After Fire
Jinwoo Lee, Michael D. Engelhardt and Eric M. Taleff
- 45 Current Steel Structures Research No. 29
Reidar Bjorhovde

ENGINEERING JOURNAL

AMERICAN INSTITUTE OF STEEL CONSTRUCTION

*Dedicated to the development and improvement of steel construction,
through the interchange of ideas, experiences and data.*

Editorial Staff

Editor: KEITH A. GRUBB, S.E., P.E.

Research Editor: REIDAR BJORHOVDE, PH.D.

Production Editor: ARETI CARTER

Officers

WILLIAM B. BOURNE, III, *Chairman*
Universal Steel, Inc., Lithonia, GA

JEFFREY E. DAVE, P.E., *Vice Chairman*
Dave Steel Company, Inc., Asheville, NC

STEPHEN E. PORTER, *Treasurer*
Indiana Steel Fabricating, Inc., Indianapolis, IN

ROGER E. FERCH, P.E., *President*
American Institute of Steel Construction, Chicago

DAVID B. RATTERMAN, *Secretary & General Counsel*
American Institute of Steel Construction, Chicago

CHARLES J. CARTER, S.E., P.E., PH.D., *Vice President and
Chief Structural Engineer*
American Institute of Steel Construction, Chicago

JACQUES CATTAN, *Vice President*
American Institute of Steel Construction, Chicago

JOHN P. CROSS, P.E., *Vice President*
American Institute of Steel Construction, Chicago

SCOTT L. MELNICK, *Vice President*
American Institute of Steel Construction, Chicago

The articles contained herein are not intended to represent official attitudes, recommendations or policies of the Institute. The Institute is not responsible for any statements made or opinions expressed by contributors to this Journal.

The opinions of the authors herein do not represent an official position of the Institute, and in every case the officially adopted publications of the Institute will control and supersede any suggestions or modifications contained in any articles herein.

The information presented herein is based on recognized engineering principles and is for general information only. While it is believed to be accurate, this information should not be applied to any specific application without competent professional examination and verification by a licensed professional engineer. Anyone making use of this information assumes all liability arising from such use.

Manuscripts are welcomed, but publication cannot be guaranteed. All manuscripts should be submitted in duplicate. Authors do not receive a remuneration. A "Guide for Authors" is printed on the inside back cover.

ENGINEERING JOURNAL (ISSN 0013-8029) is published quarterly. Subscriptions: Members: one subscription, \$40 per year, included in dues; Additional Member Subscriptions: \$40 per year. Non-Members U.S.: \$160 per year. Foreign (Canada and Mexico): Members \$80 per year. Non-Members \$160 per year. Published by the American Institute of Steel Construction at One East Wacker Drive, Suite 700, Chicago, IL 60601.

Periodicals postage paid at Chicago, IL and additional mailing offices.

Postmaster: Send address changes to ENGINEERING JOURNAL in care of the American Institute of Steel Construction, One East Wacker Drive, Suite 700, Chicago, IL 60601.

Copyright 2012 by the American Institute of Steel Construction. All rights reserved. No part of this publication may be reproduced without written permission. The AISC logo is a registered trademark of AISC.

Subscribe to *Engineering Journal* by visiting our website www.aisc.org/ej or by calling 312.670.5444.

Copies of current and past *Engineering Journal* articles are available free to members online at www.aisc.org/ej.

Non-members may purchase *Engineering Journal* article downloads at the AISC Bookstore at www.aisc.org/ej for \$10 each.

Applications of Pretensioned Anchor Rods in Industrial Facilities

SHU-JIN FANG

ABSTRACT

Base plate and anchor rod connections are key structural components. A great majority of anchor rods are designed, placed and installed without pretensioning, usually because the structures are considered to be statically loaded. Applications of pretensioned anchor rods are less common and generally limited to certain industrial facilities. This paper provides a brief overview of the current state of the practice regarding pretensioned anchor rods and reviews selected recent pretensioned anchor rod applications in power industry facilities.

Keywords: pretensioned anchor rods, column base connections.

INTRODUCTION

Base plate and anchor rod connections are key structural components of vital importance to the plumbness and safety of structures. They are not only used as column base support in every building structure, but also utilized for supporting nonbuilding structures and mounting of equipment in industrial facilities. Anchor rods, a relatively new terminology adopted by AISC, were referred to as anchor bolts in the past. A great majority of anchor rods are designed, placed and installed without pretensioning. Base plates are tied to anchor rods by nut(s) and washer, as evidenced in typical building column bases. Applications of pretensioned anchor rods are less common and generally limited to certain industrial facilities. Design of column base plates and anchor rods is governed by the AISC *Specification for Structural Steel Buildings* (AISC, 2005) and ACI 318 Appendix D (ACI, 2005). However, neither the AISC *Specification* nor ACI 318 provide specific guidelines for pretensioned cast-in-place anchors. An excellent guideline, AISC *Design Guide 1, Base Plate and Anchor Rod Design*, second edition, second printing (Fisher and Kloiber, 2006), is now available to guide engineers and fabricators for design, detailing, fabrication and erection of column-base-plate and anchor rod connections. Appendix 3 of the design guide provides limited but useful discussions on pretensioned anchors. It appears that similar guidelines or authoritative design codes/standards are still lacking with respect to design, fabrication and installation of pretensioned anchor rods, and little research has been done in this area. Engineers often have to rely on their own past

experience and engineering judgment to develop a satisfactory application. Information and design practices published in literature are not consistent, sometimes confusing and conflicting. This paper is written with two objectives: (1) to provide a brief review of the current state of the practice in pretensioned anchor rods; and (2) to present lessons and knowledge learned from selected recent project applications in power industry facilities.

For many years, AISC noted that the pretensioning of anchor rods was not recommended for building structures. Commentary Section A3.4 of the 1999 Edition AISC *LRFD Specification* noted concerns regarding prestressing relaxation due to concrete creep and the potential for stress corrosion damage. The author believes that the reason most building structures do not have pretensioned anchor rods is that the structures are statically loaded. The Commentary note is not present in the 2005 AISC *Specification*. In view of this historical background in the building industry, it would be very beneficial to examine the practices of pretensioning of anchor rods outside the building industry.

WHEN PRETENSIONING IS RECOMMENDED

According to *Design of Anchor Bolts in Petrochemical Facilities* (ASCE, 1997), pretensioning of anchor rods is recommended for the following three situations:

- Tall vessels sensitive to wind such as towers with a height-to-width ratio of 15 or more, or more than 100 feet tall.
- Dynamic machinery such as compressors or other pulsating equipment.
- High-strength anchor bolts to minimize load reversals.

These three pretensioning applications all aim to improve the long-term performance of anchor rods or to improve the

Shu-Jin Fang, Ph.D., P.E., S.E., Senior Manager/Technical Advisor, Sargent & Lundy, Chicago, IL. E-mail: shujin.fang@sargentlundy.com

performance of equipment or vessels. One common denominator among these applications is that the anchor supports are subjected to frequent load fluctuations induced by wind, thermal cycling or machine vibrations. Pretensioning helps prevent fluctuation of the tensile stress in the anchors and therefore minimizes loosening of nuts and alleviates fatigue concerns. Anchor pretensioning may also help decrease machine vibrations and the drifts of process vessels under wind or other lateral loads.

In addition, pretensioning of anchor rods will increase the frictional shear resistance at base plates, which is beneficial for the design of anchorages for tall vessels and structures subjected to heavy wind and seismic forces. Certainly, wind-sensitive structures are not limited to tall process vessels. Other examples include steel stacks, pipe rack supports, piping supports, crane column bases, transmission poles, wind turbine towers, telecommunication towers and cantilevered signal- and light-support structures for highways.

AISC *Design Guide 1* (Fisher and Kloiber, 2006) states that vibratory machine joints and double-nut joints designed for high seismic applications (Seismic Design Category D, E and F) or designed for fatigue require pretensioning according to ASCE/SEI 7 (ASCE, 2005).

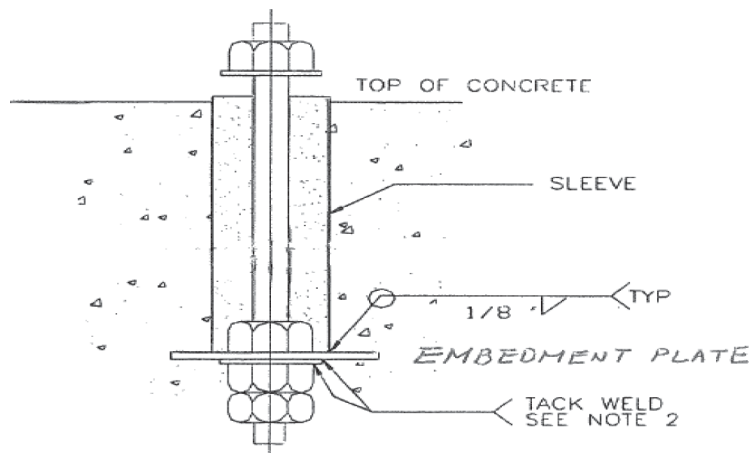
For each such application, engineers are advised to balance the previously mentioned technical advantages against the possible cost increases, which could range from little to very substantial, depending on the size of anchor rods and the pretension magnitude desired. There are a number of other potential shortcomings caused by pretensioning that should not be overlooked. One of them is the damage to concrete and grout that may result from inadequate design or excessively high pretension loads. Improper tensioning methods and/or improper tensioning sequences can cause

damage. Other shortcomings include lack of high assurance that the anchor is properly installed and pretensioned in the field. Periodic examination and testing may be needed to monitor the loss of pretension over time caused by concrete creep and anchor relaxation.

CONFIGURATIONS OF THREE TYPES OF PRETENSIONED ANCHOR ROD JOINTS

Three commonly used pretensioned anchor rod joints are shown in Figures 1a, 1b and 1c.

Figure 1a represents a typical vibratory-machine joint in which the sleeve is extended for the full depth of the anchor. The sleeve is used for both precise alignment and pre-tensioning of anchor rods. The sleeve is usually made of metal pipes. Long metal sleeves can be substituted with plastic (PVC) sleeves if no welding is required. Either single or double nuts may be located beneath the embedment plate. The space between the anchor rod and pipe sleeve can be filled with grout after the structure or equipment is set, aligned and pretensioned. Alternatively, sleeves may be sealed on top or filled with appropriate elastomeric material to prevent water or grout from filling the sleeve. It should be noted that if sleeves are not grouted, anchor rods will not be effective in resisting shear loads and will have to rely on shear friction tension or shear lugs for shear resistance. The metal sleeves are generally at least 1.0 in. larger than the anchor rod diameter. AISC *Design Guide 1* (Fisher and Kloiber, 2006) recommends that full-depth steel sleeves be used to minimize concrete creep/shrinkage. The full-depth steel sleeve permits elongation of the entire length of anchor rod and should have adequate strength for transferring anchor rod pretension from the embedment plate to the base



- Notes:
1. Base plate and grout placed above concrete are not shown for clarity in Figure 1a and 1b.
 2. If high strength anchor rods are used, welding of nuts to the anchor rods is typically not recommended.

Fig. 1a. Pretensioned anchor rods for vibratory equipment support.

plate. The embedment plate should also be capable of resisting the pretension force prior to placement of grout. Also, a hardened plate washer with appropriate thickness may need to be placed directly above the base plate when anchor pretension is high.

Figure 1b shows a pretensioned anchor rod design with a partial-depth sleeve. Partial-depth sleeves are primarily used for alignment purposes and are suitable only for applications where pretension is low or moderate. In order to allow pretensioning of anchor rods, grout below the sleeve must not be allowed to bond to the anchor rod. Typically, the portion of anchor rod shaft below the sleeve and within 1 in. of the embedment plate is taped or coated with a bond-breaker for a distance at least six times anchor rod diameter above the embedment plate, so that the anchor rods can be adequately stretched (ASCE, 1997). The sleeves are typically positioned with a distance at least six times anchor rod diameter above the embedment plate.

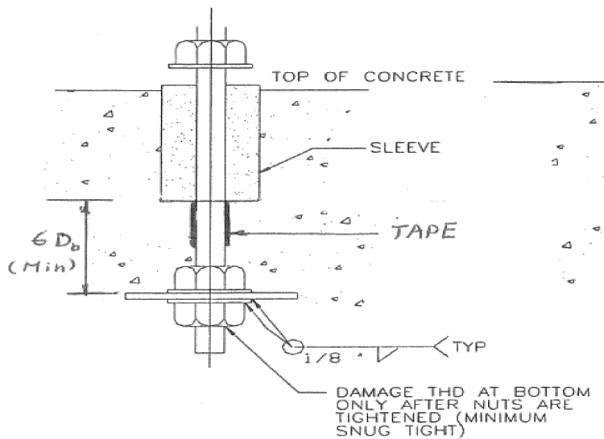


Fig. 1b. Pretensioned anchor rod with partial-depth sleeve.

Figure 1c shows configuration of a typical double-nut-moment joint at column base. The base plate is attached to anchor rods through double nuts (a leveling nut and a top nut). Washers are typically used under both nuts. The base plate stands off from the concrete foundation and bearing on leveling nuts. Grout is not typically placed beneath the base plate. Anchor rods are designed for axial loads (tension and compression), shear and moment. Double-nut-moment joints are easy to level and plumb and are also very reliable for transmitting moment to the foundation; therefore, they are satisfactory for nonredundant structures and seismic or fatigue-loaded structures. This type of column base design is commonly used in highway ancillary structures, towers and poles, which are subjected to significant moments and shears. Double-nut joints are pretensioned between nuts only. Research performed for National Cooperative Highway Research Program (NCHRP) Reports 469 and 412 (Dexter and Ricker, 2002; Kaczinski et al., 1996) shows that pretension in the rod between two nuts improves fatigue strength by good load distribution among the anchor rods.

PRETENSIONING VALUE

For any pretensioned anchor application, the first question raised by designers is how much pretension to apply. The answers to this question vary with the intended application. Table 1 gives a summary of various pretension practices in power, petrochemical process and highway industries. It can be seen from Table 1 that the pretension load desired may vary from $0.15F_y$ (15% of the specified minimum yield strength of anchor rod) to as high as $0.6F_u$ (60% of the specified minimum tensile strength of anchor rod), depending on the design objectives.

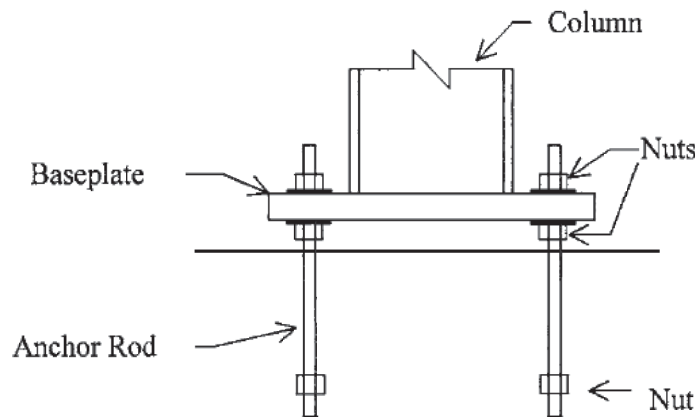


Fig. 1c. Typical double-nut-moment joint.

Table 1. Summary of Various Anchor Rod Pretensioning Practices

	Vendor 1		Vendor 2		Vendor 3	Vendor 4	Vendor 4	AISC Design Guide 1 (2006)	ACI 351-3R (2004)	ASCE Anchor Rod Design (1997)	
	Turbine Support	Generator Support	Turbine Support	Generator Support	ID/PA/FD Fan	ID/PA/FD Fan	Motor	Double-Nut-Moment Joint at Column Base	Vibratory Equipment	See Note 6	
Anchor Rod Diameter	2 in. to 2½ in.	1½ in. to 2 in.	2 in. to 2½ in.	1½ in.			1¾ in.	2 in.	≤ 4 in.	No limit	
Pretension Load	None	Approx. 55 kips for 2-in. anchor rod (17,500 psi or 0.5F _y)	18,500 psi (0.18F _y)	30,000 psi (0.28F _y)	None		32,000 psi	30,000 psi	0.5F _u for Gr. 36 and 0.6F _u for higher strength	Sufficient to resist dynamic shear loads by shear friction; 0.15F _y ≤ F _t < 0.7 F _y	F _t = 0.3; F _u unless otherwise required; 17,400 psi to 18,000 psi for A36 or A307 Gr. C; 37,500 psi for Gr. 105
Installation Torque	50 ft-lb (Notes 2, 3 and 4)	1,100 ft-lb for 2-in. anchor rods and 840 ft-lb for 1½-in. anchor rods (Notes 2 and 3)	Not specified	Not specified	None		1,560 ft-lb	1,900 ft-lb	Minimum nut rotation specified	Bolt torque should be determined based on preload required	
Sleeves	Yes	Yes	Yes	Yes	Not Required		Yes	Yes	No	Yes	Yes for vibratory machine
Grouting sleeves	Yes (Note 1)	Yes (Note 1)	Yes (Note 1)	Yes (Note 1)	N/A		Yes (Note 1)	Yes (Note 1)	No	Yes (Note 1)	No for vibratory applications; fill sleeves with elastomeric materials
Minimum Grout Strength	7,000 psi at 28 days and 5,000 psi at 7 days (Note 5)	7,000 psi at 28 days and 5,000 psi at 7 days (Note 5)	7,500 psi	7,500 psi	None		None	None	Not specified	None	None
Bolting (Rod) Materials	A307 Gr. C (A36) standard; use A449 Type 1 anchor rod when anchor rod size is large	A307 Gr. C (A36) standard; use A449 Type 1 anchor rod when anchor rod size is large	A193 B7 or equivalent	A193 B7 or equivalent	No restriction		A193-B7	A193-B7	F1554 Gr. 36, 55, 105 and A615 Gr. 60	No restriction	No restriction

Notes

1. Fill sleeve completely with grout after equipment is set and aligned.
2. Tighten the nuts of anchor bolts to snug-tight where fixators are used.
3. Where anchor rods are subject to thermal movements (expansion or contraction), nuts are backed off from tightened torque to provide a 0.01-in. nominal clearance between the bottom of nut and top of the washer; a nut-locking device or double-nutting should be provided.
4. Where thermal movement is not a concern, the anchor rods are generally tightened either snug-tight or with a 50 to 60 ft-lb final installed torque.
5. Use flowable, nonshrink, cementitious grout (ASTM C1107 Gr. A).
6. See page 1 for conditions recommended for pretensioning of anchor rods.

Vibratory Equipment Support Applications

Where pretensioned anchors are used for mounting of vibratory equipment (sometimes referred as dynamic machinery) and vibration performance is the primary objective, the pretension loads are generally set in the range of $0.15 F_y$ to $0.70 F_y$. The size, material and pretension loads or pretension stresses of anchor rods are typically specified by equipment manufacturers. Pretensioning of the anchor rods enables the equipment and foundation to act as an integral structure to allow smooth transmission of machine unbalance force to the foundation. Proper pretension provides sufficient clamping force to maintain critical alignment of the machine. Others consider the pretension has a spring effect that will absorb and dampen vibration levels. Unlike high-strength bolts in steel-to-steel connections, the pretension loads in anchor rods required may be expressed either as tensile stress or installation torque. Most rotary equipment such as gas turbines, steam turbines, generators, electric motors, pumps and fans have a specified minimum pretension of $0.15 F_y$ to $0.50 F_y$. A minimum pretension load of $0.15 F_y$ is the recommended value by ACI 351.3R (ACI, 2004) for foundation anchors supporting rotating equipment. Supports for reciprocating equipment (compressors, hammers, diesel generators, etc.) generally require larger pretension loads because the machine produces large horizontal dynamic forces. The pretension loads for these vibrating equipment supports can be as high as $0.8 F_y$. For precision machines, designing for a clamping force equal to 150% of the anticipated normal operating bolt force is a common practice to account for uncertainty in bolt tensioning and creep/shrinkage. Higher clamping force is typically achieved with more anchor bolts or larger pretension force.

In establishing anchor pretension, considerations should be given to thermal friction and the use of fixators. Where anchor rods are subject to thermal movements due to expansion or contraction of equipment, some turbine manufacturers recommend that nuts to be backed off from the tightened torque to provide a 0.01-in. nominal clearance between the bottom of nuts and top of the washer. In addition, a nut locking device or double nutting is often provided to prevent loosening of the nuts.

Leveling of mounting base for heavy machinery can be challenging and time-consuming. To achieve efficient mounting, many equipment manufacturers recommend the use of sliding shims or fixators. The later is a special anchoring and leveling device that permits precise alignment adjustments to be made after anchor nuts are tight. Where fixators are employed, anchor rods are usually installed snug-tight to avoid damage.

Highway Cantilever Structure Support Applications

Anchor pretension higher than $0.5 F_y$ may be necessary to maintain the tensile stress in the rod from fluctuating during

load reversal generated by wind induced vibrations. An excellent discussion of the minimum pretension loads is given in NCHRP Report 469 (Dexter and Ricker, 2002) for anchor rods used on highway ancillary structure supports. Extensive fatigue testing has been performed on anchor rods in the early 2000s, including NCHRP Report 412 (Kaczinski et al., 1996). The research in this report shows that the threshold tensile fatigue stress range of anchor rods is 7 ksi, which is very low. As a result, fatigue evaluation is not required if the stress in anchor rod remains in compression during the entire load cycle or if the stress range from applied loads is less than the threshold tensile stress range (7 ksi). This research showed that column base plate–anchor rod connections subjected to more than 20,000 repeated application of axial tension and/or flexure stress range must be checked for fatigue. Their testing suggested that the allowable stress range of anchor rods at 20,000 cycles is approximately 27 ksi. Thus, pretensioning of anchor rods to minimize stress fluctuation can be extremely beneficial for base plate–anchor rod connections that are subjected to large number of tensile stress cycles. Because highway cantilevered support structures are subjected to many cycles of wind loads, including vortex shedding vibrations, natural wind gust, galloping and thrust gusts, NCHRP Report 469 recommends that all anchor rods in the double-nut moment base joints be pretensioned to a minimum value equal to $0.5 F_u$ (i.e., 50% of the specified minimum tensile strength) for low-strength rod, namely, ASTM F1554 Rod Grade 36, and $0.6 F_u$ for anchor rods made of higher-grade steel. These recommended minimum pretension loads are equivalent to 80% of the specified minimum tensile yield strength for Grade 36 rods, $0.818 F_y$ for Grade 55 rods, $0.714 F_y$ for Grade 105 rods, and $0.8 F_y$ for Grade 60 ASTM A615 and A706 bars.

Since the late 1970s, studies of tensile fatigue of anchor rods have been made at several major universities. A general study of anchor rod fatigue was made by Frank (1980) at the University of Texas. This research showed that for double-nut moment base plate joints, tightening the double nut connections $\frac{1}{3}$ of a turn beyond snug-tight significantly improved fatigue life. More research, including Van Dien et al. (1996), Richards (2004), and Hodge (1996) followed after the failures of cantilevered highway signs across the country, particularly in Michigan. Research further confirms the value of preloading the anchor bolts. An excellent summary of the tensile fatigue resistance of anchor rods and recommendations is given by *NCHRP Report 469* (Kaczinski et al., 1996). It states that the S-N fatigue curve for nonpretensioned anchor rods corresponds to the Fatigue Stress Category E' of Appendix 3 of the *AISC Specification* (AISC, 2005), except that the fatigue threshold is 7 ksi, which is much higher than other Category E' details. If the anchor rod in double-nut-moment and vibratory-machinery joints is properly pretensioned, the rods will have tensile fatigue

resistance as good as Category E; however, the fatigue threshold is improved little. Because tests show that the alignment eccentricity of anchor rods in the field can have adverse effects on fatigue resistance, the report recommends that Category E' be used for design regardless of the pretension. The anchor rod misalignment should be kept below 1:40. These recommendations from *NCHRP Report 469* can serve as a guide to engineers for establishing the pretension needed for a specific application.

Support of Tall Process Vessels, Process Towers, Steel Stacks and Wind Turbine Towers

For tall process vessels, process towers, steel stacks and wind turbine towers, there is no consensus on anchor rod pretension requirements. Some engineers choose to use a very high pretension in anchor rods equal to the maximum uplift forces caused by factored wind overturning moments. This conservative pretension is intended to ensure that tension in anchor rods will never exceed the initial anchor pretension force during the life of the structure. Others have chosen to use a lower pretension equal to the maximum uplift that may be produced by the design wind (nonfactored) or a fraction (50 to 70%) of the design (factored) wind moment. Past experience and research by Dexter and Ricker (2002) shows that fatigue is generally not a problem when the number of cycles that exceed the anchor pretension force is small (less than 20,000 cycles) during the life of the structure. In any case, it will be prudent to evaluate the effect of tensile fatigue on anchor rods and compression fatigue on concrete when pretension is not set to the maximum uplift force. Where operating load spectra are not available, a minimum pretension of $\frac{1}{3}F_u$ is recommended by *Design of Anchor Bolts in Petrochemical Facilities* (ASCE, 1997).

Steel stacks are another type of wind-sensitive structure. Many stacks are susceptible to cross-wind (or vortex shedding)-induced vibrations. According to the steel stack design standard ASME STS-1 (ASME, 2006), anchor bolts should be properly torqued and retightened 30 days after stack erection. However, the standard is silent on the anchor pretension requirements, and the engineer of record must determine the pretension requirements. Where stacks are properly proportioned to preclude significant vibrations, anchor rods are typically tightened by $\frac{1}{4}$ turn beyond the snug-tight condition. The $\frac{1}{4}$ turn from snug-tight has also been a standard industry practice for tightening of anchor rods for building column base connections and static equipment supports. The pretension stresses obtained by tightening nuts $\frac{1}{4}$ turn from snug-tight vary substantially, depending on the anchor yield strength, embedment length, concrete strength, pitch of threads and the lubrication condition of nuts and anchor rods.

Thus, the level of pretension of anchor rods needed for a given application is very much influenced by the expected

service environment and past industry experience. This includes any one of the following conditions:

- Ensure the anchorage is capable of withstanding significant cyclic stress fluctuations.
- Keep anchorage tight and nuts from loosening that may be caused by operation vibrations.
- Minimize the movement or drift of structures/vessels induced by foundation rotation.
- Follow the common tightening practice for a specific industry.

For applications where anchor rods and base plates are to be subjected to a large number of significant stress cycles from live loads, wind effects or other cyclic operating loads, fatigue resistance is the single most important factor for determination of anchor pretension. It is the responsibility of foundation designers to select an adequate anchor pretension load for their specific applications.

PRETENSIONING METHODS AND INSTALLATION SEQUENCE

There are three methods commonly used for applying the required preload in the anchor rods: turn-of-the-nut method, with a torque wrench and by hydraulic jacking. Among the three, hydraulic jacking is the most accurate pretensioning method and is used where the pretension load is critical to the structural integrity of the support and/or to the serviceability of the equipment. Hydraulic bolt tensioners use an annular hydraulic jack placed around the anchor rod, stretching it axially. When the required stress level is reached, the nut is tightened snugly and then the pressure released, resulting in a preloaded bolt without any frictional or torsional stresses. The hydraulic jacking method can provide very accurate preload ($\pm 1\%$) on long bolts, but it is less accurate on short bolts. The method is often used for mounting of heavy vibratory machines with large-diameter anchor rods or high-strength anchors (Grade 75, 105 or higher strength). The method is commonly used in the power industry, petrochemical industry and wind turbine industry. Calibrated hydraulic bolt pretensioners such as those manufactured by Boltech, Tantec and others have been used satisfactorily in many applications.

Torque wrench pretensioning only provides a rough measure of anchor preload. The torque wrench method is a simple and easy method for field preloading. However, torque is not a reliable indicator of bolt tension and is sensitive to lubrication and condition of bolts and nuts. The torque coefficient used in common torque-tension relationships may vary from 0.1 to 0.3. *AISC Design Guide 1* (Fisher and Kloiber, 2006) indicates that the coefficient is 0.12 for common anchor rods. Others have suggested a larger value

of 0.2 for less-well-lubricated rods. For example, the torque needed for a pretension of $\frac{1}{3}F_u$ of a 1½-in.-diameter anchor rod made of F1554 Grade 36 would be in the range of 408 to 680 ft-lb. If the rod is made of A193 B7 steel, the range will increase to 879 to 1,465 ft-lb based on the method recommended by AISC *Design Guide 1*. Despite its inaccuracy, the torque wrench method has been the method of choice for many engineers for applications where the amount of pretension needed is either not essential or not substantial. For anchor rods greater than 1 in. diameter, the torque required for anchor tightening would require the use of a slugging wrench or a hydraulic torque wrench.

Turn-of-nut method is the easiest preloading method. It gives preloads more reliable than the preceding torque wrench method. Anchor rods are first brought to the snug-tight condition, followed by turning the nut from the snug-tight condition with a predetermined number of turns. The snug-tight is generally conceived as the condition in which base plate and grout are brought into good contact by tightening nuts with a few impacts from common impact wrench. This is the method recommended by *NCHRP Report 469* (Dexter and Ricker, 2002) for tightening of the fatigue-sensitive double-nut-moment base joints. The number of nut rotations has been developed for double-nut-moment joints based on extensive testing. For other pretensioned joints, the nut rotation required beyond the snug-tight condition is not known and may have to be established by testing. It is important to note that anchor rods are typically much longer than high-strength structural bolts, varying from eight times the rod diameter to 30 ft in length. Thus, the amount of nut rotations beyond snug-tight to achieve pretension is substantially larger than high-strength structural bolts. According to *Design of Anchor Bolts in Petrochemical Facilities* (ASCE, 1997), the amount of nut rotation for the targeted pretension stress can be estimated by an approximate formula based on displacement compatibility between anchor rod and nut rotations. However, the amount of nut rotation for a given preload estimated by the formula is often found to be too low because the compression deformation of concrete and grout is ignored in the approximation. Caution must be exercised when using any approximate turn-of-nut formula.

Both torque wrench and turn-of-nut pretensioning method have been used for applications where anchor rods have a diameter of 1½-in. or smaller or where anchor rods have a shallow embedment length (less than or equal to 15 times the anchor diameter). However, for anchor rods of larger diameter or greater embedment length, pretensioning by hydraulic tensioners will be more effective.

Aside from these three methods, load indicating mechanisms, such as direct tension indicators (DTI), are getting more popular. They are often used in verifying preloads installed by torque wrench and turn-of-nut method. They serve as an alternative means to hydraulic jacking to achieve accurate pretension desired.

Multiple anchor rods are used for mounting heavy equipment, large process vessels, cantilevered poles and tower masts, and steel stacks. Anchor rods may be tightened in two or three stages. The three-stage tightening sequence is a more current trend in the industry, with 50% of full-pretension applied to all anchors in the first stage, 90% in second stage and 100% full pretension applied in the last stage. *Design of Anchor Bolts in Petrochemical Facilities* recommends that anchor rods should be tightened in criss-cross or star pattern. Similar tightening sequence is also followed in anchoring wind turbine towers.

Installation sequence for pretensioned joints is provided in Appendix A of AISC *Design Guide 1* (Fisher and Kloiber, 2006). Due to creep and stress relaxation, anchor pretension should be monitored periodically and anchors should be retightened if necessary. ACI 355.1R (ACI, 1997) reported that the final tension in headed anchors are typically in the range of 40 to 80% of the initial preload due to creep of highly stressed concrete under the anchor head. The loss of pretension depends on bearing stress under the anchor head, concrete deformation and the anchor depth. It also reported that pretensioning the anchor 90 days after the initial tightening can reduce the pretension loss by more than 50%. Anchors tightened 90 days after concrete placement then retightened 1 year later can further reduce loss in pretension (80% less). For fatigue critical applications such as wind turbine tower supports, engineers often specify that anchor rod pretension be checked once within 6 months after anchor installation and every 3 years thereafter. Loosened anchors should be retightened with hydraulic jacking. AISC *Design Guide 1* also recommends that all pretensioned anchor joints designed for Seismic Design Categories D, E or F be inspected and maintained after a significant seismic event.

Where epoxy grout is used, creep under high compression can cause a significant loss in anchor bolt pretension, which reduces the ability of the anchor bolt to maintain high frictional resistance to relative motion between vibrating equipment and tie-downs. The effects of creep must be considered in pretensioning of anchor bolts as well as in the engineering of grout thickness, anchor bolt length and preload tension as recommended by *Design of Anchor Bolts in Petrochemical Facilities* (ASCE, 1997) and *PCI Design Handbook* (PCI, 2008).

SPECIAL DESIGN CONSIDERATIONS

Designs of pretensioned anchor rods and regular anchor rods have many common aspects. Anchor rods must be capable of withstanding design loads (uplift tension loads, shear loads, compression loads and pretension force) and allowing the loads to be transferred to base plate, grout and concrete. Anchor rods should possess adequate strength to guard against bolt tensile failure and concrete pull out failure. Anchor rods located near the edge of concrete piers or foundations

should be designed for possible lateral (side) bursting failure. ACI 318 Appendix D (ACI, 2005) and AISC *Design Guide 1* (Fisher and Kloiber, 2006) provide excellent provisions/guidelines for design of nonpretensioned base plates and anchor rods.

There are, however, a few design aspects in which pretensioned anchors differ from nonpretensioned anchors and would require special consideration. These include the following:

- Pretensioned anchors should have adequate fatigue strength to resist cyclic loads (see Example 1), and bolt forces due to pry action should be included in the fatigue evaluation.
- Embedment plate, sleeve and base plate should have adequate static strength and stiffness for anchors with large pretension as discussed in *Design of Anchor Bolts in Petrochemical Facilities* (ASCE, 1997).
- Grout and concrete supporting base plates and anchors are susceptible to localized bearing damage and concrete splitting cracks when pretension force is high. A

number of recent wind turbine foundation applications required the use of 12,000-psi grout and 7,000-psi concrete.

- Friction due to anchor pretension is available for shear resistance. As a result, shear lugs are not often used in pretensioned anchors. According to *Design of Anchor Bolts in Petrochemical Facilities*, friction resistance may also be considered for seismic shear if anchor rods are pretensioned to twice the seismic uplift force, except that no more than 50% of friction resistance should be provided by pretension.

SELECTED EXAMPLES OF PRETENSIONED ANCHOR APPLICATIONS

Example 1

This example involves the design of a spread footing with a central pedestal to support a wind turbine tower as shown in Figure 2. The turbine tower is anchored to the concrete pedestal via a base ring plate and 140 high-strength anchor rods. Anchor rods are to be fabricated from No. 10 A615 Grade

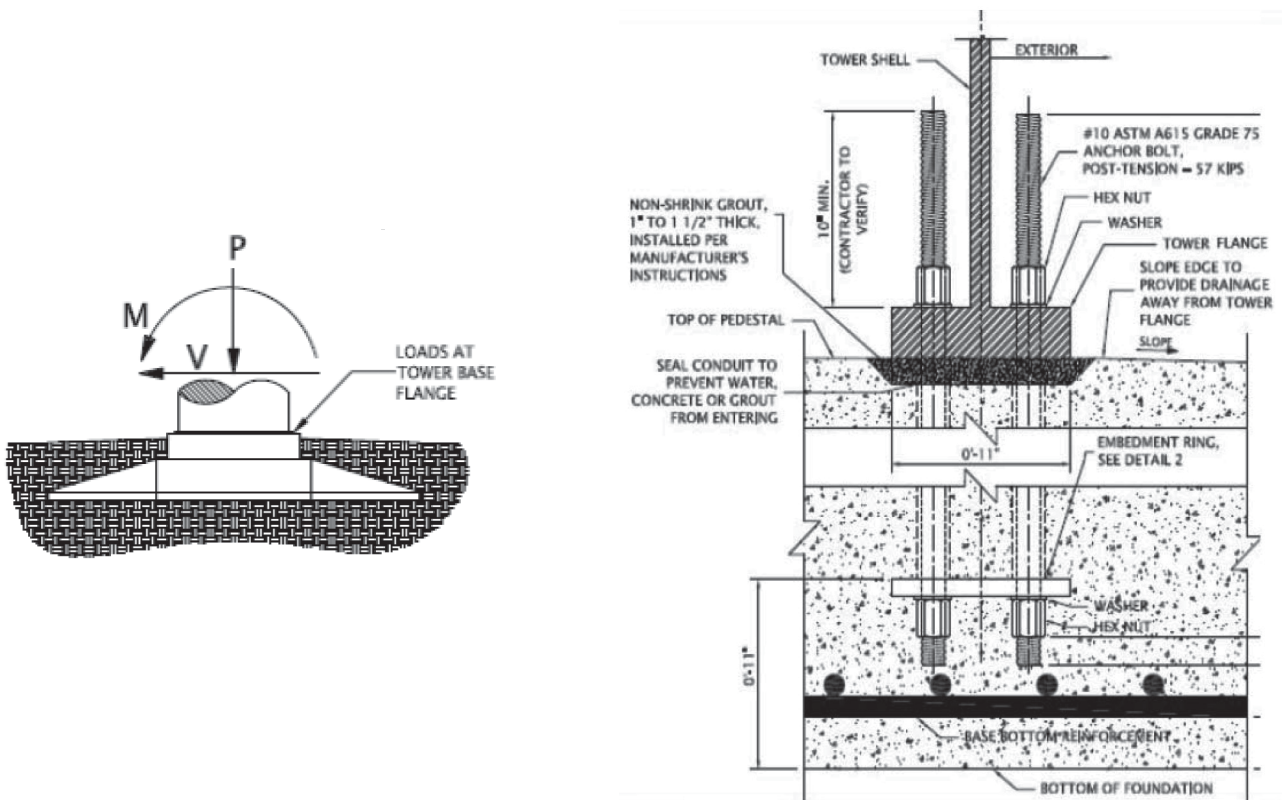


Fig. 2. Sketch of wind turbine foundation and tower anchorage to foundation for Example 1.

75 threaded bars. The anchor rods are arranged in two concentric circles with 70 anchor rods evenly spaced along each bolt circle. The diameter of the inner bolt circle is 13 ft 6 in.; the diameter of the outer bolt circle is 14 ft 6 in. The tower anchorage is designed for an unfactored wind moment, M_w , of 25,747 kip-ft, a horizontal shear load (V) of 118 kips, and a dead load, P , of 415 kips. In addition, the turbine manufacturer requires the anchorage to have adequate fatigue resistance against operating load spectra with cyclic overturning moment changes from nominal to a value as large as the design wind moment. A complete design of this wind turbine foundation will require a geotechnical evaluation, a static strength design, a structural stability analysis, a foundation dynamic stiffness analysis, and a static and fatigue strength of anchorage. However, the focus of this example is limited to the determination of anchor rod pretension only.

Note that Grade 75 threaded bars are the anchor rods most commonly used in the wind turbine industry, although their use at building column base is rare. The material has excellent strength: $F_y = 75$ ksi (minimum yield strength) and $F_u = 100$ ksi (minimum tensile strength) and excellent bond strength to concrete. Grade 75 threaded rods are available in many diameters ($\frac{3}{4}$ to $3\frac{1}{2}$ in.) and in lengths up to 50 ft. The net tensile area at the threads of a No. 10 threaded bar is 1.27 in.²

First, the maximum uplift force in anchor rods, T_b , due to unfactored design moment can be estimated by the following approximation equation given by ASME STS-1 2006:

$$T_b = \frac{4M_w}{ND_b} - \frac{P}{N} + \frac{V}{(\text{friction coefficient at grout} \times N)}$$

where

D_b = average diameter of the inner and outer bolt circles

N = number of anchor rods

$$\begin{aligned} T_b &= \frac{4(25,747 \text{ kip-ft})}{(140)(14 \text{ ft})} - \frac{415 \text{ kips}}{140} + \frac{118 \text{ kips}}{(0.55)(140)} \\ &= 51.3 \text{ kips} \end{aligned}$$

A more accurate determination can be made on the basis of moment of inertia considering exact locations of anchor rods. Maximum tension in the outer anchor rods is 57.1 kips.

There is no unique way for prescribing the pretension loads. One can set the pretension in the anchor rods equal to 57.1 kips (45% of the tensile strength of the rod) or 72.4 kips at the factored moment (57% of the tensile strength of the rod), or at a pretension of 42.0 kips (which is close to one-third of the rod tensile strength). If the pretension is set at 72.4 kips, the anchor rods will not be subjected to net uplift

forces during their service life, and tensile fatigue of anchor rods is unlikely. Conversely, the tensile fatigue resistance of anchor rods should be evaluated for the other two cases where lower anchor pretension loads are selected.

According to the turbine manufacturer for this project, the turbine tower is expected to experience a mean overturning moment of 10,873 kip-ft and a fatigue damage equivalent cyclic moment range of 30,393 kip-ft at 1,000,000 cycles using a method recommended by *Guidelines for Design of Wind Turbines* (DNV/RSO, 2002). Therefore, the anchor rods will be stressed to a tensile stress 1.3% higher than the initial pretension at the maximum cyclic moment if pretension is set at 57 kips. Thus, the anchor rods should have adequate fatigue strength. However, the anchor rods will be stressed to a maximum tensile stress 37.4% higher than the initial pretension if the anchor rod pretension load is set at 42 kips. The tensile stress range is therefore equal to $(0.374)(\frac{1}{3})(100 \text{ ksi}) = 12.5$ ksi.

Per AISC *Specification* (AISC, 2005) and ACI 351.3R-04 (ACI, 2004), the allowable stress range of the anchor rods can be determined as follows:

$$F_{sr} = \left(\frac{C_f}{N} \right)^{0.333} \geq 7 \text{ ksi} = \text{fatigue threshold}$$

where

$$C_f = \text{fatigue constant} = 3.90 \times 10^8$$

$$N = 1,000,000 \text{ cycles}$$

$$F_{sr} = \left(\frac{3.90 \times 10^8}{1,000,000} \right)^{0.333} = 7.3 \text{ ksi}$$

The tensile stress range of 12.5 ksi from the operating load spectra will exceed the above allowable stress range by 70%. Therefore, the pretension of 42.0 kips is too low and has to be adjusted to a higher value.

Note that the effective pretension in anchor rods with an initial tension of 57.1 kips will decrease to 42.8 kips if a 25% loss is considered. Hence, anchor rods with an initial pretension of 57.1 kips may not have adequate fatigue strength unless the anchor tension is periodically monitored and readjusted.

This example shows that the fatigue strength of anchor rods is sensitive to anchor pretension. A proper selection of initial pretension is critical to the long-term fatigue performance of wind sensitive structures.

Example 2

A compressor weighing 600 kips is supported on a concrete block foundation via soleplate and epoxy grout. The compressor is expected to produce a maximum dynamic

horizontal force of 200 kips. Assume the machine will require a total of eight 1³/₄-in.-diameter anchor bolts and the coefficient of friction at the critical interface is 0.15. This example will determine the preload tension required in the anchor bolts and the bolt material required.

To avoid slippage under dynamic loads at any interface, the friction force, F , at any interface between the compressor frame and soleplate, or soleplate and epoxy grout, or grout and foundation top surface must exceed the maximum horizontal dynamic force, H_{max} :

$$F = C_f (W_m + NT_{min}) \geq H_{max}$$

where

C_f = friction coefficient = 0.15

T_{min} = minimum preload tension

W_m = machine weight = 600 kips

H_{max} = maximum horizontal load = 200 kips

N = number of bolts = 8

$$\begin{aligned} T_{min} &= \frac{H_{max}/C_f - W_m}{N} \\ &= \frac{(200 \text{ kips}/0.15) - (600 \text{ kips})}{8} \\ &= 91.7 \text{ kips} \end{aligned}$$

Because the recommended clamping force is 150% of the required value, the minimum pretension is 137.5 kips. The bolt stress due to pretension is $137,500 \text{ lb}/1.90 \text{ in.}^2 = 72,368 \text{ psi}$, where net tensile area of anchor rod is 1.90 in.^2 . Per ACI 351.3R, the ratio of prestress to yield stress should be between 0.15 and 0.8. Thus, the minimum required yield stress of anchor bolts is $72,368 \text{ psi}/0.8 = 90,460 \text{ psi}$.

Select ASTM A193 B7 anchor bolts, which have a minimum yield strength of 105 ksi.

REFERENCES

- ACI (1997), "Report on Anchorage to Concrete," ACI 355.1R-91, reapproved 1997, American Concrete Institute, Farmington Hills, MI.
- ACI (2004), *Foundations for Dynamic Equipment*, ACI 351.3R-04, American Concrete Institute, Farmington Hills, MI.
- ACI (2005), *Building Code Requirements for Structural Concrete and Commentary*, ACI 318-05, American Concrete Institute, Farmington Hills, MI.
- AISC (2005), *Specification for Structural Steel Buildings*, American Institute of Steel Construction, Chicago, IL.
- ASCE (2005), *Minimum Design Loads for Buildings and Other Structures*, ASCE/SEI 7-05, American Society of Civil Engineers, Reston, VA.
- ASCE (1997), *Design of Anchor Bolts in Petrochemical Facilities*, Task Committee on Anchor Bolts, American Society of Civil Engineers, New York, NY.
- ASME (2006), *Steel Stacks*, STS-1 2006, American Society of Mechanical Engineers, New York, NY.
- Dexter, R.J. and Ricker, M.J. (2002), "Fatigue-Resistant Design of Cantilevered Signal, Sign and Light Supports," *National Cooperative Highway Research Program (NCHRP) Report 469*, Transportation Research Board, Washington, DC.
- DNV/RSO (2002), *Guidelines for Design of Wind Turbines*, Second Edition, Denmark.
- Fisher, J.M. and Kloiber L.A. (2006), *Design Guide Series No. 1: Base Plate and Anchor Rod Design*, 2nd edition, 2nd printing, American Institute of Steel Construction, Chicago, IL.
- Frank, K.H. (1980), "Fatigue Strength of Anchor Bolts," *Journal of Structural Division*, ASCE, Vol. 106, No. 6, pp. 1279-1293.
- Hodge, J.B. (1996), "Fatigue Analysis of High Mast Luminaire Anchor Bolts," MS Thesis, Texas A&M University, College Station, TX.
- Kaczinski, M.R., Dexter, R.J. and Van Dien, J.P. (1996), "Fatigue-Resistant Design of Cantilevered Signal, Sign and Light Supports," *National Cooperative Highway Research Program (NCHRP) Report 412*, Transportation Research Board, Washington, DC.
- PCI (2008), *PCI Design Handbook*, 7th edition, Precast/Prestressed Concrete Institute, Chicago, IL.
- Richards J.H. (2004), "Turn-of-the-nut Tightening of Anchor Bolts," MS Thesis, Texas A&M University, College Station, TX.
- Van Dien, J.P. Kaczinski, M.R., and Dexter, R.J. (1996), "Fatigue Testing of Anchor Bolts," *Proceedings of the 14th Structural Congress*, American Society of Civil Engineers, Reston, VA, pp. 337-344.

Recommendations for Shear Lag Factors for Longitudinally Welded Tension Members

PATRICK J. FORTNEY and WILLIAM A. THORNTON

ABSTRACT

Section J2.2b of the 2010 AISC *Specification for Structural Steel Buildings* requires the length of longitudinal welds, used to connect flat plate tension members, to be greater than the distance between the longitudinal welds. Currently, weld lengths less than the distance between the welds are not permitted for connections of flat plate members. The procedure for the calculation of the shear lag factor, U , for this type of connection is given by Case 4 in Table D3.1 of the AISC *Specification*, where U is a function of the length of the longitudinal weld and the width of the plate. Although Case 4 is explicitly defined for plates only, the generally accepted practice in the design of similar welded connections of angles, channels, tees and wide flange members is to apply the same limitation on weld length, and calculate the effect of shear lag as $1 - \bar{x}/l$ as given by Case 2 in Table D3.1 of the AISC *Specification*, while ignoring shear lag effects with weld lengths between one and two times the distance between the welds. Furthermore, for connection geometries meeting those for Case 2 or Case 4, there is no guideline for considering connection strengths where the longitudinal welds on each side of the member have unequal lengths (e.g., skewed web members or braces) or weld lengths less than the distance between the welds.

This paper presents recommendations for a generalized design procedure for welded connections of plate, angle, channel and tee tension members regardless of the length of the weld or if the length of the longitudinal welds are unequal. A summary of the treatment of various current building codes/specifications (AISC and CSA) on this topic is presented along with the results of several published experimental research projects that evaluated the behavior of these types of connections. Two analytical models are presented, and recommendations for changes to the current AISC *Specification* are made, followed by an example problem illustrating the practical application of the recommendations.

Keywords: shear lag, longitudinal welds.

In November 2005, a task group was formed under the AISC Committee on Specifications to evaluate Table D3.1 of the 2005 AISC *Specification for Structural Steel Buildings*. One of the tasks assigned to the group was to evaluate shear lag coefficients for longitudinally welded flat plate connections, shown as Case 4 in Table D3.1, for cases where the weld length, l , is less than the width, w , of the connected plate. Since then, the same question was posted in the Steel Interchange section of the June 2009 edition of *Modern Steel Construction*. While reviewing the provisions for Case 4, the authors of this paper decided to evaluate the potential of revising Case 4 to address longitudinally welded end connected members in a more general fashion and to address similar connections, as shown in Case 2 for angles, channels, wide flange and WT sections.

Case 4 shown in Table D3.1 provides direction for end-connected plate material. The limitations for this condition

are (1) only plates are considered, (2) both edges of the plate must be welded, (3) the longitudinal welds on each side of the plate must be of equal length, and (4) the length of the welds must be equal to or greater than the distance between the welds. Presented in this paper are recommendations for generalizing Case 4 in Table D3.1, while incorporating conditions where the length of the welds are less than the distance between them, and for conditions where the weld lengths are unequal (e.g., skewed brace or web connections).

SUMMARY OF CURRENT DESIGN PROVISIONS

The AISC *Specification* (2010) and *Design of Steel Structures* (Canadian Standards Association, 2009) were reviewed. The following is a summary of the treatment of longitudinally welded tension members as presented in the two codes/specifications.

2010 AISC *Specification* (ANSI/AISC 360-10)

$$A_e = A_n U = wtU \quad (D3-1)$$

where

A_e = effective cross-sectional area

A_n = net cross-sectional area

Patrick J. Fortney, Ph.D., P.E., Manager and Chief Engineer, Cives Engineering Corp., Roswell, GA. E-mail: pfortney@cives.com

William A. Thornton, Ph.D., P.E., Corporate Consultant, Cives Engineering Corp., Roswell, GA. E-mail: bthornton@cives.com

t = thickness of plate
 w = width of plate
 U = shear lag factor

Shear lag factor, U ; Table D3.1 (Case 4)

For $l \geq 2w$

$$U = 1.0$$

$$\therefore A_e = wt$$

For $2w > l \geq 1.5w$

$$U = 0.87$$

$$\therefore A_e = 0.87wt$$

For $1.5w > l \geq w$

$$U = 0.75$$

$$\therefore A_e = 0.75wt$$

For $w > l$

Per AISC Specification Section J2.2b, the length of the

welds shall not be less than the perpendicular distance between the welds.

$\therefore l < w$ is not permitted.

In all of the preceding expressions, l is the length of each longitudinal weld.

CSA-2009 (Section 12.3.3.3)

$$A_{ne} = A_{n1} + A_{n2} + A_{n3}$$

For elements connected with transverse welds,

$$A_{n1} = wt$$

(Note that this type of weld is outside the scope of this paper.)

For elements connected with a pair of parallel longitudinal welds,

For $L \geq 2w$

$$A_{n2} = 1.00wt$$

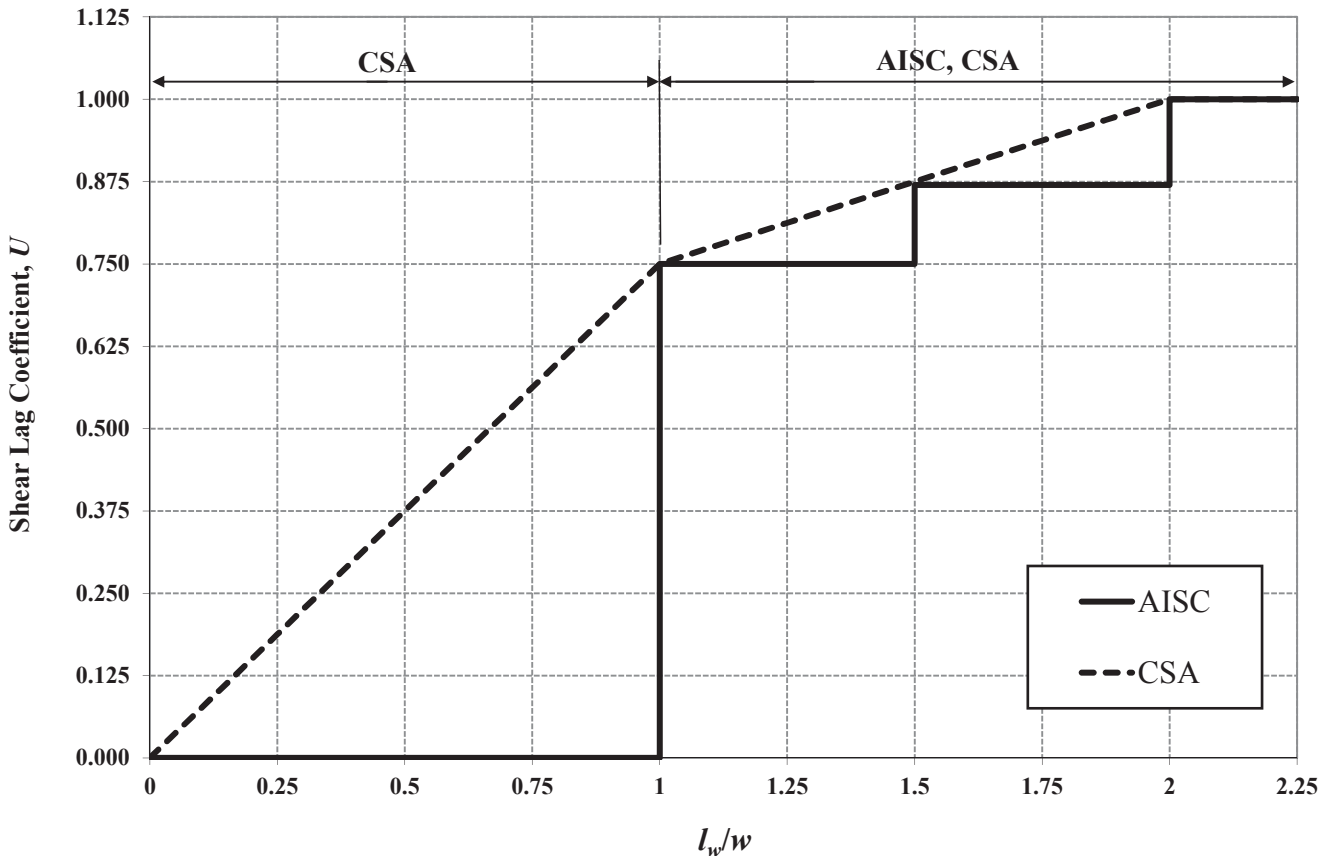


Fig. 1. Comparison of AISC and CSA shear lag requirements for plates connected with a pair of parallel longitudinal welds (l_w = length of weld).

For $2w > L \geq 1.0w$

$$A_{n2} = 0.5wt + 0.25Lt$$

For $w > L$

$$A_{n2} = 0.75Lt$$

(Note that these provisions are CSA's counterpart to AISC's provisions for plate tension members connected with longitudinal welds.)

For elements connected by a single line of weld,

$$A_{n3} = \left(1 - \frac{\bar{x}}{L}\right)wt$$

(Note that AISC does not have such a provision.)

where

A_{n1} = net cross-sectional area of an element connected with a transverse weld

A_{n2} = net cross-sectional area of an element connected by a pair of parallel longitudinal welds

A_{n3} = net cross-sectional area of an element connected with a single longitudinal weld line

w = the width of the element being considered

t = the thickness of the element being considered

L = length of longitudinal weld

\bar{x} = the distance from the connected edge to the centroid of the area of the element

Evaluating AISC 360-10 Against CSA-2009

The CSA provisions for calculating the effective area, A_{n2} , are CSA's method for computing shear lag effects in longitudinally welded plates. The CSA A_{n2} provisions are evaluated and compared to AISC's provisions for longitudinally welded plates.

Substituting w for L in the CSA equation for A_{n2} , it can be seen that the CSA provisions are the same as AISC for $w \leq L < 2w$. Note that the Canadian Standard uses L to denote weld length.

$$A_e = A_{n2}$$

For $L \geq 2w$

$$A_{n2} = 1.00wt = A_e = wt \quad (\because \text{AISC and CSA equal})$$

For $2w > L \geq 1.0w$

$$A_{n2} = 0.5wt + 0.25Lt$$

At $L = 2w$

$$A_{n2} = 0.5wt + 0.25(2w)t = 1.0wt$$

(at $L = 2w$, \therefore AISC and CSA equal)

At $l_w = 1.5w$

$$A_{n2} = 0.5wt + 0.25(1.5w)t = 0.875wt$$

(at $L = 1.5w$, \therefore AISC and CSA equal)

At $l_w = w$

$$A_{n2} = 0.5wt + 0.25(1.0w)t = 0.75wt$$

(at $L = w$, \therefore AISC and CSA equal)

For $w > L$

$$A_{n2} = 0.75Lt = 0.75\alpha wt$$

where $\alpha = L/w < 1.0$

So, there are two differences between AISC and CSA standards relative to plates used as tension members, and connected with longitudinal welds. Refer to Figure 1.

1. When $2w > L \geq w$, the reduction varies linearly in the CSA standard where the AISC standard has a step function with the steps located at $L = 1.5w$ and $L = 2w$.
2. When $L < w$, AISC does not permit this condition. The CSA standard allows this condition, and strength reduction varies linearly from $U = 0$ at $L = 0$ to $U = 0.75$ at $L = w$.

Rationale for CSA Provisions

Figure 2 is an illustration of a possible schematic representing the CSA shear lag model for plates connected with a pair of longitudinal welds (i.e., A_{n2}). Referring to Figure 2, the following equations are developed.

Assumptions:

1. Only cross-sectional area contained within w' is effective in resisting tension.
2. Stress acting on the effective cross-sectional area is uniformly distributed with magnitude of F_u .
3. The effective width, w' , varies bi-linearly from $l_w = 0$ to $l_w = w$ and from $l_w = w$ to $l_w = 2w$, as shown in Figure 2, where l_w = length of weld.

For $l_w \geq 2w$

$$w' = w$$

$$A_n = wt$$

For $2w > l_w \geq 1.0w$

$$\frac{w'}{2} = \frac{3w}{8} + \frac{0.125w}{w}(l_w - w)$$

$$w' = 0.5w + 0.25l_w$$

$$A_n = (0.5w + 0.25l_w)t$$

For $w > l_w$

$$\frac{3w}{8w} = \frac{w'}{2l_w}$$

$$w' = 0.75l_w$$

$$A_n = 0.75l_w t$$

Conclusion: this model is the same model as AISC with the exceptions that (1) the effective width varies linearly from $l_w = w$ to $l_w = 2w$ in the CSA model, where the AISC model has step functions at l_w/w ratios of 1.0, 1.5 and 2.0, and (2) the CSA model allows $w > l_w$ where AISC currently does not.

Fixed-Fixed Beam Model

Figure 3 illustrates the theoretical deformed shape of a welded tension member over the connected region. As axial tension load is applied, longitudinal and transverse strain is induced over the connected region resulting from a combination of axial tension and bending resulting from the Poisson effect. The following derivation neglects Poisson's effect, but it assumes that normal longitudinal stresses develop in the plate during bending; are approximately equal to the normal stresses in the transverse direction, resulting from bending in an assumed fixed-fixed beam with a uniformly distributed load along the width of the plate; and are equal to T/w , where T is the applied axial load and w is the width of the plate.

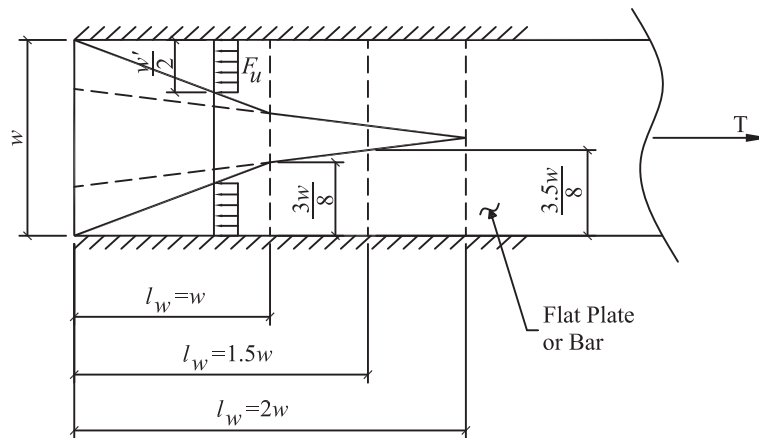


Fig. 2. Representation of CSA shear lag model for welded flat-plate tension members.

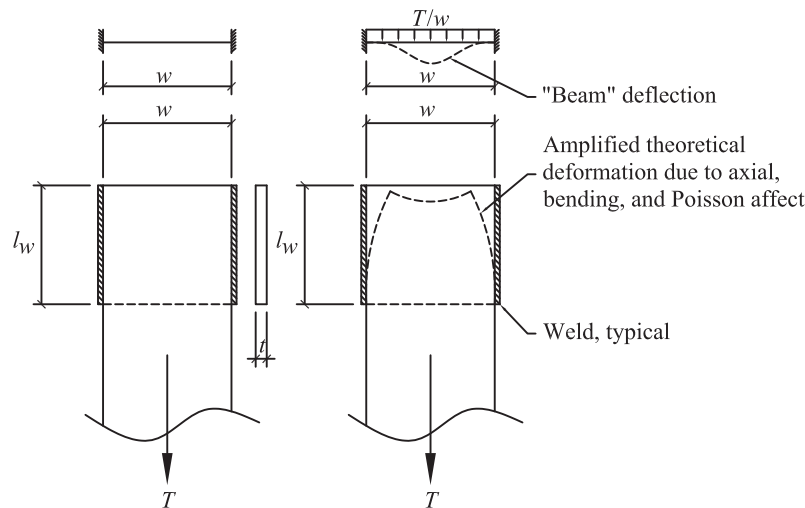


Fig. 3. Fixed-fixed beam shear lag model.

Assuming a fixed-fixed beam with a uniformly distributed load along its length and plastic hinges formed at locations of maximum positive and negative moments, the required nominal flexural strength, M_r , and flexural capacity, M_c , at the weld is

$$M_r = \frac{T_w}{16} \quad (1)$$

$$M_c = F_y Z = \frac{F_y t l_w^2}{4} \quad (2)$$

Similarly, the required nominal axial strength, P_r , and tensile capacity, P_c , is

$$P_r = T \quad (3)$$

$$P_c = F_u t w \quad (4)$$

Using the moment-axial interaction equation of AISC Section H1.1, and assuming that $P_r/P_c > 0.2$, for uniaxial bending,

$$\frac{P_r}{P_c} + \frac{8M_r}{9M_c} = 1.0 = \frac{T}{F_u t w} + \frac{8}{9} \frac{T_w}{16 F_y t l_w^2} \quad (5)$$

$$1.0 = \frac{T}{F_u t w} + \frac{2T_w}{9F_y t l_w^2} \quad (6)$$

Rearranging Equation 6 to take the form of $T = F_u A_n U = F_u t w U$

$$T = F_u t w \left(\frac{1}{1 + \frac{2}{9} \left(\frac{F_u}{F_y} \right) \left(\frac{w}{l_w} \right)^2} \right) \quad (7)$$

Conservatively taking F_u/F_y approximately equal to 1.5, the shear lag factor reduces to

$$U = \frac{1}{1 + \frac{1}{3} \left(\frac{w}{l_w} \right)^2} \quad (8)$$

As can be seen in Figure 4, the shear lag model defined

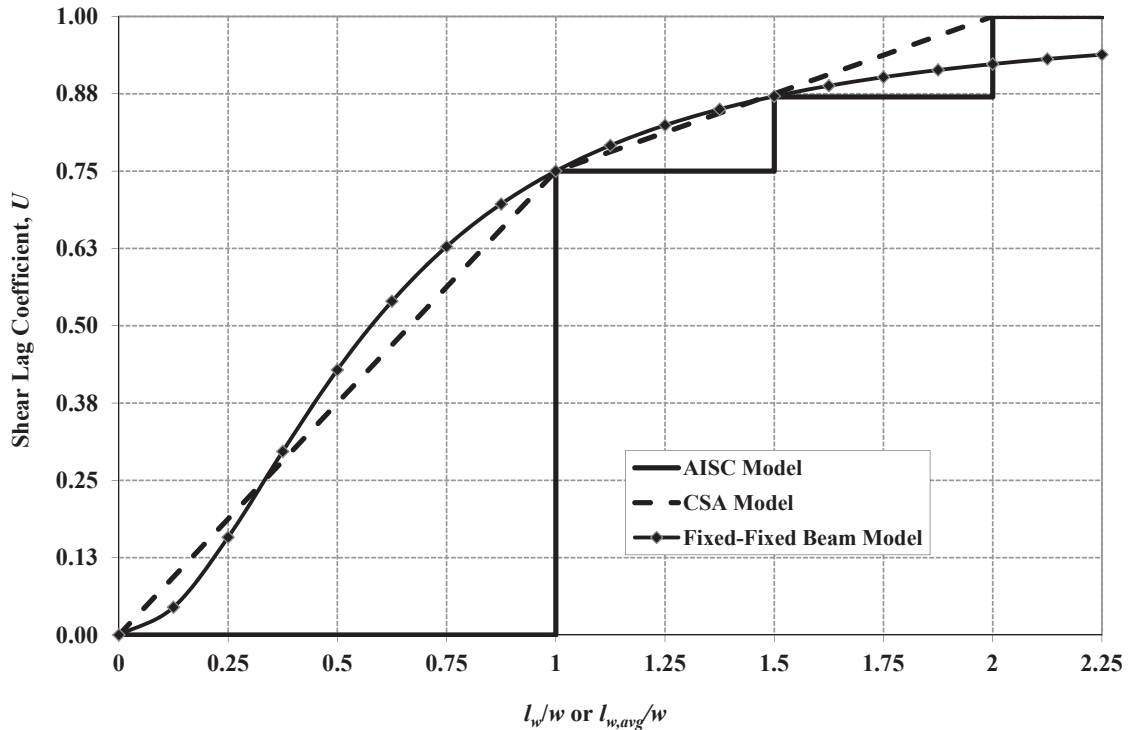


Fig. 4. Comparison of fixed-fixed beam model to current AISC and CSA models used for plates connected with a pair of longitudinal welds.

by Equation 8 is a good approximation to the CSA model currently used for plates connected with a pair of longitudinal welds. Comparing Equation 8 to the current AISC model, Equation 8 is a good approximation if the step functions are neglected. Note that the fixed-fixed beam model, surprisingly because of its simplicity, intersects with the AISC model at l_w/w values of 1.0 and 1.5.

In regard to the fixed-fixed beam model presented, it is worth noting that the authors evaluated several different beam models assuming various boundary conditions (fixed or pinned), loading conditions (uniform or concentrated) and beam stress distributions (elastic or plastic), as well a plane stress lower bound solution. The fixed-fixed beam with a uniformly distributed load along the width of the plate has the best correlations with the AISC and CSA models, as well as the experimental data, as will be presented in the following section.

This fixed-fixed beam model, which closely follows both the AISC and CSA models, gives a continuous curve that is a function of l_w and w for U rather than a series of four discrete straight lines. This is much simpler to use relative to the current AISC and CSA procedures and will be part of the recommendations given in this paper.

THE SHEAR LAG FACTOR, U

The shear lag factor used in AISC procedures, U , is generally thought to be a factor applied to the main member and not the weld—and not the connection region either. But, equally generally understood is that the weld arrangement in a welded connection, such as that considered in this paper, affects both the main member and the weld. The Poisson effect, for example, results in stresses on the welds over the connection region that are not accounted for in the usual weld strength calculations, where only longitudinal stress is considered. The beam models presented previously in this paper, although not exact models that describe the structural mechanics occurring, are generated in an effort to at least capture the phenomena that occur in the connection region.

The discussion in this paper is based on the authors' assertion that the shear lag factor is more accurately used to capture the strength reduction of the system, rather than simply the member. It is also important to recognize that the strength of the weld is usually the controlling limit state in the design of a longitudinally welded tension member. Commonly, these types of connections are designed based on a given load, which is usually less than the tensile strength of the member ($F_u A_g$). For a longitudinally welded tension member, where the connection is designed to resist a given load, it should be expected that the failure of such a system would be a weld failure because the weld strength is controlling limit state. However, consider a welded connection designed to resist the tensile strength of the member.

Assume a $\frac{3}{8}$ -in. \times 6-in. A36 plate is used as a tension

member and is connected using 6-in.-long longitudinal welds on each side of the plate. The design would be set up as shown in the following.

The design tensile yielding strength of the plate is

$$\phi P_{ny} = \phi F_y A_g = (0.9)(36 \text{ ksi})(\frac{3}{8} \text{ in.})(6 \text{ in.}) = 72.9 \text{ kips}$$

The weld required to resist this load is

$$1.392 D L n = 72.9 \text{ kips}$$

$$n = 2$$

$$L = 6 \text{ in. (given)}$$

$$D = \frac{72.9 \text{ kips}}{(1.392)(6 \text{ in.})(2)} = 4.36 \text{ sixteenths}$$

The design tensile rupture strength of the plate is

$$U = 0.75$$

$$\phi P_{nu} = \phi F_u U A_n$$

$$= (0.75)(58 \text{ ksi})(0.75)(\frac{3}{8} \text{ in.})(6 \text{ in.})$$

$$= 73.4 \text{ kips}$$

The weld required to resist this load is

$$1.392 D L n = 73.4 \text{ kips}$$

$$n = 2$$

$$L = 6 \text{ in. (given)}$$

$$D = \frac{73.4 \text{ kips}}{(1.392)(6 \text{ in.})(2)} = 4.39 \text{ sixteenths}$$

Thus, a $\frac{5}{16}$ -in. weld 6 in. long will be used.

The nominal strengths of the plate and weld are

$$\text{Plate yield: } R_{ny} = (36 \text{ ksi})(\frac{3}{8} \text{ in.})(6 \text{ in.}) = 81 \text{ kips}$$

$$\text{Plate rupture: } R_{nu} = (58 \text{ ksi})(\frac{3}{8} \text{ in.})(6 \text{ in.}) = 131 \text{ kips}$$

$$\text{Weld: } R_w = \frac{(1.392)(2)(5)(6)}{0.75} = 111 \text{ kips}$$

Considering the calculated nominal strengths, the weld will fail prior the plate reaching rupture strength. Generally speaking, it should be no surprise that weld failure occurs in these types of connections.

Table 1. Summary of Test Specimens

No.	Researcher	Specimen Type	Quantity	Weld Length
1	Easterling and Giroux (1993)	Flat plates	7	Equal
		Double angles	3	Equal (balanced)
		Double channels	6	Equal
		Double tees	4	Equal
2	Structural Steel Welding Society (1931)	Flat plates	151	Equal
3	Gibson and Wake (1942)	Single angles	4	Unequal (balanced)

The following sections of this paper discuss previous physical research projects evaluating the strength of longitudinally welded tension members. In these research reports, the researchers report failure loads where weld failures occur. The data points of these specimens are included in the data points presented in this paper. For example, as is presented in the following section, 151 longitudinally welded plate specimens were tested by the Structural Steel Welding Committee (1931). Of the 151 data points presented, 149 of the specimens were reported as weld failures at the reported failure load. Of the 149 specimens reported as having weld failures, 126 of these specimens have calculated weld strengths, using AISC 360-10 strength equations, greater than the reported failure load. In most cases, the calculated weld strengths vary from 2 to 10 times larger than the weld size that would be required to produce the reported failure load. Although apparently contrary to prevailing opinion (which assumes that shear lag is limited to the member), referring to these SSWC results and also to the preceding example calculations where a weld size of at least a $R_{nu}/5R_w = 131/(5)(111) = 3/8$ in. fillet weld would be needed to cause the member to fail first, it is the authors' assertion that the 151 SSWC tests are all valid data points for evaluating the shear lag phenomena.

PREVIOUS RESEARCH

To evaluate the potential for generalizing the shear lag model for the various shapes discussed in this paper, a literature review was conducted to gather all possible pertinent experimental data. The following is a discussion and summary of experimental data collected from past research reports.

Three research projects, as shown in Table 1, were evaluated for load capacities of longitudinally welded tension members. Specimens meeting the configuration as shown in Cases 2 and 4 of Table D3.1 were included in the evaluation. Measured U factors, P_{fail}/F_uA_{net} , plotted against the ratio of weld length to width (l_w/w), were determined for each of the specimens reported in the three research projects considered. P_{fail} is the reported load at which the specimen

failed, and F_uA_{net} is the calculated net tension capacity using (1) measured material properties for research projects Nos. 1 and 2 and (2) mill test reported values for research project No. 3.

Considering that flat plate connections have negligible eccentricity in the direction normal to the axis of the member, whereas angles, channels and tees have eccentricity, connections of flat plate members and connections of members with out-of-plane eccentricity are considered separately.

Welded Flat Plates

The measured shear lag factors, U , for Easterling and Giroux (7 specimens) and the Structural Steel Welding Committee (SSWC) (151 specimens) are plotted in Figure 5. Referring to Figure 5, for $l_w/w \geq 1$, the majority of the tensile strengths measured by the SSWC fall below the model currently adopted by AISC; all specimen strengths measured by Easterling and Giroux are larger than the current models. Evaluating the SSWC test data, all current specifications are unconservative, but conservative compared to the Easterling and Giroux results.

For $l_w/w < 1$, only two values were considered in the SSWC project (0.67 and 0.80). At $l_w/w = 0.67$, 78 specimen results are available; 8 specimens at $l_w/w = 0.80$. As can be seen in Figure 5, the CSA model is conservative from $l_w/w = 0$ up to $l_w/w = 1.0$. Note that the SSWC tested multiple numbers of the same specimen type, and many data points exist in the same space.

Also noteworthy is that the stepped model adopted by AISC has a better correlation with the experimental results relative to the CSA straight line functions for l_w/w values greater than 1.0.

Members with Eccentricity (Out-of-Plane Unconnected Elements)

AISC procedures account for out-of-plane eccentricity by reducing tensile strength by $(1 - \bar{x}/l)$, where \bar{x} is the distance from the connection surface to the centroid of the connected member and l is the length of the connection (in the context

Table 2. Comparison of Measured Shear Lag to AISC Requirements (Uni-planar Model)											
Double Angles (Easterling and Giroux)						Single Angles (Gibson and Wake)					
Test	P_{fail} (kips)	I_w/W	$P_{fail}/F_u A_g$ U_{exp}	$1 - x/l$ U_{AISC}	U_{exp}/U_{AISC} (%)	Test	P_{fail} (kips)	$I_w, avg/W$	$P_{fail}/F_u A_g$ U_{exp}	$1 - x/l$ U_{AISC}	U_{exp}/U_{AISC} (%)
L-L1	50.0	2.25	0.81	0.89	91.4	1	80.8	1.95	1.28	0.90	142
L-L2	50.5	2.25	0.82	0.89	92.2	2	78.2	1.95	1.23	0.90	138
L-L3	50.4	2.25	0.82	0.89	92.7	3	77.3	1.45	1.22	0.86	142
						4	76.8	1.28	1.21	0.84	144
Double Channels (Easterling and Giroux)						Double Tees (Easterling and Giroux)					
Test	P_{fail}	I_w/W	$P_{fail}/F_u A_g$ U_{exp}	$1 - x/l$ U_{AISC}	U_{exp}/U_{AISC} (%)	Test	P_{fail} (kips)	I_w/W	$P_{fail}/F_u A_g$ U_{exp}	$1 - x/l$ U_{AISC}	U_{exp}/U_{AISC} (%)
C-L-1a	79.9 [†]	2.16	0.84	0.93	90.2	T-L-1a	71.7 [†]	1.41	0.55	0.75	73.4
C-L-1b	87.0 [‡]	1.66	0.89	0.91	97.9	T-L-1b	85.3	1.65	0.80	0.90	88.6
C-L-2a	85.0 [†]	2.16	0.92	0.93	98.5	T-L-2	85.1 [†]	1.65	0.82	0.90	90.4
C-L-2b	86.7 [‡]	1.65	0.90	0.91	98.3	T-L-3	86.5	1.65	0.79	0.90	87.2
C-L-3a	76.3 [†]	2.16	0.83	0.93	89.4						
C-L-3b	86.9 [‡]	1.65	0.92	0.91	100.8						

[†] Test stopped due to weld failure.

[‡] Test stopped due to cross-sectional rupture away from connection region.

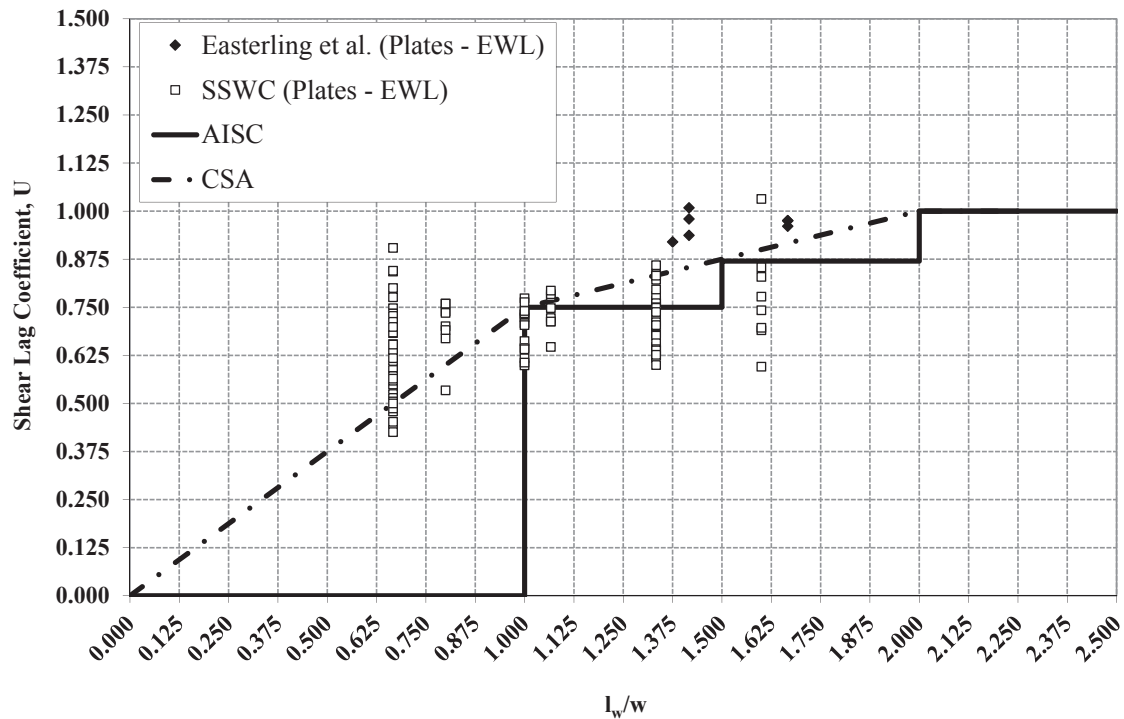


Fig. 5. Data for plates with equal-length longitudinal welds.

of this paper, the length of the weld). Note that previous versions of the the AISC *Specification* limited the upper bound of U to 0.9 for reductions calculated using the $(1 - \bar{x}/l)$ term (the fixed-fixed beam model described previously for flat plate members reaches 0.9 at $l_w/w \approx 2.0$). Consider a WT connected with longitudinal welds at the flange only. Currently, the AISC procedure accounts for shear lag effect of the out-of-plane eccentricity but does not account for the length of the weld (in-plane shear lag effect). The following is an evaluation to determine if eccentricity due to out-of-plane effects, as well as the in-plane effects, should be considered. Note that this evaluation is for members where not all of the member's elements are connected.

Easterling and Giroux (1993) tested several welded tension members consisting of double angles, double channels and double tees. A total of 13 specimens were reported; three, six, and four specimens, respectively. All specimens

had equal length longitudinal welds. The longitudinal welds used for the angles were sized appropriately to create balanced connections.

Table 2 summarizes the shear lag factors measured for each of the specimens and compares those values to the shear lag calculated using the current AISC procedure. As can be seen in Table 2, the experimental data results in a larger strength reduction compared to the procedure currently required by AISC. On average, the AISC procedure would result in connection strength approximately 10% larger than what is reported by Easterling and Giroux (1993). It should be noted that several of the failure loads reported for the channels and tees are a result of weld failures. Refer to the footnotes to the table.

Referring to the results shown in Table 2, the experimental strengths are less than the strength predicted with $(1 - \bar{x}/l)$ (with the exception of the single angles).

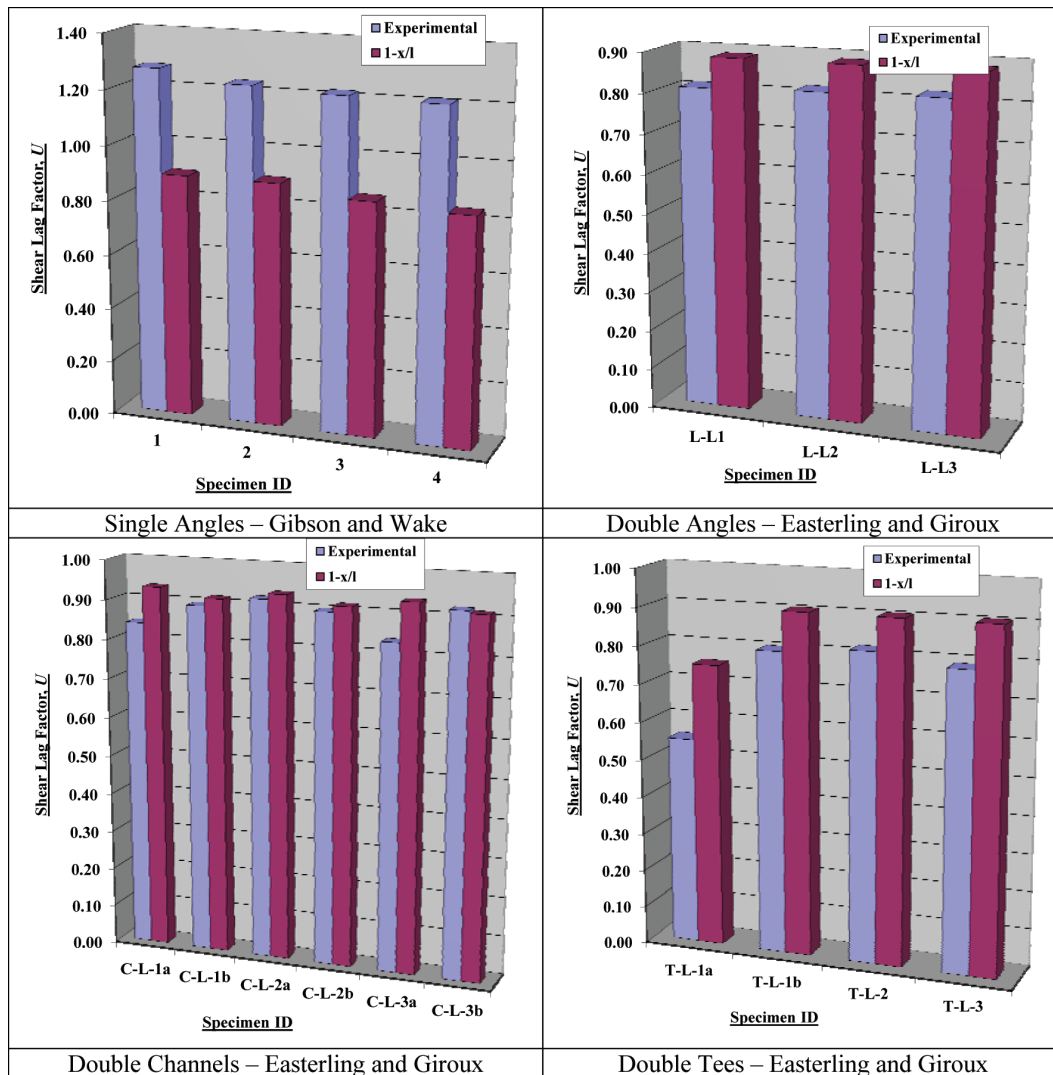


Fig. 6. Comparison of measured shear lag to AISC current procedures.

Considering that the effect of the in-plane shear lag is not considered in the values shown, the following discussion evaluates the need for accounting for the in-plane effects.

Figure 6 shows a graphical representation of the data shown in Table 2. As can be seen in the figure, the experimentally measured strengths for all specimens, except for the single angles, are less than the strength predicted using the current AISC procedure (i.e., $1 - \bar{x}/l$). This may be a result of not considering the in-plane shear lag effect resulting from the length of the connection. However, consider that several of the specimens shown in Table 2 have weld lengths greater than two times the width of the connected element. For these connection lengths, consideration of weld length will not have an impact if no strength reduction is taken for weld lengths equal to or greater than two times the distance between the welds.

Unequal-Length Welds and Unconnected Elements

A generalized procedure for determining shear lag in tension members should consider welded connections where the longitudinal welds are not equal in length. Very little experimental evidence was able to be located during the literature review. Gibson and Wake (1942) tested four single-angle tension members connected with unequal length longitudinal welds. For each of the four tests, the angles were connected with different size, unequal-length welds, and

proportioned appropriately to achieve a balanced connection. Table 2 also summarizes the results of those four tests. As can be seen in Table 2, the measured failure load was considerably larger than the strength computed using the current AISC procedure. The measured failure load is, on average, 42% larger than what the AISC procedure allows.

It is also worth noting that the CSA shear lag provisions explicitly provide direction for determining strength reduction in tension members connected with longitudinal welds on some, but not all, of the elements that make up the member cross-section.

Effects of Shear Lag in Two Planes

As discussed previously, shear lag is considerably different in the connected region of a plate as opposed to angles, channels and tee sections. This is an effect primarily due to the eccentricity of the geometric centroid relative to the faying surface of the connected element of the member. The total shear lag is a combination of the in-plane shear lag effect in the connected element and the out-of-plane shear lag effect associated with the unconnected element of the section. Referring to Figure 7, the total shear lag in an end-connected plate is fully due to the in-plane shear lag effect, whereas the total shear lag in angles, channels and tees is a combination of the in-plane and out-of-plane effects.

The contribution to the total shear lag effect in the

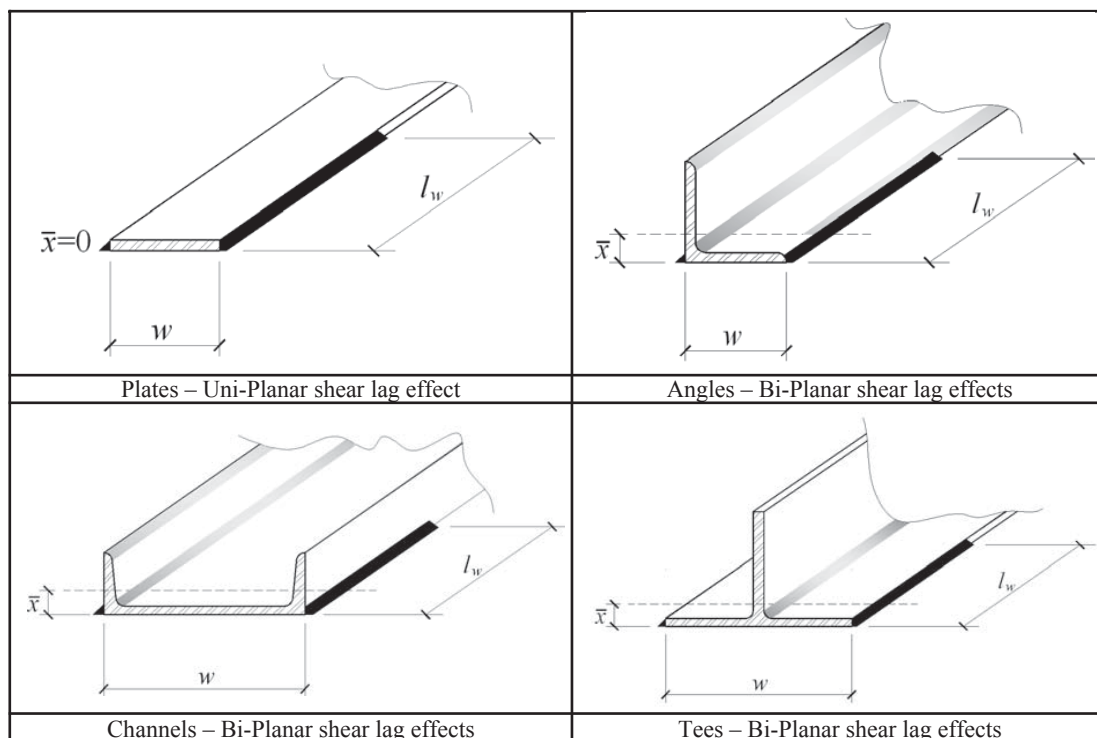


Fig. 7. Examples of shear lag effects in one and two planes.

connected element, due to in-plane effects, may be assumed to be captured using the guidelines of the AISC *Specification* for plates (Case 4), as given in Equation 9, where U_{CE} is the shear lag factor for the connected element (similar to A_{n2} used by CSA).

$$U_{CE} = f(l_w, w) = \begin{cases} 1.0 & \text{for } l_w \geq 2w \\ 0.875 & \text{for } 1.5w \leq l_w < 2w \\ 0.75 & \text{for } 1.0w \leq l_w < 1.5w \\ 0.75 \left(\frac{l_w}{w} \right) & \text{for } l_w < w \end{cases} \quad (9)$$

The contribution to the total shear lag effect in the unconnected element, due to out-of-plane effects, may be assumed to be captured using the guidelines of the AISC *Specification* for tension members (Case 2) as given in Equation 10, where U_{OE} is the shear lag factor for the unconnected (out-standing) element(s).

$$U_{OE} = 1 - \frac{\bar{x}}{l_w} \quad (10)$$

The combined effect of Equations 9 and 10 can be approximated as the product of the two component effects as

$$U = U_{CE} U_{OE} = \left(f(l_w, w) \right) \left(1 - \frac{\bar{x}}{l_w} \right) \quad (11)$$

Equation 11 is the method proposed in this paper for combining Cases 2 and 4 of Table D3.1 of the current AISC Specification (2005) for welded connections. This is referred to subsequently as the bi-planar model. As will be discussed later in this paper, two bi-planar models are recommended: the bi-planar (AISC method) model, which uses current AISC provisions for determining the shear lag effect of the connected element, and the bi-planar (beam method), which uses the proposed fixed-fixed beam model to account for the shear lag effect in the connected element.

Evaluating the stepped function of the AISC shear lag model for the four regions defined by Equation 9 results in four shear lag equations as a function of the l_w/w ratio, as given in Equations 12 through 15. Note that current AISC provisions do not permit weld lengths less than the width of the connected element. However, as the following equations are part of the development of the recommendations made in this paper, Equation 15 provides for a strength reduction similar to the CSA provisions for weld lengths in that range.

For weld lengths where $l_w \geq 2w$,

$$U = 1.0 \left(1 - \frac{\bar{x}}{l_w} \right) \quad (12)$$

For weld lengths where $1.5w \leq l_w < 2w$,

$$U = 0.875 \left(1 - \frac{\bar{x}}{l_w} \right) \quad (13)$$

For weld lengths where $1.0w \leq l_w < 1.5w$,

$$U = 0.75 \left(1 - \frac{\bar{x}}{l_w} \right) \quad (14)$$

For weld lengths where $l_w < w$,

$$U = 0.75 \left(\frac{l_w}{w} \right) \left(1 - \frac{\bar{x}}{l_w} \right) \quad (15)$$

Figures 8 and 9 illustrate the shear lag factors that the bi-planar (AISC method) model produces. In these figures, the shear lag factor is plotted against the l_w/w ratio. To produce the plots, an assumption must be made regarding the width of the connected element, w . Widths of 4 and 24 in. were selected, respectively, to cover a range of conditions that illustrate the range of the proposed model. The eccentricity of the connection, \bar{x} , is chosen to range from $\bar{x} = 0$ to $\bar{x} = 16$ in. From $\bar{x} = 0$ to $\bar{x} = 1.00$ in., the eccentricity increases in 8-in. increments. These ranges were chosen to illustrate the difference between relatively narrow connections with large eccentricities to that of relatively wide connections with small eccentricities.

Figure 8 presents the shear lag factors for a 4-in.-wide connection (i.e., $w = 4$ in.). As expected, if the eccentricity of the connection is zero, the member is a flat plate, and the $1 - \bar{x}/l$ term in the bi-planar model is 1.0, leaving the shear lag factor a function of only the l_w/w ratio. As the eccentricity increases slightly, the out-of-plane term decreases from 1.0, reducing the strength of the connection. When the eccentricity is as large as the width of the connection (e.g., $\bar{x} = 4.0$ in.), the strength reduction becomes more severe, penalizing the strength. If the eccentricity is as much as four times the width of the connection (i.e., $\bar{x} = 16$ in.), the connection has no calculable strength regardless of the length of the welds.

Figure 9 presents the shear lag factors for a 24-in.-wide connection (i.e., $w = 24$ in.). As expected, if the eccentricity of the connection is zero, the member is a flat plate, and the $1 - \bar{x}/l$ term in the bi-planar model is 1.0, leaving the shear lag factor a function of only the l_w/w ratio. As the eccentricity increases slightly, the out-of-plane term decreases from 1.0, reducing the strength of the connection. Although the trend of strength reduction for the wide connection is similar to that of the narrow connection shown in Figure 6, the penalty for eccentricity is less severe relative to a narrow connection.

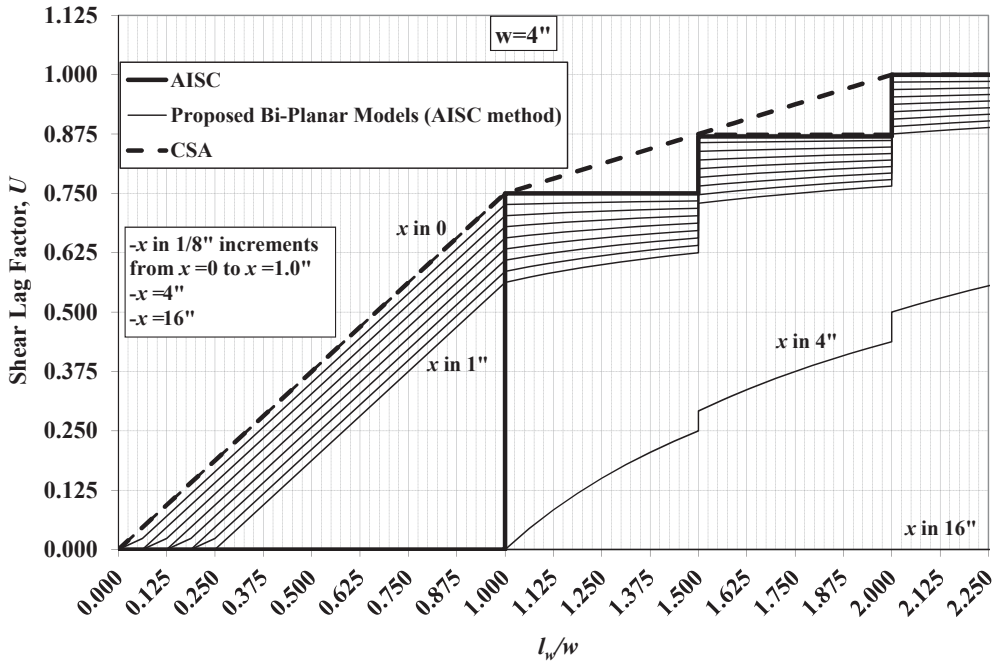


Fig. 8. Comparison of proposed bi-planar model to current AISC model (width of connected element equal to 4 in.).

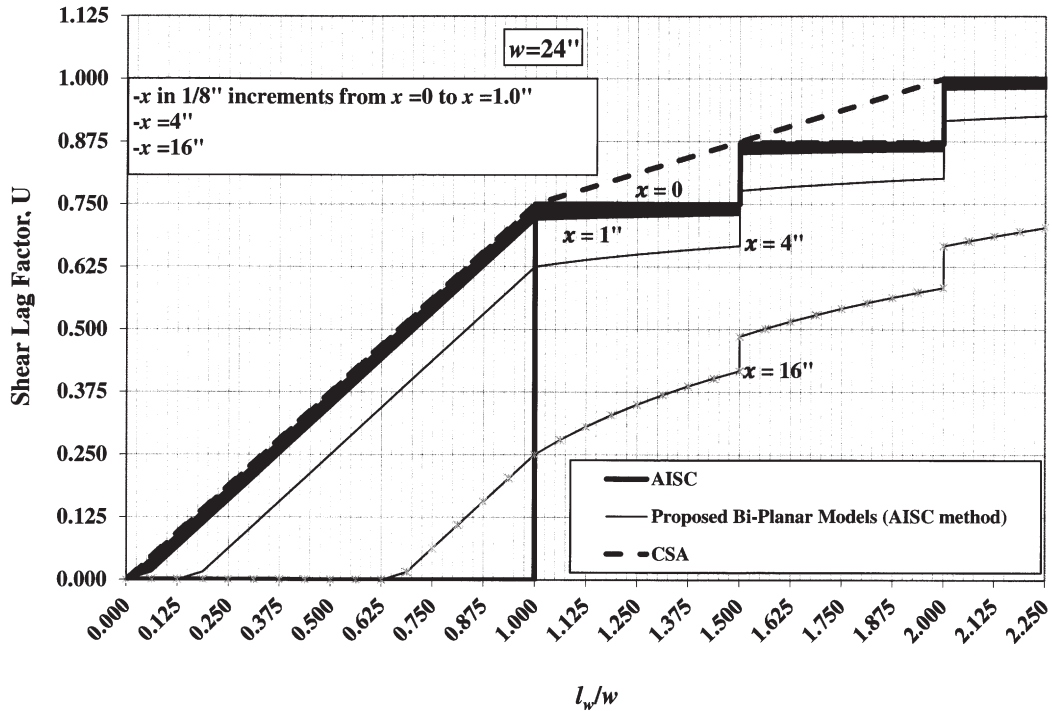


Fig. 9. Comparison of proposed bi-planar model to current AISC model (width of connected element equal to 24 in.).

**Table 3. Comparison of Measured Shear Lag to AISC Requirements
(Bi-Planar Model Using AISC Method for Connected Element)**

Double Angles (Easterling and Giroux)						Single Angles (Gibson and Wake)					
Test	P_{fail}	l_w/W	$\frac{P_{fail}/F_u A_g}{U_{exp}}$	$\frac{U_{plane}}{U_{1-x/l}}$	Bi-Planar Model $\frac{U_{exp}/U_{plane}}{U_{1-x/l}}$ (%)	Test	P_{fail}	$l_w, avg/W$	$\frac{P_{fail}/F_u A_g}{U_{exp}}$	$\frac{U_{plane}}{U_{1-x/l}}$	Bi-Planar Model $\frac{U_{exp}/U_{plane}}{U_{1-x/l}}$ (%)
L-L1	50.0	2.25	0.81	0.89	91.4	1	80.8	1.95	1.28	0.82	163
L-L2	50.5	2.25	0.82	0.89	92.2	2	78.2	1.95	1.23	0.78	157
L-L3	50.4	2.25	0.82	0.89	92.7	3	77.3	1.45	1.22	0.64	189
						4	76.8	1.28	1.21	0.63	192
Double Channels (Easterling and Giroux)						Double Tees (Easterling and Giroux)					
Test	P_{fail}	l_w/W	$\frac{P_{fail}/F_u A_g}{U_{exp}}$	$\frac{U_{plane}}{U_{1-x/l}}$	Bi-Planar Model $\frac{U_{exp}/U_{plane}}{U_{1-x/l}}$ (%)	Test	P_{fail}	$l_w, avg/W$	$\frac{P_{fail}/F_u A_g}{U_{exp}}$	$\frac{U_{plane}}{U_{1-x/l}}$	Bi-Planar Model $\frac{U_{exp}/U_{plane}}{U_{1-x/l}}$ (%)
C-L-1a	79.9 [†]	2.16	0.84	0.93	90.2	T-L-1a	71.7 [†]	1.41	0.55	0.56	97.9
C-L-1b	87.0 [‡]	1.66	0.89	0.68	131	T-L-1b	85.3	1.65	0.80	0.68	118
C-L-2a	85.0 [†]	2.16	0.92	0.93	98.5	T-L-2	85.1 [†]	1.65	0.82	0.68	120
C-L-2b	86.7 [‡]	1.65	0.90	0.68	131	T-L-3	86.5	1.65	0.79	0.68	116
C-L-3a	76.3 [†]	2.16	0.83	0.93	89.4						
C-L-3b	86.9 [‡]	1.65	0.92	0.68	134						

[†] Test stopped due to weld failure.

[‡] Test stopped due to cross-sectional rupture away from connection region.

Similar plots as shown in Figures 8 and 9 were generated to illustrate the strength reduction due to shear lag when the shear lag effect of the connected element is determined using the fixed-fixed beam model. Those plots are shown in Figures 10 and 11. Note that the resulting strength reduction between the two methods is similar. The primary difference is that the bi-planar (beam method) model is simpler to apply due to the continuous function through the l_w/w range. That is, the l_w/w ratio does not need to be evaluated when using the beam method. One other difference is that the beam method requires approximately a 10% strength reduction for weld lengths equal to or greater than $2w$, where the AISC method requires no strength reduction for the same range. Although the beam method is asymptotic to 1.0, the weld length needs to be approximately six times the width of the connected region to mathematically achieve no strength reduction. The mathematical model used for the beam method uses the general equation shown in Equation 11. However, the function $f(l_w, w)$ is computed using Equation 8. Equation 16 gives the bi-planar (beam method) model.

$$U = f(l_w, w) \left(1 - \frac{\bar{x}}{l_w}\right) = \left(\frac{1}{1 + \frac{1}{3} \left(\frac{w}{l_w}\right)^2} \right) \left(1 - \frac{\bar{x}}{l_w}\right) \quad (16)$$

Tables 3 and 4 summarize the comparisons of the experimental shear lag factors to the bi-planar models. The same experimental data as presented in Table 2 is given in this table. However, the percent difference in the experimental data is compared to the shear lag factors computed using the bi-planar models. Referring to Tables 3 and 4, the bi-planar models provide a conservative estimate of strength reduction relative to the current AISC procedure, with the exception of the double angles tested by Easterling and Giroux (1993). Note that because the l_w/w ratio for the double angles is greater than 2.0, the U_{CE} term in the bi-planar models is 1.0. Thus, the uni-planar and bi-planar models yield the same shear lag factor. Figures 12 and 13 present graphical representations of the shear lag comparisons summarized in Tables 3 and 4, respectively.

Of the recommended bi-planar models considered in Tables 3 and 4, the beam method is closer to predicting the failure load than is the AISC method, except for one case (T-L-1a). Considering the 17 tests listed in Tables 3 and 4, the

AISC method of Table 3 results in an average $\frac{U_{exp}}{U_{plane} U_{1-x/l}}$

of 124%, whereas the beam method of Table 4 results in an

**Table 4. Comparison of Measured Shear Lag to AISC Requirements
(Bi-Planar Model Using Fixed-Fixed Beam Method for Connected Element)**

Double Angles (Easterling and Giroux)						Single Angles (Gibson and Wake)					
Test	P_{fail}	l_w/W	$P_{fail}/F_u A_g$ U_{exp}	U_{plane} $U_{1-x/l}$	Bi-Planar Model U_{exp}/U_{plane} $U_{1-x/l}$ (%)	Test	P_{fail}	$l_w, avg/W$	$P_{fail}/F_u A_g$ U_{exp}	U_{plane} $U_{1-x/l}$	Bi-Planar Model U_{exp}/U_{plane} $U_{1-x/l}$ (%)
L-L1	50.0	2.25	0.81	0.83	97.5	1	80.8	1.95	1.28	0.82	155
L-L2	50.5	2.25	0.82	0.83	98.3	2	78.2	1.95	1.23	0.78	157
L-L3	50.4	2.25	0.82	0.83	98.8	3	77.3	1.45	1.22	0.64	189
						4	76.8	1.28	1.21	0.63	192
Double Channels (Easterling and Giroux)						Double Tees (Easterling and Giroux)					
Test	P_{fail}	l_w/W	$P_{fail}/F_u A_g$ U_{exp}	U_{plane} $U_{1-x/l}$	Bi-Planar Model U_{exp}/U_{plane} $U_{1-x/l}$ (%)	Test	P_{fail}	$l_w, avg/W$	$P_{fail}/F_u A_g$ U_{exp}	U_{plane} $U_{1-x/l}$	Bi-Planar Model U_{exp}/U_{plane} $U_{1-x/l}$ (%)
C-L-1a	†79.9	2.16	0.84	0.87	96.6	T-L-1a	†71.7	1.41	0.55	0.64	85.8
C-L-1b	‡87.0	1.66	0.89	0.81	110	T-L-1b	85.3	1.65	0.80	0.81	99.4
C-L-2a	†85.0	2.16	0.92	0.87	106	T-L-2	†85.1	1.65	0.82	0.81	101
C-L-2b	‡86.7	1.65	0.90	0.81	110	T-L-3	86.5	1.65	0.79	0.81	97.9
C-L-3a	†76.3	2.16	0.83	0.87	95.8						
C-L-3b	‡86.9	1.65	0.92	0.81	113						

† Test stopped due to weld failure.

‡ Test stopped due to cross-sectional rupture away from connection region.

average $\frac{U_{exp}}{U_{plane} U_{1-x/l}}$ of 115%, an improvement in prediction accuracy of 7.8%.

Wide Flange Shapes

Although reports of experimental studies investigating welded connections of wide flange tension members were not able to be found, the bi-planar shear lag models can be easily adopted. Where only the flanges or web of a W-shape are connected with longitudinal welds, the U_{CE} term can be determined based on the length of the welds, and the U_{OE} term computed by considering the eccentricity of the shape's corresponding T-shape (see Case 2 of Table D3.1 in the AISC *Specification*).

SUMMARY

The objective of this work was to develop a generalized procedure for computing shear lag in plate, angle, channel and tee members connected with longitudinal welds. The procedure was to include consideration of connections with welds lengths less than the distance between them and where unequal weld lengths are permitted. Of the three research projects presented, only the SSWC project considered weld lengths less than the distance between them; a total of 86 specimens were evaluated. A large majority of

the experimental strengths are larger than the strengths using the CSA procedure. In regard to unequal weld lengths, only four specimens were tested (Gibson and Wake). The experimental results have significant variation, as can be seen in Figure 14. Although both the AISC and CSA appear to capture average test result values, AISC's stepped model better captures the experimental results. This is especially true for l_w/w ratios greater than 1.0.

Two analytical uni-planar models were investigated: the effective width model and the fixed-fixed beam model. The effective width model is identical to the CSA procedure, and unlike the AISC procedure, includes l_w/w ratios less than 1.0. The fixed-fixed beam model correlates very well with the CSA procedure up to $l_w/w = 1.5$ and is conservative beyond ratios greater than 1.5. However, it is important to recognize that these two models consider only shear lag within the plane of the connected element, and therefore are only appropriate for flat plate tension members.

The bi-planar models can be used in a general sense regardless of the type of tension member discussed in this paper. For typical connection widths and out-of-plane eccentricities, the bi-planar model is somewhat conservative but has the advantage of easy adoption for flat plate, angle, channel or tee tension members. The current AISC procedure does not account for bi-planar effects of shear lag in welded connected elements of angle, channel, wide flange and tee tension members. Not accounting for the bi-planar

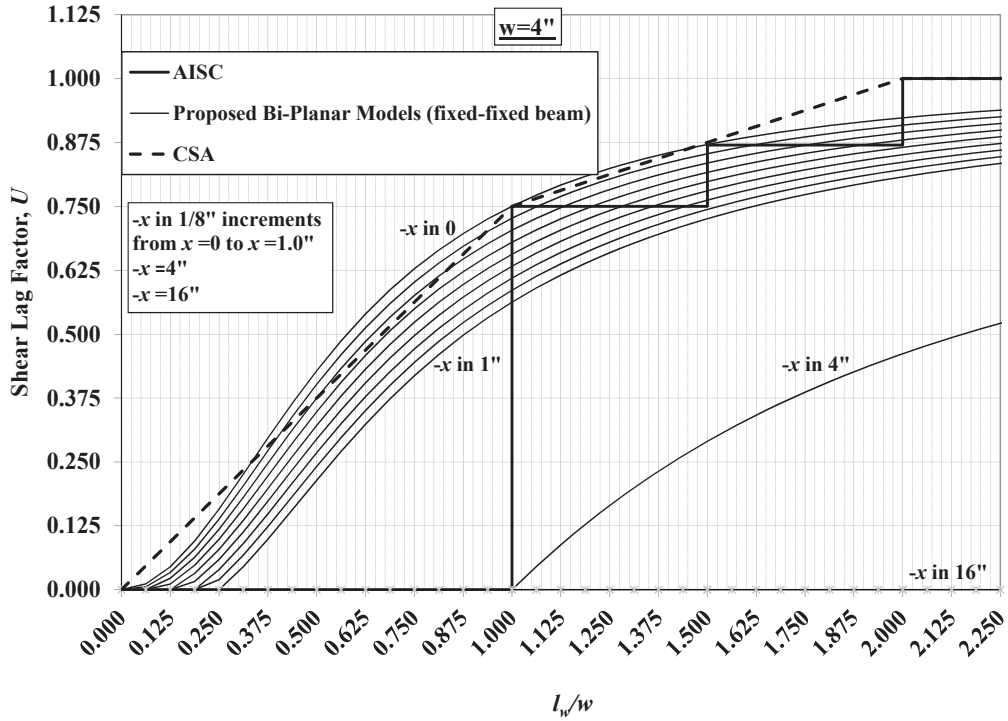


Fig. 10. Comparison of proposed beam bi-planar model to current AISC model (width of connected element equal to 4 in.).

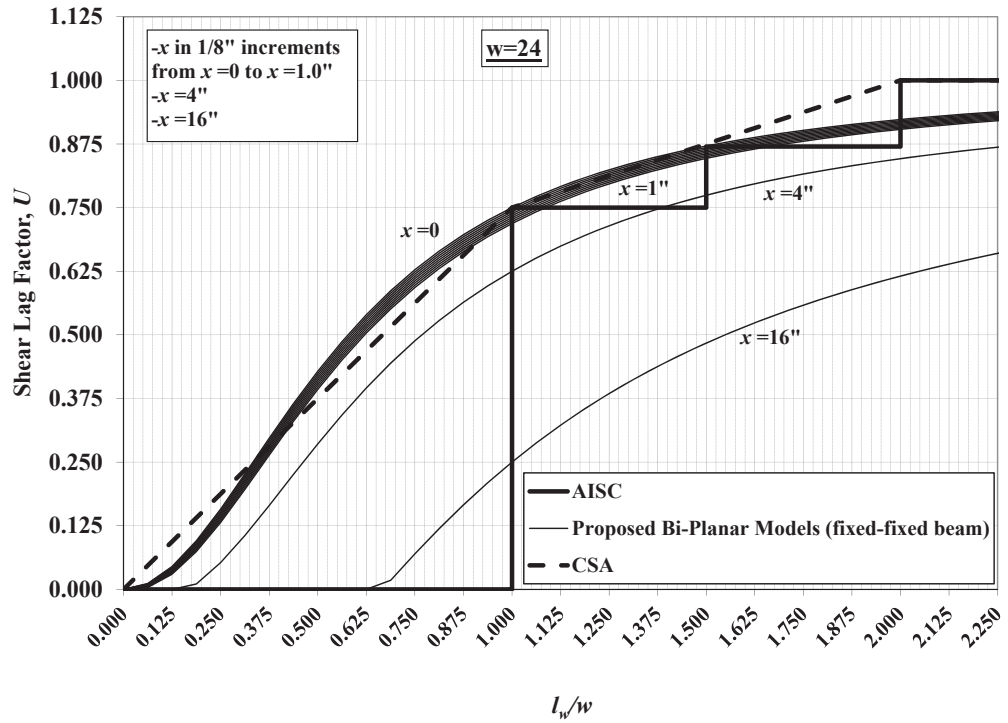


Fig. 11. Comparison of proposed beam bi-planar model to current AISC model (width of connected element equal to 24 in.).

affect tends to overestimate the connection strength relative to the experimental results presented.

RECOMMENDATIONS

Recommendation No. 1: The bi-planar model using stepped functions for the connected element as currently used by AISC.

The following are recommendations for revisions of AISC 360-10 regarding shear lag in longitudinally welded tension members,

1. Recommended changes to Table D3.1 of the AISC *Specification*:

Replace the description for Case 2 with the following:

“All tension members, except HSS, where the tension load is transmitted to some but not all of the cross-sectional elements by fasteners. Alternatively, Case 7 may be used for W, M, S, and HP shapes.”

Replace Case 4 with that shown in Figure 15.

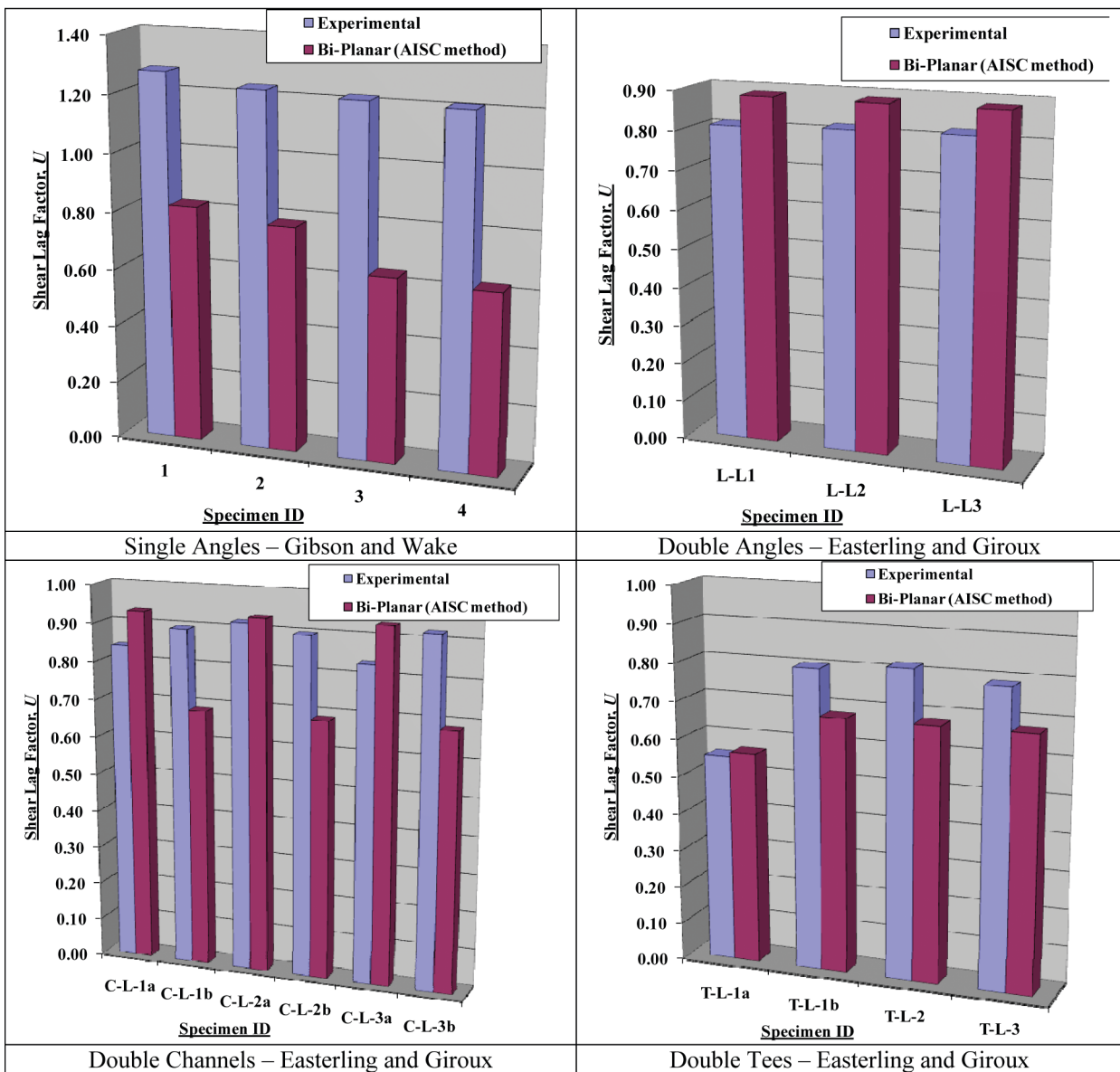


Fig. 12. Comparison of measured shear lag to proposed bi-planar model using AISC method for connected element.

- Remove the portion of *Specification* paragraph J2.2(b) that states, “If longitudinal fillet welds are used alone in end connections of flat-bar tension members, the length of each fillet weld shall not be less than the perpendicular distance between them.”
- Remove the fourth paragraph of Commentary to J2.2(b), which states that the length of longitudinal fillet welds must be equal to or greater than the distance between them.

Recommendation No. 2: The bi-planar model using the continuous fixed-fixed beam model for the connected element. This recommendation is the same as Recommendation

No. 1, with the exception that Case 4 is replaced with that shown in Figure 16.

EXAMPLE PROBLEM — UNEQUAL LENGTH WELDS AND UNCONNECTED ELEMENTS

The following is an example evaluation of a skewed angle, used as a web member of a truss, connected to the truss chord using unequal length welds. First, assume that the internal member is a 2-L4×4×2; and second, assume the internal member is back-to-back 4-in.-wide by ½-in.-thick flat bars. Compute the shear lag factor using

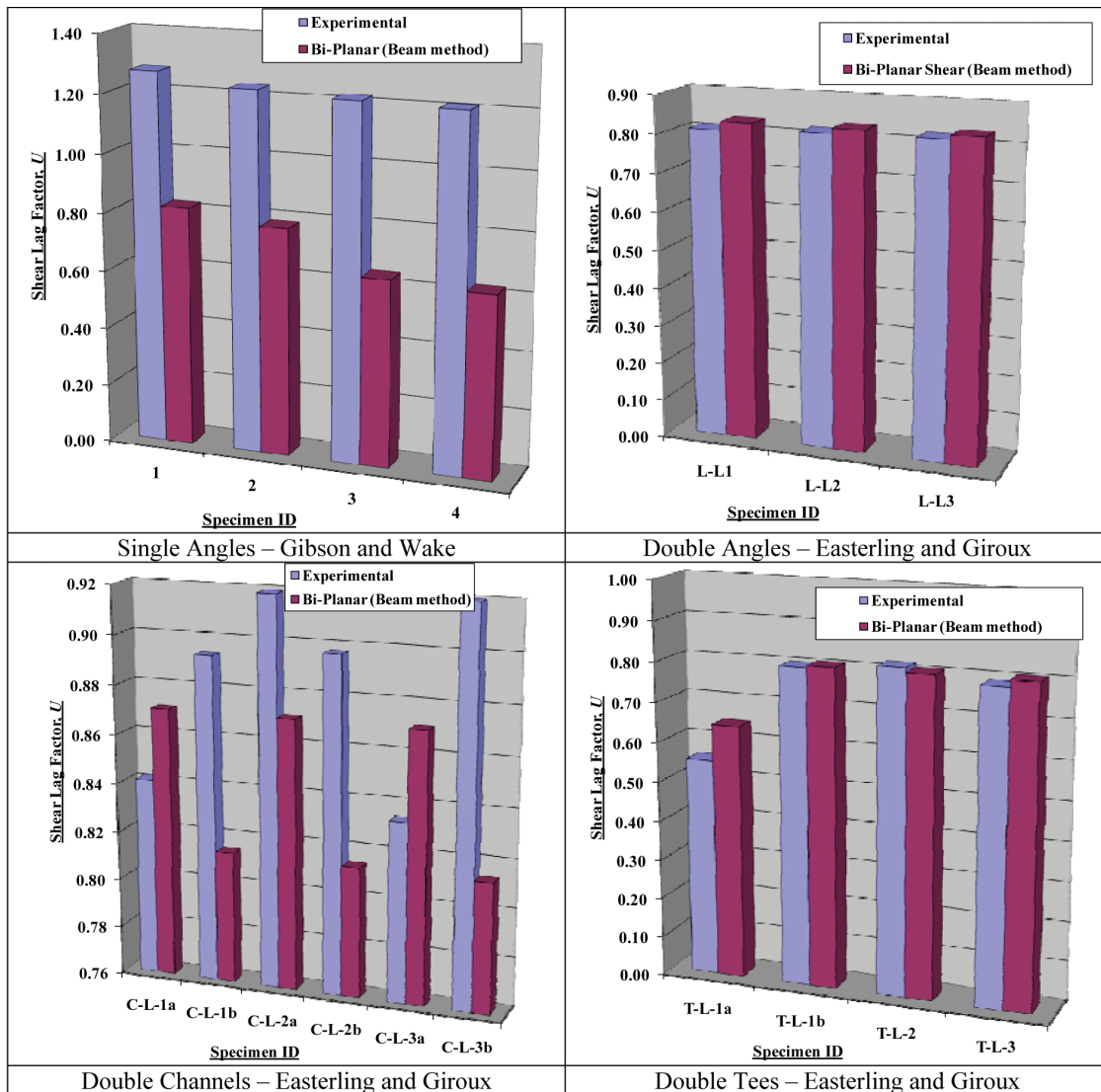


Fig. 13. Comparison of measured shear lag to proposed bi-planar model using beam method for connected element.

1. The current specified AISC procedure.
2. The current practice AISC procedure
3. The current CSA procedure.
4. The procedure as given in Recommendation No. 1.
5. The procedure as given in Recommendation No. 2.

Figure 17 shows the connection details. Given for a L4×4×2:
 $\bar{x} = 1.18$ in.

Although the following example demonstrates the procedure for a plate and angle member, the procedure can be easily applied to channels and WT sections where not all of the elements of the member are connected (with perpendicular or skewed orientation). Furthermore, this example problem illustrates the procedure considering unequal length welds, having a weld length less than the distance perpendicular to the line of the welds.

Double Angles

Part 1: Current Specified AISC Procedure

This connection is not permitted. Therefore, $U = 0$.

Part 2: Current Practice AISC Procedure

The current AISC procedure requires Case 2 be used to compute the shear lag factor, U . However, unequal length welds are not addressed currently nor is the in-plane effect. Because there are no guidelines currently, the length of the connection, l , will be taken as the average weld length ($l = 5.00$ in.), because this is what would probably be assumed in practice. Neglecting that one of the weld lengths is less than the width of the connected part, and therefore, would not be permitted using current procedures,

$$U = 1 - \frac{1.18 \text{ in.}}{5.00 \text{ in.}} = 0.764$$

Part 3: Current CSA Procedure

The portion of the shear lag accounted for in the connected leg of the angle is:

$$l = \frac{3.00 \text{ in.} + 7.00 \text{ in.}}{2} = 5.00 \text{ in.}$$

$$2w = 2(4.00 \text{ in.}) = 8.00 \text{ in.} > 5.00 \text{ in.}$$

$$w = 4.00 \text{ in.} < 5.00 \text{ in.}$$

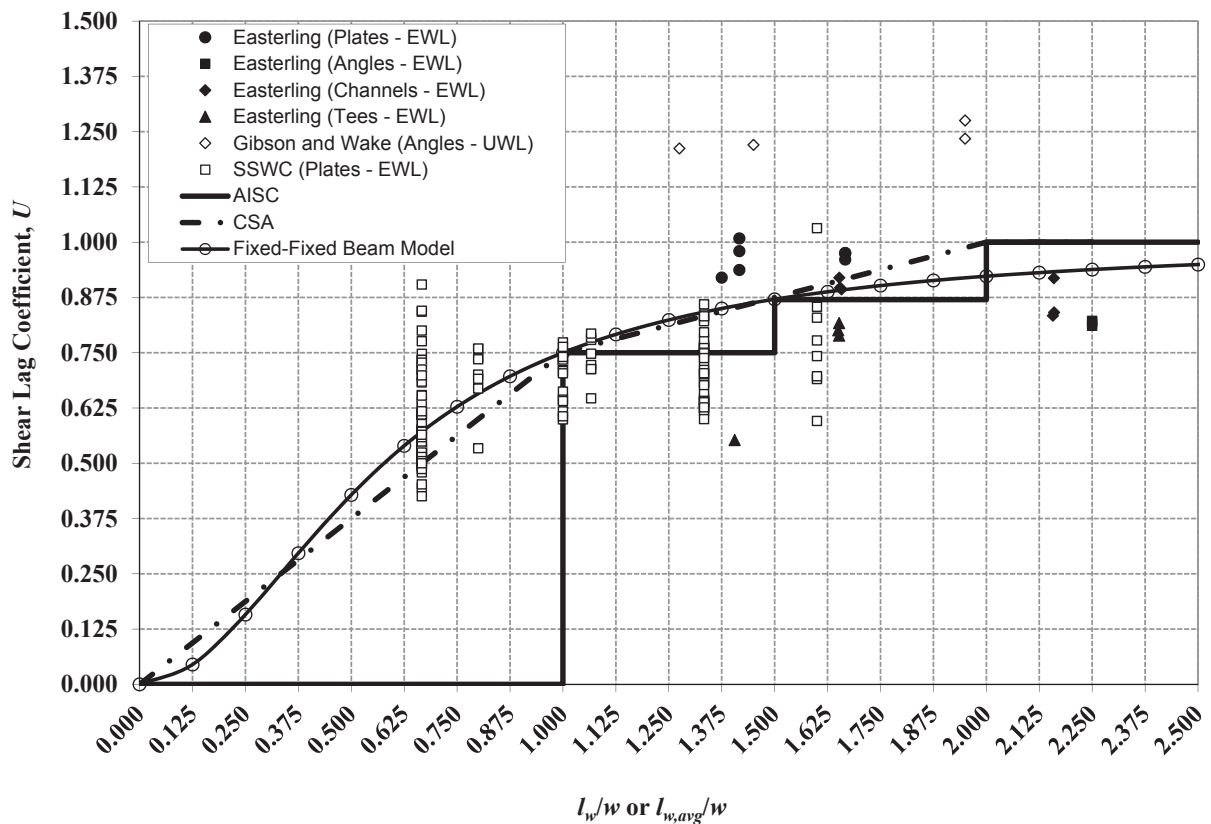


Fig. 14. Comparison of fixed-fixed beam model to current design models and experimental data.

Because l is less than $2w$ but greater than w ,

$$\begin{aligned} A_{n2} &= 0.5wt + 0.25Lt \\ &= (0.5)(4.00 \text{ in.})(0.500 \text{ in.}) \\ &\quad + (0.25)(5.00 \text{ in.})(0.500 \text{ in.}) \\ &= 1.63 \text{ in.}^2 \end{aligned}$$

The portion of the shear lag accounted for in the unconnected (or outstanding) leg of the angle is:

$$\begin{aligned} A_{n3} &= wt \left(1 - \frac{\bar{x}}{l} \right) \\ \bar{x} &= 0.500 \text{ in.} + \left(\frac{4.00 \text{ in.} - 0.5 \text{ in.}}{2} \right) \\ &= 2.25 \text{ in.} \\ A_{n3} &= (4.00 \text{ in.} - 0.500 \text{ in.})(0.500 \text{ in.}) \left(1 - \frac{2.25 \text{ in.}}{5.00 \text{ in.}} \right) \\ &= 0.963 \text{ in.}^2 \end{aligned}$$

Taking a shear lag factor, U , which is not used in the CSA

treatment, as the sum of the cross-sectional areas of the elements divided by the gross area of the member,

$$U = \frac{A_{n2} + A_{n3}}{A_g} = \frac{1.63 \text{ in.}^2 + 0.963 \text{ in.}^2}{3.75 \text{ in.}^2} = 0.691$$

Part 4: Recommendation No. 1

This recommended procedure takes into account shear lag in both planes, as well as explicit treatment of the unequal weld lengths, and weld lengths less than w .

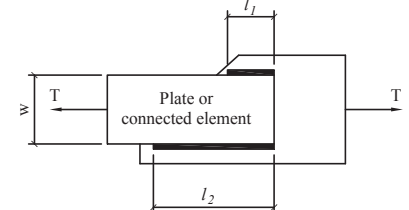
$$U = U_{CE} \left(1 - \frac{\bar{x}}{l} \right)$$

$$l_{avg} = \frac{7.00 \text{ in.} + 3.00 \text{ in.}}{2} = 5.00 \text{ in.}$$

$$\frac{l}{w} = \frac{5.00 \text{ in.}}{4.00 \text{ in.}} = 1.25 \quad \therefore U_{CE} = 0.75$$

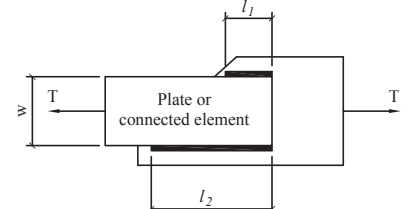
$$U_{OE} = 1 - \frac{\bar{x}}{l} = 1 - \frac{1.18 \text{ in.}}{5.00 \text{ in.}} = 0.764$$

$$U = U_{CE}U_{OE} = (0.75)(0.764) = 0.573$$

4^x	Plates; and angles, channels, tees, and W shapes with connected elements; where the tension load is transmitted by longitudinal welds only	$U = U_{CE} \left(1 - \frac{\bar{x}}{l} \right)$ $l \geq 2w \dots \dots \dots U_{CE} = 1.0$ $2w > l \geq 1.5w \dots U_{CE} = 0.87$ $1.5w > l \geq w \dots \dots U_{CE} = 0.75$ $w > l \dots \dots \dots U_{CE} = 0.75l/w$	
-------	--	--	--

^xWeld lengths l_1 and l_2 must be non-zero, $(l_1, l_2)_{\min} = 4$ times weld size; where $l_1 = l_2$, $l = l_1 = l_2$; where $l_1 \neq l_2$, $l = \frac{l_1 + l_2}{2}$.

Fig. 15. Recommended revision to Table D3.1 (Recommendation No. 1)

4^x	Plates; and angles, channels, tees, and W shapes with connected elements; where the tension load is transmitted by longitudinal welds only	$U = U_{CE} \left(1 - \frac{\bar{x}}{l} \right)$ $U_{CE} = \frac{1}{1 + \frac{1}{3} \left(\frac{w}{l} \right)^2}$	
-------	--	---	--

^xWeld lengths l_1 and l_2 must be non-zero, $(l_1, l_2)_{\min} = 4$ times weld size; where $l_1 = l_2$, $l = l_1 = l_2$; where $l_1 \neq l_2$, $l = \frac{l_1 + l_2}{2}$.

Fig. 16. Recommended revision to Table D3.1 (Recommendation No. 2).

Part 5: Recommendation No. 2

This recommended procedure takes into account shear lag in both planes, as well as explicit treatment of the unequal weld lengths, and weld lengths less than w .

$$\begin{aligned}
 U &= U_{CE} \left(1 - \frac{\bar{x}}{l} \right) \\
 &= \left(\frac{1}{1 + \frac{1}{3} \left(\frac{w}{l} \right)^2} \right) \left(1 - \frac{\bar{x}}{l} \right) \\
 &= \left(\frac{1}{1 + \frac{1}{3} \left(\frac{4.00 \text{ in.}}{5.00 \text{ in.}} \right)^2} \right) \left(1 - \frac{1.18 \text{ in.}}{5.00 \text{ in.}} \right) \\
 &= 0.630
 \end{aligned}$$

Flat Plates

Part 1: Current Specified AISC Procedure

This connection is not permitted. Therefore, $U = 0$.

Part 2: Current Practice AISC Procedure

The current AISC procedure requires Case 4 be used to compute the shear lag factor, U . However, unequal length welds are not addressed currently, so the length of the connection,

l , will be taken as the average weld length ($l = 5.0$ in.), because this is what would probably be assumed in practice. Neglecting that one of the weld lengths is less than the width of the connected part, and therefore, would not be permitted using current procedures:

$$\begin{aligned}
 \frac{l}{w} &= \frac{5.00 \text{ in.}}{4.00 \text{ in.}} = 1.25 \\
 \therefore U &= 0.75
 \end{aligned}$$

Part 3: Current CSA Procedure

Because $l = 5$ in. is between w and $2w$,

$$\begin{aligned}
 A_2 &= 0.5wt + 0.25Lt \\
 &= (0.5)(4.00 \text{ in.})(0.500 \text{ in.}) \\
 &\quad + (0.25)(5.00 \text{ in.})(0.500 \text{ in.}) \\
 &= 1.63 \text{ in.}^2
 \end{aligned}$$

Taking a shear lag factor, U , which is not used in the CSA treatment, as the ratio of A_{n2} divided by the gross cross-sectional area of the plate,

$$U = \frac{A_{n2}}{A_g} = \frac{1.63 \text{ in.}^2}{(4.00 \text{ in.})(0.500 \text{ in.})} = 0.815$$

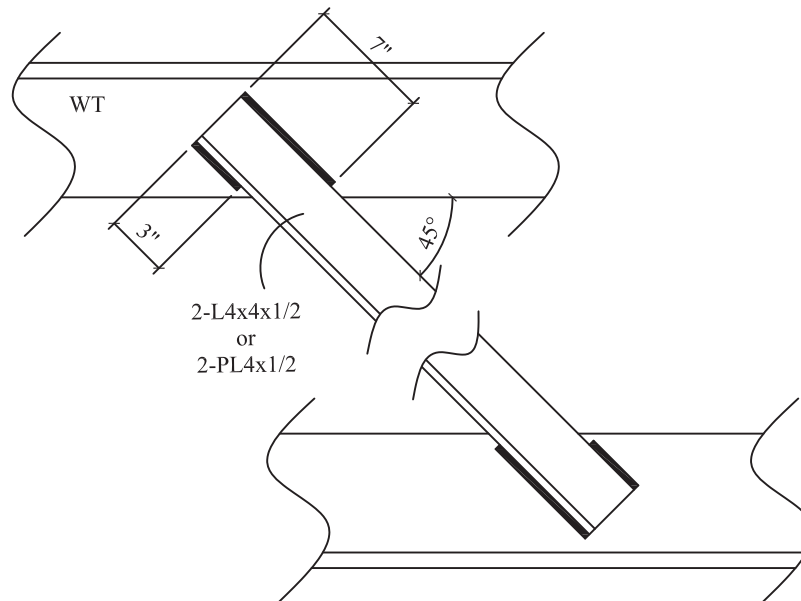


Fig. 17. End connection illustration for example problem.

Table 5. Summary of Example Problem Results

Member	Current Specified AISC Procedure ^a (Part 1)	Current Practice AISC Procedure ^b (Part 2)	Current CSA Procedure (Part 3)	Recommendation No. 1 (AISC Method) (Part 4)	Recommendation No. 2 (Beam Method) (Part 5)
Double angle	0	0.76	0.69	0.57	0.63
Flat plate	0	0.75	0.81	0.75	0.82

^a The current AISC provisions do not allow for unequal weld lengths. Additionally, one of the welds is only 3 in. long, which is less than the width of the connected element. Therefore, the connection would have to be considered as having no strength.

^b The shear lag factors shown for this category neglect that AISC provisions do not currently permit unequal weld lengths. The weld length is taken as the average of the lengths of the two longitudinal welds.

Part 4: Recommendation No. 1 [Bi-Planar (AISC Method)]

The recommended procedure takes into account shear lag in both planes, as well as explicit treatment of the unequal weld lengths and weld lengths less than w . In the case of a plate,

$\bar{x} = 0$, so the $1 - \frac{\bar{x}}{l}$ term is 1.0.

$$U = U_{CE} \left(1 - \frac{\bar{x}}{l} \right) = U_{CE}$$

$$l_{avg} = \frac{7.00 \text{ in.} + 3.00 \text{ in.}}{2} = 5.00 \text{ in.}$$

$$\frac{l}{w} = \frac{5.00 \text{ in.}}{4.00 \text{ in.}} = 1.25 \quad \therefore U_{CE} = 0.75$$

$$U = U_{CE} = 0.75$$

Part 5: Recommendation No. 2 [Bi-Planar (Beam Method)]

$$U = \frac{1}{1 + \frac{1}{3} \left(\frac{4.00 \text{ in.}}{5.00 \text{ in.}} \right)^2} = 0.824$$

Table 5 summarizes the results of the example problem. Note that because the parameters of the example problem are not currently addressed by the AISC procedure, assumptions regarding connection length were required. Without the assumptions (ignoring that the 3-in. length is less than the width of the angle leg and using the average weld length

of 5 in.), the current specified AISC procedure (Part 1 of the example problems above) yields no estimated strength. The bi-planar (AISC method) model is more conservative than that of the bi-planar (beam method). It is worth considering that although the bi-planar (beam method) is less than conservative than the bi-planar (AISC method), the beam method has better correlation with the experimental data and the CSA model.

Also note that the current AISC procedure and the bi-planar (AISC method) procedure give the same shear lag factor for the plate. This is expected, considering that there is no out-of-plane eccentricity in the plate (i.e., the $(1 - \bar{x}/l)$ term is zero).

REFERENCES

AISC (2010), *Specification for Structural Steel Buildings*, American Institute of Steel Construction, Chicago, IL.

American Bureau of Welding (1931), "Report of Structural Steel Welding Society," American Welding Society, New York, NY.

Canadian Standards Association (2009), "Design of Steel Structures," CSA-S16, Rexdale, Ontario, Canada.

Easterling, W.S. and Giroux-Gonzalez, L. (1993), "Shear Lag Effects in Steel Tension Members," *Engineering Journal*, American Institute of Steel Construction, Third Quarter, pp. 77-88.

Gibson G.J. and Wake, B.T. (1942). "An Investigation of Welded Connections for Angle Tension Members," *Welding Journal*, Vol. 21, No. 1, pp. 44-49.

Mechanical Properties of ASTM A992 Steel After Fire

JINWOO LEE, MICHAEL D. ENGELHARDT and ERIC M. TALEFF

ABSTRACT

When evaluating the condition and safety of a steel structure following a fire, an issue of concern is the mechanical properties of the steel after the fire. The exposure of the steel to high temperatures during the fire, and the subsequent cooling of the steel after the fire, can potentially affect the mechanical properties of the steel. A testing program was undertaken to measure the mechanical properties of ASTM A992 steel after being subjected to various patterns of heating and cooling. This paper presents results of the test program and provides data on the effect of various heating and cooling cycles on key mechanical properties, including yield strength, tensile strength, elastic modulus, elongation, Charpy V-Notch (CVN) impact values and hardness.

Keywords: fire, mechanical properties, steel, ASTM A992.

INTRODUCTION

When a structure has been exposed to fire, an issue of concern following the fire is evaluating the safety of the structure and the need for repairs (Gosain et al., 2008; Tide, 1998). In the case of a steel structure, questions arise on the effect that the exposure to heating and cooling may have had on the mechanical properties of the structural steel. Limited past studies have addressed the post-fire mechanical properties of structural steel (Smith et al., 1981; Outinen and Makelainen, 2004), whereas other studies have examined the effects of various cooling rates from a more fundamental metallurgical and microstructure point of view (Davis and King, 1993; Dhua et al., 2003; Pyshmintsev et al., 2008). However, the available experimental data pertinent to post-fire evaluation of structural steel are limited. Further, a review of the literature suggests there are no data available on the effects of heating and cooling on the mechanical properties of ASTM A992 steel, which is currently the most common structural steel used for rolled wide flange shapes in the United States. To address the need for such data, the authors conducted an extensive series of tests on A992 steel to help engineers assess the post-fire mechanical properties of this material. More complete details of this investigation will be reported in an upcoming publication by Lee (2012).

Jinwoo Lee, P.E., Ph.D. candidate, Department of Civil, Architectural and Environmental Engineering, University of Texas at Austin, Austin, TX. E-mail: jinwoo@mail.utexas.edu

Michael D. Engelhardt, Ph.D., P.E., Dewitt C. Greer Centennial Professor, Department of Civil, Architectural and Environmental Engineering, University of Texas at Austin, Austin, TX (corresponding author). E-mail: mde@mail.utexas.edu

Eric M. Taleff, Ph.D., Professor, Department of Mechanical Engineering, University of Texas at Austin, Austin, TX. E-mail: taleff@mail.utexas.edu

TEST PROGRAM

Material Samples

For the purposes of this study, a series of coupons were prepared as shown in Figure 1. The coupons were made from material taken from the web of a W30×99 shape of ASTM A992 steel. The longitudinal dimension of the coupon corresponded with the longitudinal axis of the member, i.e., along the rolling direction. Room temperature tension tests on this material prior to heating and cooling showed $F_y = 52$ ksi for yield strength and $F_u = 66$ ksi for tensile strength. The results of a chemical analysis of the steel are shown in Table 1. Two different lengths of coupons were made for testing; 14 in. and 18 in. The longer coupons were used to extract samples for Charpy V-Notch testing.

Heating

The coupons were heated in an ATS (Applied Test Systems) 3160 electric furnace. The basic heating system is shown in Figure 2, including the furnace, the furnace controller, and the data acquisition system for recording temperatures. The coupons were hung from the top of the furnace using wire and were thus surrounded by air on all sides. The temperature of the coupons was measured using K-type thermocouple wire. The thermocouple wire was wrapped around the center portion of the coupon and covered with stainless steel foil to minimize radiation effects of the furnace heating coils on the thermocouple. Most of coupons were heated up to the target temperature within a half-hour and then held at that target temperature for one hour. Coupons were heated to target temperatures that ranged from 200 to 1,000 °C, in increments of 100 °C. In this paper, all temperatures are reported in the Celsius scale ($t^{\circ}\text{F} = 1.8 \times t^{\circ}\text{C} + 32$).

Table 1. Chemical Composition of the Test Material											
Element	C	Si	Mn	P	S	Cr	Mo	Ni	V	Al	Cu
Weight (%)	0.079	0.20	0.97	0.014	0.024	0.09	0.026	0.13	0.027	0.001	0.38

Cooling

The actual cooling rates for structural steel after a fire can depend on a number of factors, including the cooling rate of the fire itself, whether or not the steel is insulated, whether or not the steel is exposed to water from fire-fighting operations or sprinklers, and others. Three different cooling methods were used for the test coupons in an attempt to provide a range of cooling rates that might reasonably bracket realistic conditions. The three cooling methods are referred to as cooled-in-blanket (CIB), cooled-in-air (CIA) and cooled-in-water (CIW). Figure 3 shows photos of coupons being cooled by these methods. The CIB method provided the slowest cooling. For this method, the coupon was wrapped in a ceramic fiber blanket after removal from the furnace and allowed to cool to room temperature. For the CIA method, the coupon was removed from the furnace and allowed to cool to room temperature while exposed to ambient air. For the CIW method, the coupon was removed

from the furnace and placed in a container of water for very rapid cooling. The time required for the coupons at 1,000 °C to return to room temperature was on the order of 14 hours for CIB, 4 hours for CIA and 1 minute for CIW. The actual cooling rates were monitored for each coupon. Typical cooling data are shown in Figure 4. Figure 4a plots temperature versus time for both the heating and cooling of the coupons heated to 1,000 °C. All three cooling methods are shown in the plot. Figure 4b shows the cooling rate (in °C/min) for coupons heated to various temperatures and then cooled by the CIB method. The actual cooling rate varied over time for each cooling method. An example of cooling rates measured 1-minute after removal of the coupon from the furnace for the CIA and CIB methods is given in Table 2.

Cleaning

After the heating and cooling process, a number of the coupons had a significant amount of scale and corrosion. To

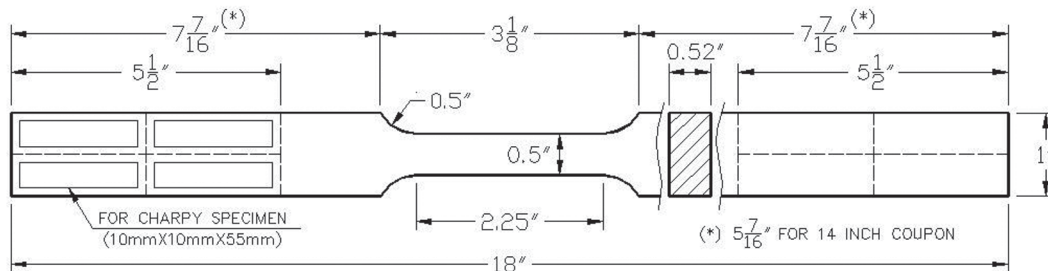


Fig. 1. Coupon dimensions.

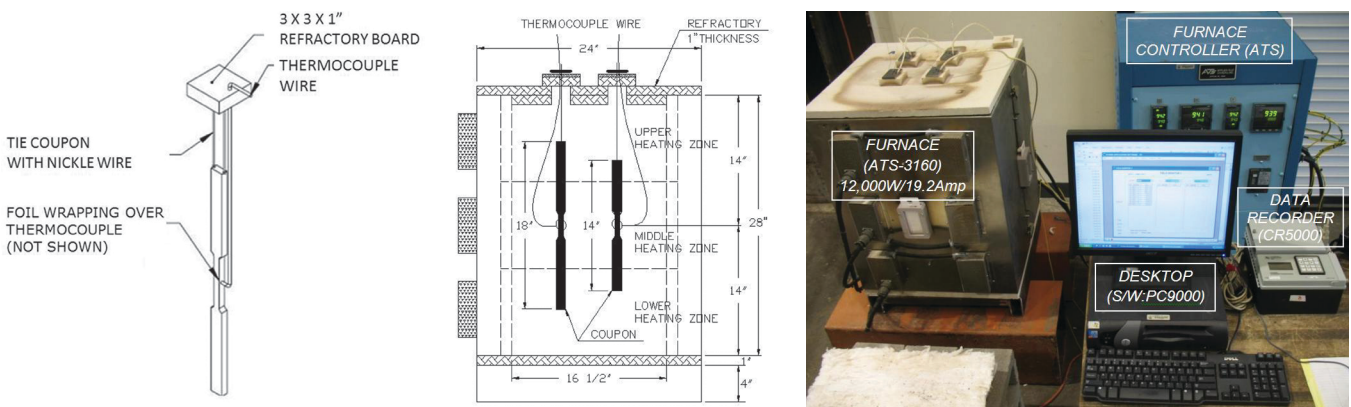
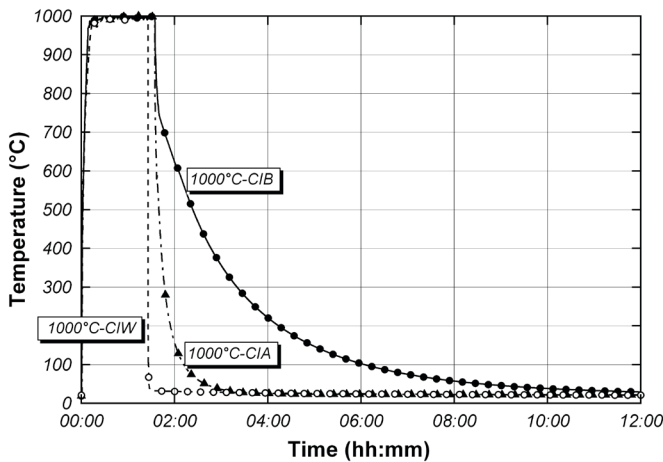


Fig. 2. Coupon heating system.

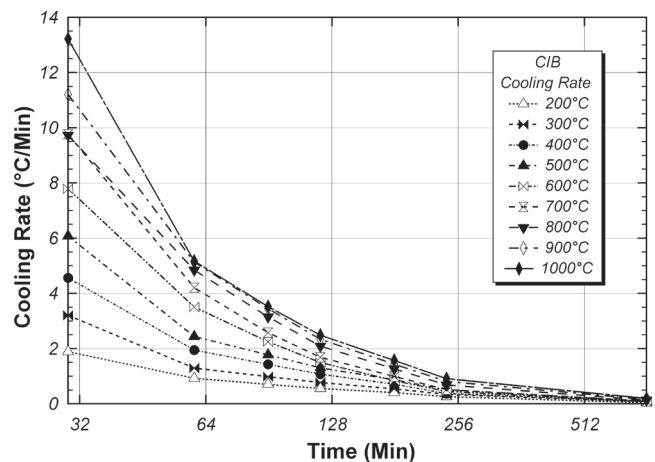
Table 2. Measured Cooling Rates 1-Minute After Removal from Furnace										
Temp (°C)	CIA (°C/Min)					CIB (°C/Min)				
	0~30	60	90	120	180	0~30	60	90	120	180
200	4.48	0.97	0.32	0.13	0.04	1.89	0.93	0.70	0.56	0.41
300	7.26	1.46	0.36	0.14	0.05	3.21	1.30	0.99	0.77	0.55
400	10.49	1.61	0.39	0.09	0.01	4.57	1.95	1.43	1.07	0.71
500	13.32	1.88	0.55	0.19	0.05	6.08	2.44	1.77	1.30	0.87
600	16.87	1.83	0.37	0.1	0.02	7.79	3.51	2.25	1.50	0.84
700	19.28	2.27	0.64	0.23	0.07	9.77	4.21	2.58	1.69	1.00
800	22.62	2.27	0.62	0.18	0.04	9.73	4.85	3.15	2.09	1.27
900	25.05	2.95	0.75	0.23	0.06	11.21	5.14	3.45	2.34	1.44
1,000	28.97	2.52	0.70	0.24	0.06	13.22	5.17	3.52	2.49	1.57



Fig. 3. Cooled-in-air (CIA), cooled-in-blanket (CIB) and cooled-in-water (CIW).



(a) Temperature vs. Time for 1,000 °C coupons



(b) Cooling Rate vs. Time for CIB coupons

Fig. 4. Typical temperature data.

allow for accurate measurement of cross-section area and for secure attachment of the extensometer, the coupons were cleaned with a wire brush grinder prior to testing. Figure 5 shows photos of typical coupons before and after cleaning.

Testing

After heating, cooling and cleaning, tensile tests were performed on the coupons using an MTS 810, 22-kip capacity, computer-controlled, test machine. Coupons were loaded with displacement control at a cross-head rate of 0.01 in. per minute. The strain was measured with a 2-in. gage length MTS extensometer. Charpy V-Notch tests as well as hardness tests were also conducted.

TEST RESULTS

Stress-Strain Curves

Figures 6 through 11 show the measured stress strain curves for all coupons for each type of cooling. The temperatures shown in these plots indicate the temperature to which the

coupon was heated (and held for 1-hour) prior to cooling. The full stress-strain curves are shown as well as the initial portion of the curves up to 1% strain. Each plot also shows the virgin stress-strain curve at 20 °C, which was for the coupon not subjected to heating and cooling. The full stress-strain curves are replotted in Figures 12 through 20 according to the heating temperature of the coupon. The virgin stress-strain curve for unheated steel is again also plotted for comparison. Note that for the CIA and CIB cooling methods, the coupons were heated to temperatures varying from 200 to 1,000 °C in increments of 100 °C. For the CIW cooling method, the coupons were heated to temperatures varying from 500 to 1,000 °C in increments of 100 °C. These data show that for heating temperatures up to about 500 °C, the stress-strain curves for the heated and cooled coupons are very similar to the virgin unheated coupon for all cooling methods. However, for heating temperatures of 600° C and above, some changes from the virgin coupon become somewhat more noticeable. For the heating range of 600 to 1,000 °C, the CIA and CIB coupons show some reduction in yield and tensile strength. The stress-strain curves, however,



Fig. 5. Coupons before and after cleaning.

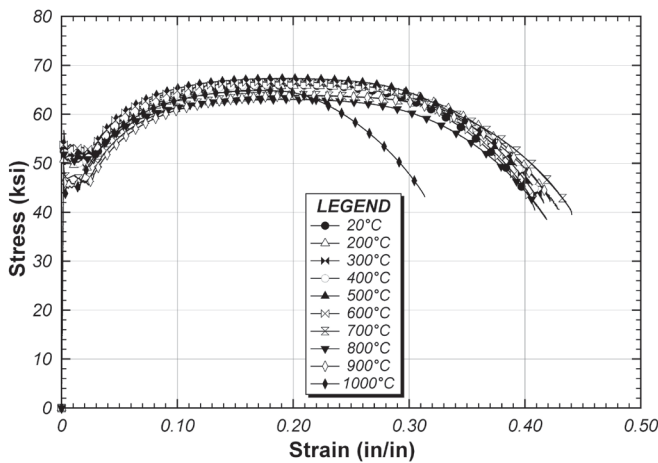


Fig. 6. CIA full stress-strain curves.

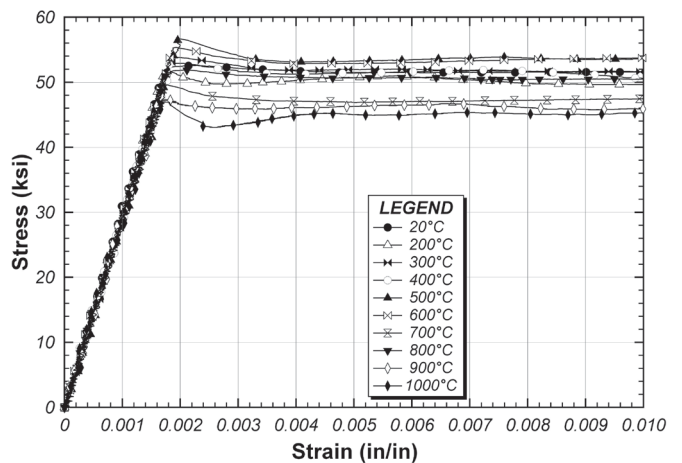


Fig. 7. CIA initial portion of stress-strain curves.

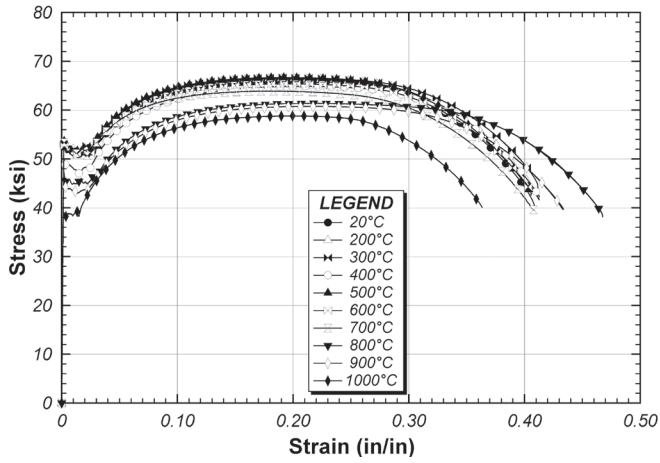


Fig. 8. CIB full stress-strain curves.

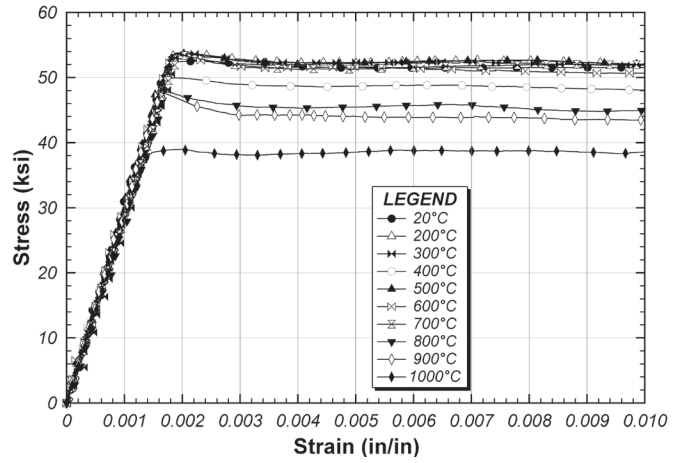


Fig. 9. CIB initial portion of stress-strain curves.

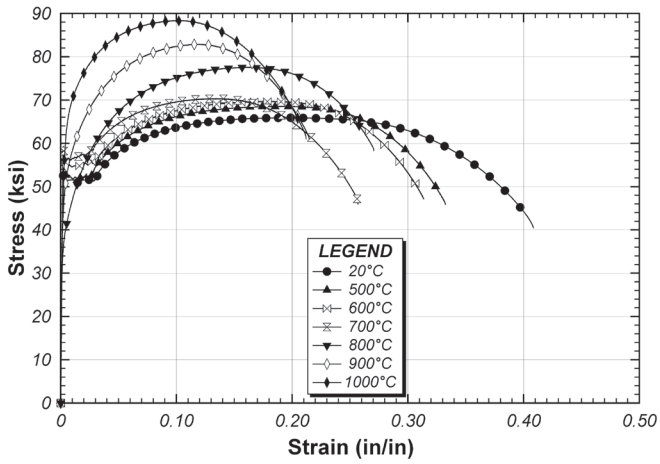


Fig. 10. CIW full stress-strain curves.

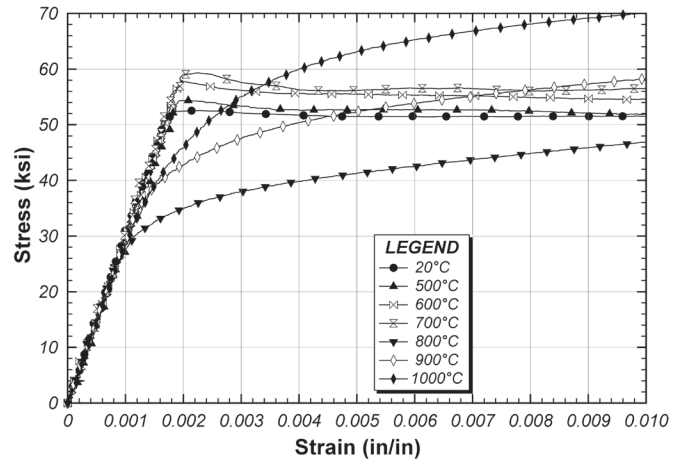


Fig. 11. CIW initial portion of stress-strain curves.

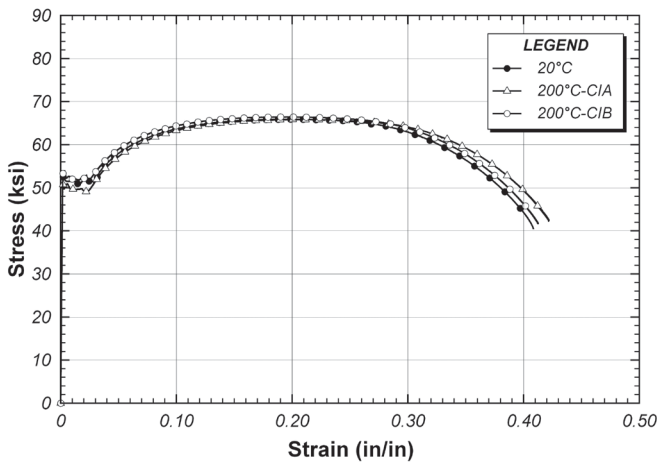


Fig. 12. Stress-strain curves for 200 °C.

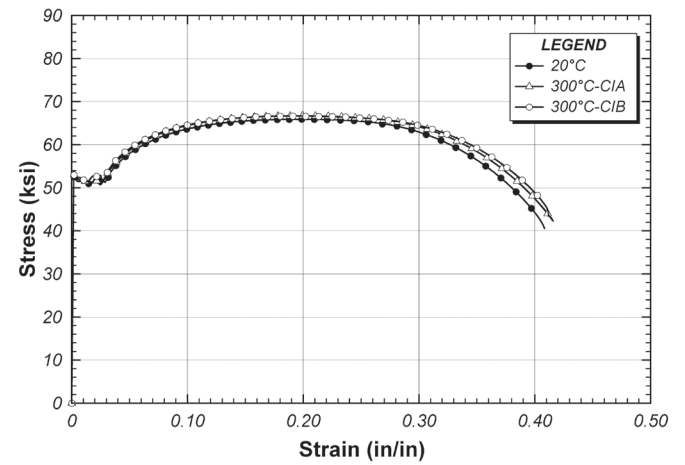


Fig. 13. Stress-strain curves for 300 °C.

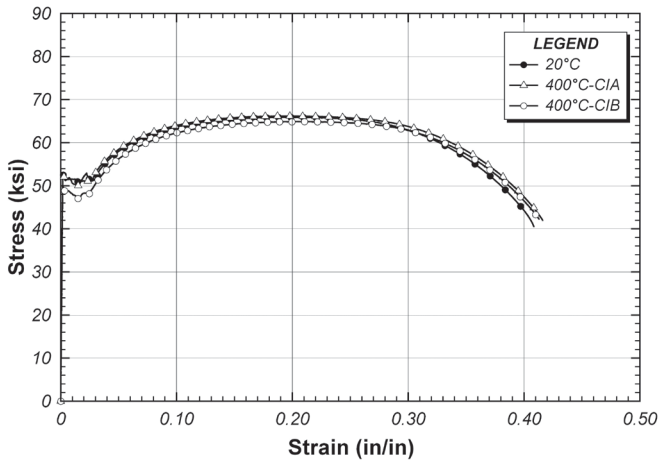


Fig. 14. Stress-strain curves for 400 °C.

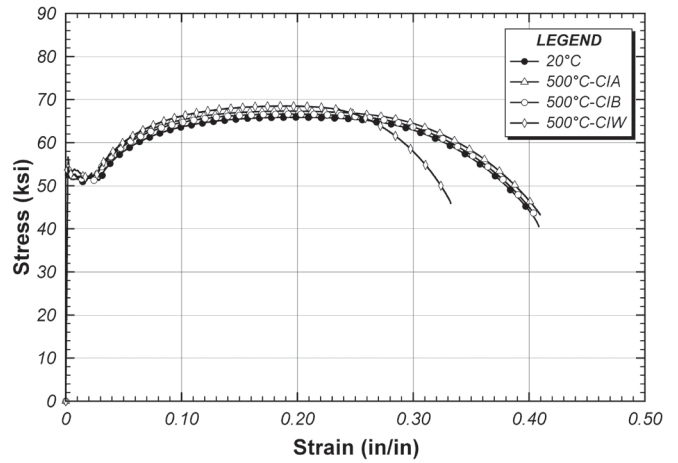


Fig. 15. Stress-strain curves for 500 °C.

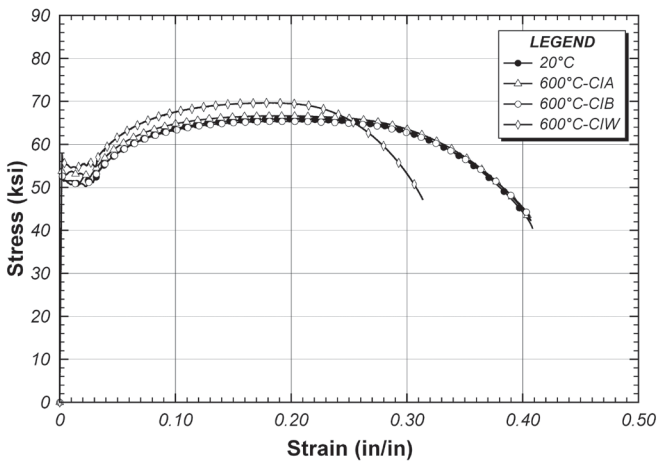


Fig. 16. Stress-strain curves for 600 °C.

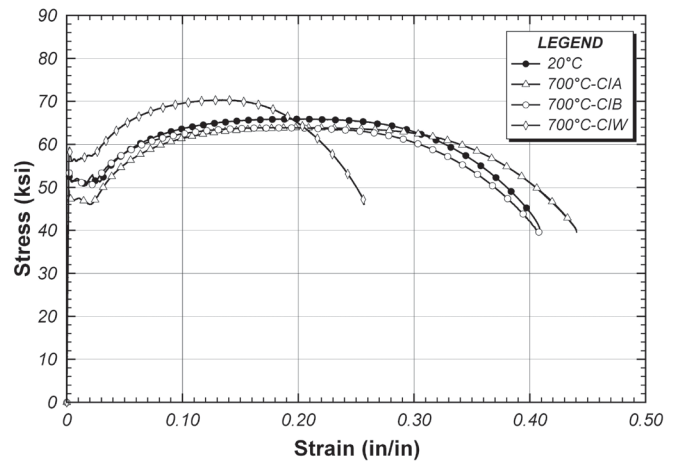


Fig. 17. Stress-strain curves for 700 °C.

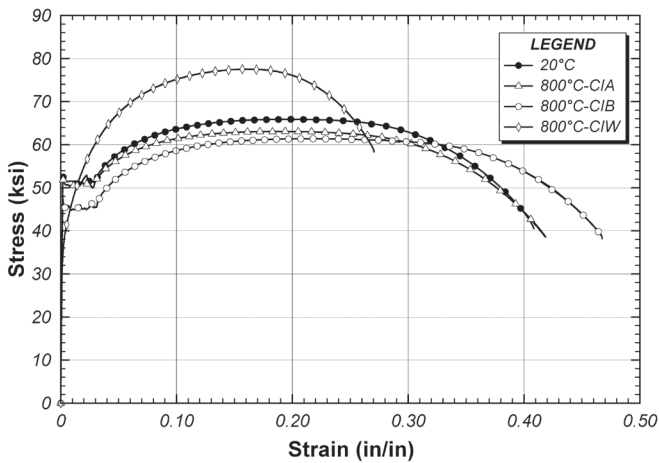


Fig. 18. Stress-strain curves for 800 °C.

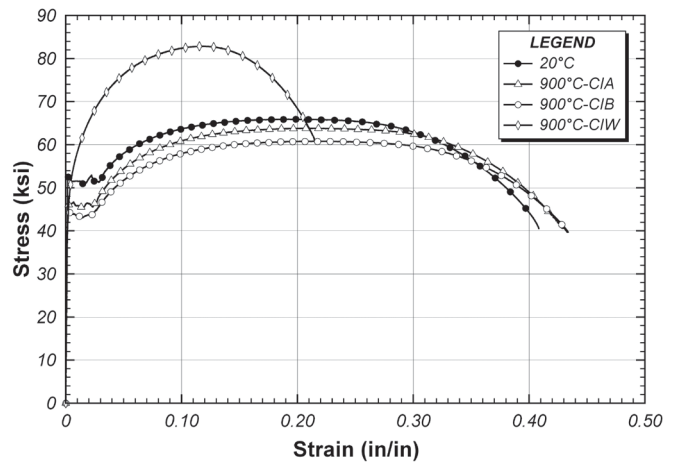


Fig. 19. Stress-strain curves for 900 °C.

Temp. (°C)	20	200	300	400	500	600	700	800	900	1,000
CIA	51.9	50.1	52.1	51.3	53.1	52.9	50.8	47.1	46.0	44.6
CIB	51.9	52.4	52.3	48.7	52.2	51.6	51.4	45.4	44.3	38.3
CIW	51.9	—	—	—	52.7	55.6	56.6	38.7	49.4	60.1

maintain the same basic shape of the virgin curve, exhibiting a well-defined yield plateau. Within the 600 to 1,000 °C heating range, more significant changes are evident in the CIW coupons. Compared to the virgin coupon, the CIW coupons exhibit a significant increase in tensile strength and a significant loss of ductility. For heating temperatures in the range of 800 to 1,000 °C, the CIW stress-strain curves do not exhibit a yield plateau and show significant nonlinearity starting at relatively low stress levels. In general, more significant changes in the stress-strain curves are expected for

coupons heated in the range of 800 to 1,000 °C, because steel undergoes a phase change near 730 °C from ferrite (α -Fe) to austenite (γ -Fe).

Yield Strength

The yield strength of the coupons after heating and cooling was determined from the stress-strain curves by using the 0.2% offset method shown on Figure 21. Results are listed in Table 3 and are plotted in Figure 22. The right plot in

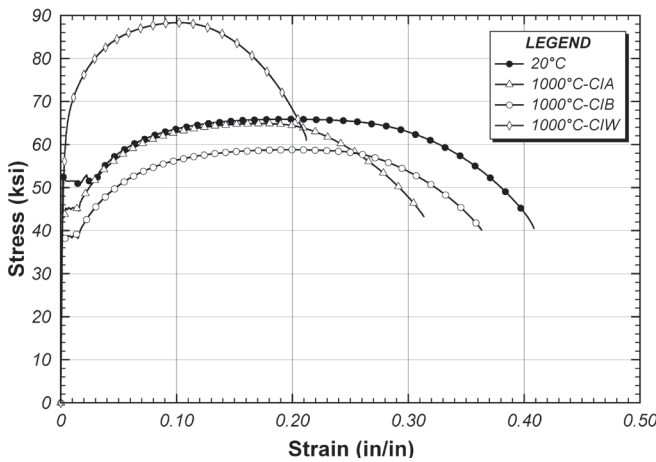


Fig. 20. Stress-strain curves for 1,000 °C.

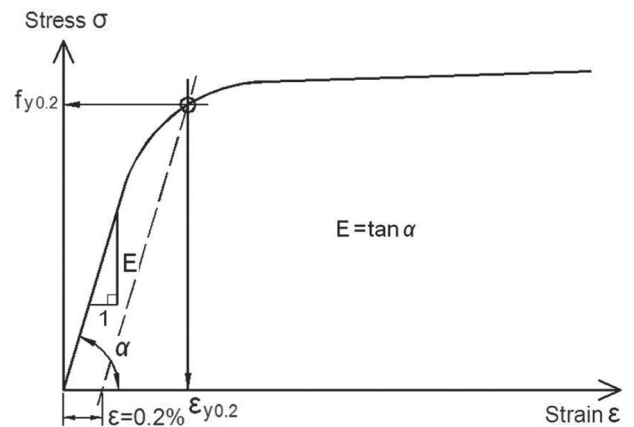


Fig. 21. Definition of 0.2% offset yield stress.

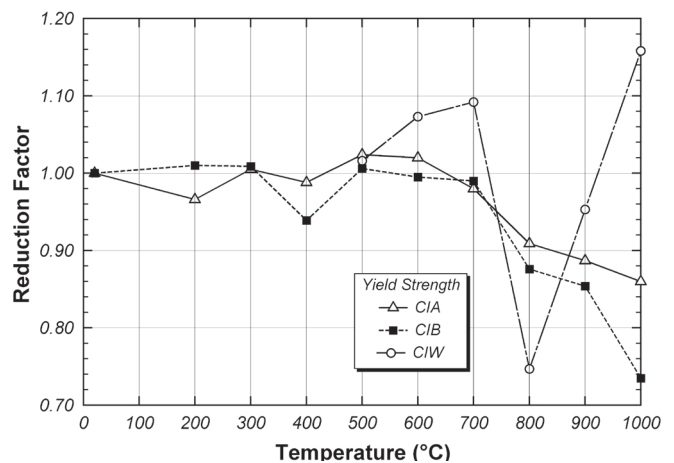
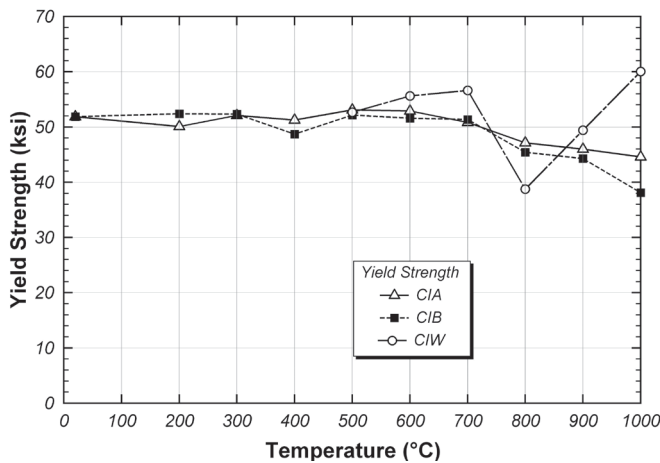


Fig. 22. Yield strength and yield strength reduction factors after heating and cooling.

Temp. (°C)	20	200	300	400	500	600	700	800	900	1,000
CIA	65.9	65.9	66.8	66.2	67.4	66.7	63.1	63.9	63.8	64.9
CIB	65.9	66.5	66.7	64.9	66.7	65.4	63.9	61.5	60.8	58.8
CIW	65.9	—	—	—	68.6	69.7	70.4	77.6	82.9	88.4

Figure 22 shows the reduction in yield strength relative to the virgin unheated coupon. Reasonably significant reductions in yield strength, up to about 25% for CIA and CIB cooling are seen for coupons heated to temperatures of 800 to 1,000 °C. The CIW coupons also show significant changes in yield strength in the range of 800 to 1,000 °C, with the yield strength first dropping and then increasing within this temperature range.

Specimens heated to temperatures higher than 727 °C at least partially transform to austenite (γ -Fe), and subsequent cooling can produce microstructures different from the original material. This is one reason that yield strength does not change significantly in specimens heated to 700 °C and lower temperatures. The decrease in yield strength with increase in temperature at 800 °C and higher in the CIB and CIA specimens results from increasing volume fractions transformed to austenite during heating. Upon subsequent cooling, the ferrite (α -Fe) produced may be coarser than that of the original material, leading to decreased yield strength. A992 steel has sufficient carbon to potentially form some pearlite following cooling from these temperatures. Pearlite consists of ferrite (α -Fe) and cementite (Fe_3C) in a lamellar configuration. The amount of pearlite possible increases with the amount of austenite transformed during heating, which should increase from 727 °C up to a maximum near 900 °C. The microstructures expected after cooling from

800 °C or higher are a normalized microstructure with some coarse pearlite for slow cooling rates (e.g., CIB) and some slightly finer pearlite for moderate cooling rates (e.g., CIA). This may explain the slightly greater yield strength reduction observed for the CIB specimens compared to the CIA specimens. An increase in cooling rate (e.g., CIW) will reduce the pearlite interlamellar spacing and, in accordance with the continuous cooling transformation curve, will lead to an increase in yield strength, such as that observed for the CIW specimen heated at 1,000 °C. Thus, the variations of yield strength with heating temperature and cooling rate, as seen in Figure 22, are consistent with the expected microstructural transformations.

Tensile Strength

The tensile strength of the coupons after heating and cooling was determined from the stress-strain curves. Results are listed in Table 4 and are plotted in Figure 23. For the CIA and CIB cooling methods, there is a modest reduction in tensile strength for coupons heated above about 600 °C. On the other hand, for the CIW cooling method, there is a large increase in tensile strength for coupons heated above about 600 °C due to quenching effect, which induced a martensite microstructure of metal with quick cooling process. A transformed martensite generally represents strength increasing

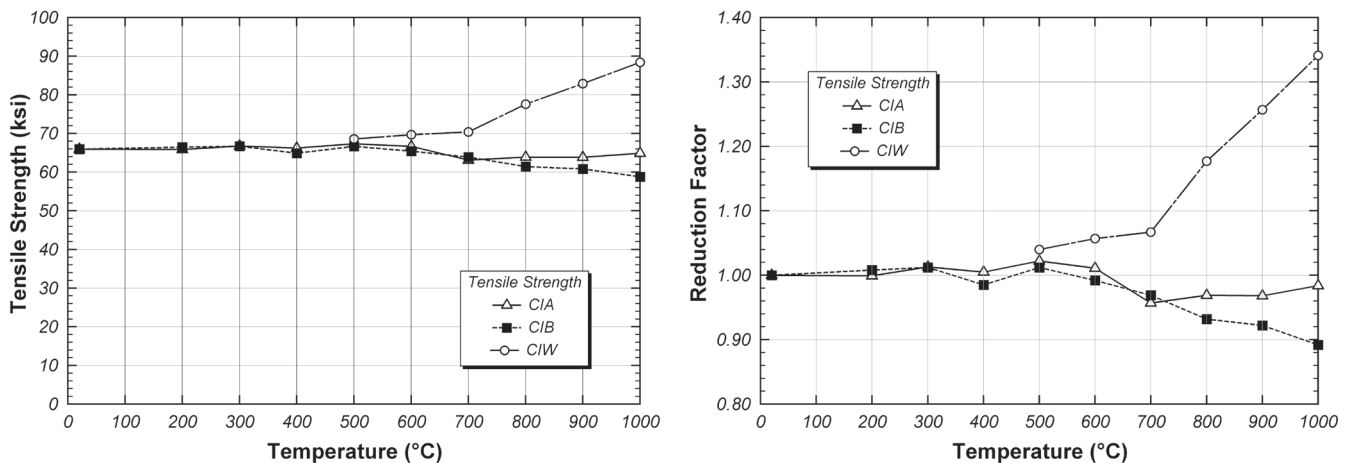


Fig. 23. Tensile strength and tensile strength reduction factors after heating and cooling.

Table 5. Elastic Modulus (ksi)										
Temp. (°C)	20	200	300	400	500	600	700	800	900	1,000
CIA	29,910	29,900	29,420	28,780	28,930	29,510	29,040	28,830	29,010	28,200
CIB	29,910	28,720	29,270	29,360	29,590	28,800	28,060	28,080	29,680	27,610
CIW	29,910	—	—	—	29,090	29,690	30,380	29,380	29,520	28,650

and ductility decreasing trend because of trapped austenite microstructures produced by rapid cooling period.

Elastic Modulus

The elastic modulus of the coupons after heating and cooling was estimated from the initial linear portion of the stress-strain curves. Strains were measured in the tension coupon tests using a nonaveraging type extensometer; i.e. strains were measured on only one side of the coupon. Consequently, errors at small strain levels can occur due to bending of the coupon, resulting in errors in the measured strain. As such, the elastic modulus values derived from the stress-strain curves may be subject to some error. Nonetheless, the elastic modulus data were still examined for general trends. Results are listed in Table 5 and are plotted in Figure 24. The data show minor variations in elastic modulus over the full temperature range. These variations may be indicative of strain measurement errors and so the data are considered somewhat inconclusive. Note, however, that even considering possible strain measurement errors, the data show no dramatic changes in elastic modulus.

Elongation

The elongation of the coupons after heating and cooling was determined from the stress-strain curves. The elongation

was taken as the strain at fracture of the coupon. Results are listed in Table 6 and are plotted in Figure 25. For the CIA and CIB cooling methods, there is no significant change in elongation for temperatures up to 900 °C. There is a reduction in the measured elongation for the coupons heated to 1,000 °C. Even for this case, however, the elongation was still above 30%. The CIW coupons, on the other hand, show a rather significant reduction in elongation over the 500 to 1,000 °C range of temperatures tested.

Charpy V-Notch (CVN) Impact Tests

Charpy V-Notch impact tests were conducted on samples of steel that were subjected to heating and cooling. Results are listed in Table 7 and are plotted in Figure 26. The results for the CIA and CIB specimens show an increase in CVN values over the full temperature range tested. The CIW specimens, on the other hand, show a large reduction in CVN values for the temperature range tested, which was 500 to 1,000 °C. Note that specimens heated to 1,000 °C and then cooled in water showed a CVN value that was only 20% of the original virgin specimen.

Hardness Tests

Hardness tests were conducted on samples of steel subjected to heating and cooling. An objective of these tests was to

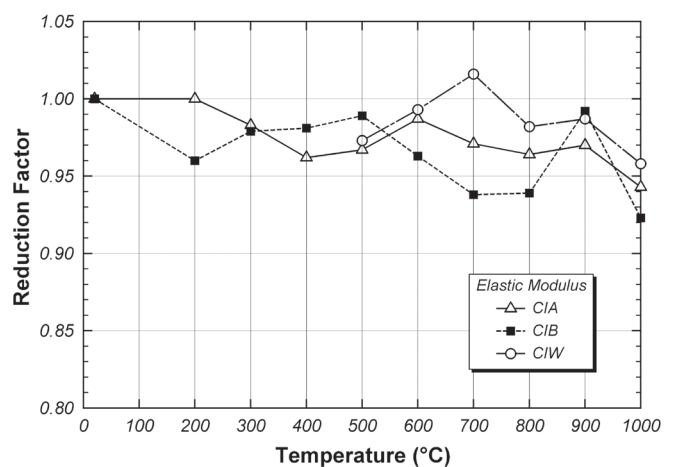
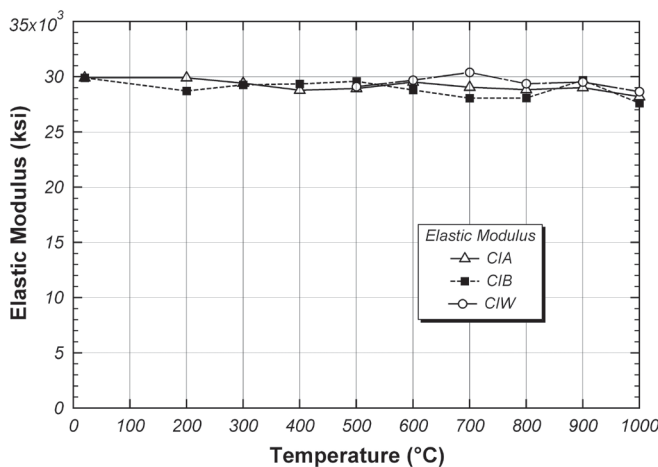


Fig. 24. Elastic modulus and elastic modulus reduction factors after heating and cooling.

Temp. (°C)	20	200	300	400	500	600	700	800	900	1,000
CIA	0.41	0.42	0.42	0.42	0.41	0.41	0.44	0.42	0.43	0.31
CIB	0.41	0.41	0.41	0.41	0.41	0.41	0.41	0.47	0.43	0.36
CIW	0.41	—	—	—	0.33	0.32	0.26	0.27	0.21	0.21

determine if hardness testing can be used as a diagnostic tool to evaluate steel after exposure to fire. Hardness measurements were made using a Wilson Rockwell Hardness Tester. All hardness results were within the B scale range except for the 1,000 °C CIW coupon, which was in the C scale Rockwell hardness range. The measured hardness values are plotted in Figure 27 and are listed in Table 8. The trends in Rockwell hardness with heating temperature and cooling method are very similar to the corresponding trends in tensile strength (Figure 23). This is expected because there is typically a strong correlation between hardness and tensile strength. On the other hand, the correlation between hardness (Figure 27) and yield strength (Figure 22) is rather poor. Consequently, when evaluating steel after a fire, hardness testing may not be effective in diagnosing loss of yield strength. Hardness testing, on the other hand, may be useful for diagnosing steel that has been exposed to high temperatures and then rapidly cooled by water.

CONCLUSIONS

This paper has presented results of tension tests and CVN tests on samples of A992 steel subjected to heating and cooling. These tests were intended to provide insights into the post-fire mechanical properties of A992 steel. The trends in the data can be summarized as follows. In terms of yield

strength, there was no significant reduction until the temperature exceeded 700 °C. For temperatures of 800 up to 1,000 °C, some reduction in yield strength was observed. The largest reduction in yield strength observed in these tests was approximately 25%. This occurred for the coupon heated to 1,000 °C and then cooled very slowly (CIB). For tensile strength, there is little change, even for coupons heated to 1,000 °C. It is noted that the CIW case actually increased the tensile strength. The most significant effect of water cooling appears to be in CVN values. Steel samples that were heated above 500 °C and then cooled rapidly in water showed a large drop in CVN values. CVN values are indicative of fracture toughness, and the loss of fracture toughness due to heating and then rapid cooling in water may be of concern in some applications—for example, in a steel bridge girder subjected to fire and then cooled rapidly by water from fire-fighting operations. It may be possible to identify steel in a structure that was subjected to fire and then cooled rapidly by the use of field hardness measurements.

The data presented in this paper can assist in assessing the post-fire condition of a steel structure. However, these data presume that the maximum temperature achieved in the steel during the fire is known. This, of course, is rarely the case. A review of the literature suggests there are no simple and reliable approaches for estimating the maximum temperature achieved in a steel element during a fire. Some approaches

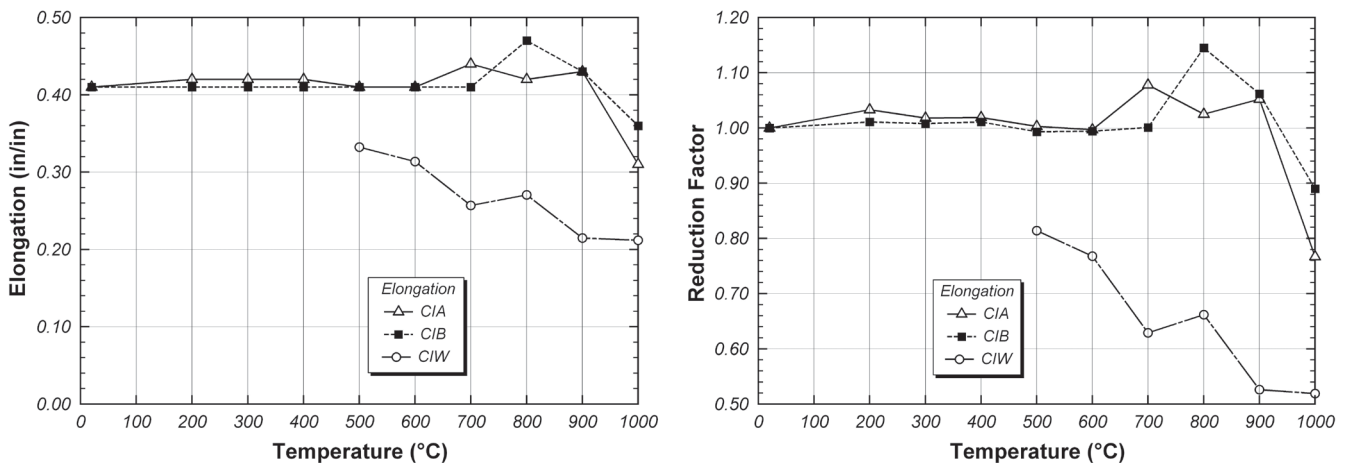


Fig. 25. Elongation and elongation reduction factors after heating and cooling.

Table 7. CVN Impact Energy (ft-lb)										
Temp. (°C)	20	200	300	400	500	600	700	800	900	1,000
CIA	171	220	244	244	240	206	247	245	252	188
CIB	171	233	238	226	219	250	247	259	251	239
CIW	171	—	—	—	95	93	76	79	86	38

Table 8. Rockwell Hardness Test Results (All B scale except for CIW at 1,000 °C)										
Temp. (°C)	20	200	300	400	500	600	700	800	900	1,000
CIA	89	91	87	83	84	86	83	84	82	88
CIB	89	88	88	89	89	89	86	84	81	84
CIW	89	—	—	—	84	85	88	93	97	25.9 (HRC)

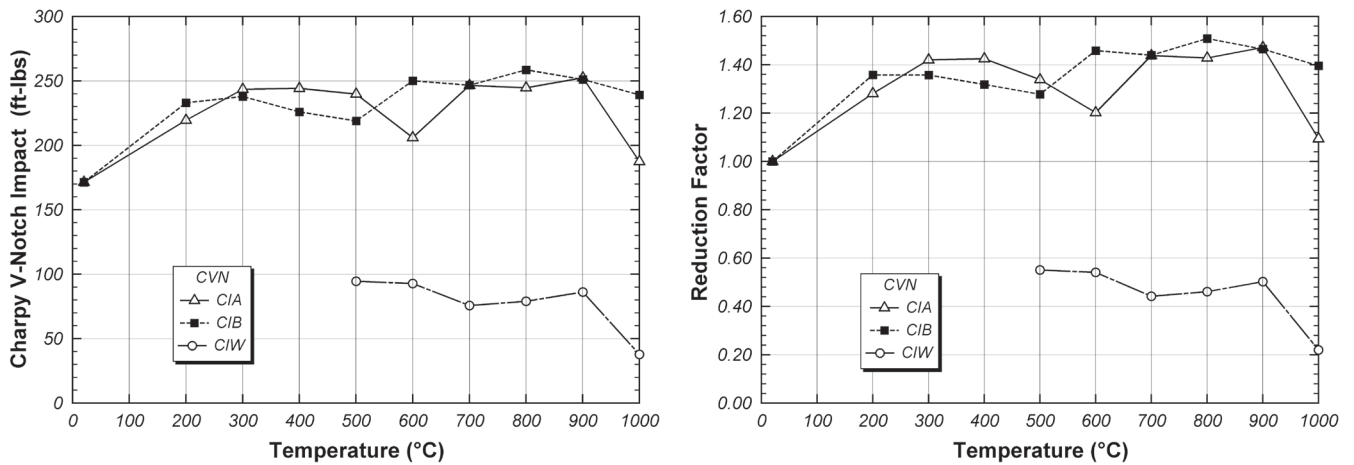


Fig. 26. CVN impact energy and CVN reduction factors after heating and cooling.

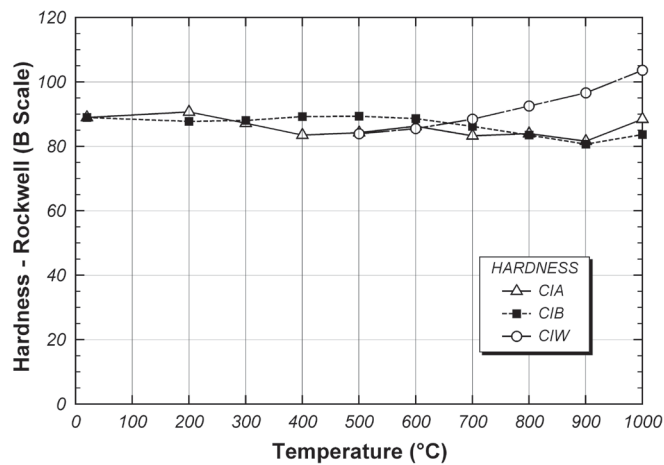


Fig. 27. Rockwell hardness after heat and cooling.

for addressing this question are discussed in Banovic and Foecke (2005). Nonetheless, the tests reported herein examined temperature exposures up to 1,000 °C, which would represent quite an extreme exposure. Even when exposed to such an extreme temperature, there was little degradation in mechanical properties after cooling, with the possible exception of steel cooled rapidly in water. It is important to note, however, that tests on high-strength bolts have shown significant loss of strength after heating and cooling (Yu and Frank, 2009). Thus, when assessing the condition of a steel structure following a fire, the effect of the fire on the strength of bolts is likely to be a greater concern than the effect of the fire on the structural steel members.

ACKNOWLEDGMENTS

The research reported herein was partially supported by the National Science Foundation under Grant No. 0927819. The support of the National Science Foundation and of NSF Program Director M.P. Singh is gratefully acknowledged. Any opinions, findings and conclusions or recommendations expressed in this paper are those of the authors and do not necessarily reflect the views of the National Science Foundation.

REFERENCES

- Banovic, S.W. and Foecke, T. (2005), "Federal Building and Fire Safety Investigation of the World Trade Center Disaster: Damage and Failure Modes of Structural Steel Components," Report NIST NCSTAR 1-3C, National Institute of Standards and Technology, Gaithersburg, MD.
- Davis, C.L. and King, J.E. (1993), "Effect of Cooling Rate on Inter-critically Reheated Microstructure and Toughness in High-Strength Low-Alloy Steel," *Materials Science and Technology*, Vol. 9, No. 1, pp. 8–15.
- Dhua, S.K., Mukerjee, D. and Sarma, D.S. (2003), "Effect of Cooling Rate on the As-Quenched Microstructure and Mechanical Properties of HSLA-100 Steel Plates," *Metallurgical and Materials Transactions a-Physical Metallurgy and Materials Science*, Vol. 34A, No. 11, pp. 2493–2504.
- Gosain, N.K., Drexler, R.F. and Choudhuri, D. (2008), "Evaluation and Repair of Fire Damaged Buildings," *Structure*, September 2008, pp. 18–22.
- Lee, J. (2012), "Elevated Temperature Properties of Steel for Structural Fire Engineering Analysis," Ph.D. Dissertation, Department of Civil, Architectural and Environmental Engineering, University of Texas at Austin (expected completion in 2012).
- Outinen, J. and Makelainen, P. (2004), "Mechanical Properties of Structural Steel at Elevated Temperatures and After Cooling Down," *Fire and Materials*, Vol. 28, Nos. 2–4, pp. 237–251.
- Panigrahi, B.K. (2006), "Microstructures and Properties of Low-Alloy Fire Resistant Steel," *Bulletin of Materials Science*, Vol. 29, No. 1, pp. 59–66.
- Pyshmintsev, I., Boryakova, I.A. and Smirnov, M.A. (2008), "Effect of Cooling Rate on the Structure and Properties of Low-Carbon Tube Steel," *Metallurgist*, Vol. 52, Nos. 7–8, pp. 464–469.
- Smith, C.I., Kirby, B.R., Lapwood, D.G., Cole, K.J., Cunningham, A.P. and Preston, R.R. (1981), "The Reinstatement of Fire Damaged Steel Framed Structures," *Fire Safety Journal*, Vol. 4, No. 1, pp. 21–62.
- Tide, R.H.R. (1998), "Integrity of Structural Steel After Exposure to Fire," *Engineering Journal*, AISC, Vol. 35, No. 1, pp. 26–38.
- Yu, L. and Frank, K.H. (2009), "Shear Behavior of A325 and A490 High-Strength Bolts in Fire and Post-Fire," *Engineering Journal*, AISC, Vol. 46, No. 2, pp. 99–106.

Current Steel Structures Research

No. 29

REIDAR BJORHOVDE

INTRODUCTION

This issue of “Current Steel Structures Research” for the *Engineering Journal* focuses on a selection of research projects at universities in Europe and New Zealand. Not all current projects at each school will be discussed. Instead, selected studies provide a representative picture of the research work and demonstrate the importance of the schools to their respective home countries—and indeed their importance to the efforts of industry and the profession worldwide.

The universities and many of their researchers are very well known in the world of steel construction: the Czech Technical University in Prague, the Czech Republic; the University of Ljubljana in Ljubljana, Slovenia; and the University of Auckland in Auckland, New Zealand. Segments of some of the projects at these institutions have been discussed in previous research papers, but the studies that are presented here reflect additional elements of the projects as well as other significant long-time efforts. All of the projects are multi-year efforts, emphasizing the need for careful planning and implementation of research needs and applications, including the education of graduate students and advanced researchers. As in the United States, the outcomes of the studies focus on design standards and industry needs.

The lead researchers have been active for many years, as evidenced by their leading roles in the design standards development of their countries, but they have also been frequent participants in the work of other countries and regions. Large numbers of English-language technical papers and conference presentations have been published, contributing to a collection of studies that continue to offer solutions to complex problems for designers as well as fabricators and erectors. Many of the projects also complement current work in the United States and elsewhere. The broad sharing of knowledge that is taking place promises significant results, not the least because of issues of finances and the sheer cost of research: synergism is a critical feature of multi-institutional, indeed multinational, activities.

References are provided throughout this paper when they

are available in the public domain. However, much of the work is still in progress, and in some cases reports or publications have not yet been prepared for public dissemination.

SOME CURRENT RESEARCH WORK AT THE CZECH TECHNICAL UNIVERSITY IN PRAGUE, THE CZECH REPUBLIC

The Czech Technical University (CTU) has been one of the leading academic institutions in Europe for many years. The faculty has pursued an aggressive development of technical programs and research facilities. In spite of its location “behind the Iron Curtain” for many years, with somewhat limited access and communication with researchers in other areas of the world, a number of the faculty members at CTU pursued contacts with colleagues in the West. However, the amount of activity that has taken place since the early 1990s has been impressive, particularly after the Czech Republic joined the European Union (EU). There have been numerous significant projects addressing the performance of steel materials, members and connections for steel structures, steel and composite frames, bridge structures, and the response of steel structures subjected to fire.

Design of Connections to Composite Columns for Improved Fire Robustness: Professor Frantisek Wald is the director of this project, which has been sponsored by the Research Fund for Coal and Steel (RFCS), an arm of the European Union. Additional support has been provided by TATA Steel Tubes Europe. The CTU staff has been working together with researchers from the University of Coimbra (Portugal), the universities of Manchester and Sheffield in England, and the University of Luleå in Sweden.

Focusing on the behavior and robustness of practical beam-to-column connections between wide-flange beams and both concrete-filled tubular (HSS) columns and partially encased wide-flange columns, the project aims to determine the following criteria for the connections and related design requirements:

1. Thermal effects in composite connections under different types of fire loading, including the cooling phase.
2. Component behavior in composite connections under arbitrary internal stress resultants and imposed displacements at elevated temperatures.

3. The influence of the connections on the global behavior of frames at elevated temperatures.
4. Using full-scale demonstrations, determining the influence of improved connection designs on the structural robustness under realistic fire conditions.
5. Development of connection design guides for practical applications.

The connections that are being examined are flush end-plate types and so-called reverse channel types, both of which are commonly used in European construction practice. Current results are partial and only tentative; the project will be completed by the end of 2012.

Modeling of Membrane Action of Floor Slabs Exposed to Fire: Professor Frantisek Wald is the director of this project, which has been funded by the Grant Agency of the Czech Republic, an institution similar to the National Science Foundation in the United States.

Using fiber-reinforced concrete for the slab, a yield line model was developed and tested computationally by finite element analyses. Interestingly, in addition to the traditional steel and concrete composite slab, a composite system using glulam beams was also designed and tested, in recognition of the use of wood for certain structures in the Czech Republic.

At this time, four steel-concrete composite floor

assemblies have been tested at ambient temperature and two have been tested for fire-level temperatures (Bednar et al., 2011). Figure 1 shows the appearance of the floor system at the completion of the ambient temperature test and Figure 2 shows a collapsed slab during the fire test. As expected, the yield line modeling predicted the ambient results very well, and the fire test demonstrated the ductility of the fiber-reinforced slab and steel system. The final results will be available in 2012.

Composite Beams with High Ribbed Concrete Deck: Professors Jiri Studnicka and Stepan Thoendel direct this project.

Using trapezoidal steel deck 135 mm (5.3 in.) high and IPE 200 (200 mm high or 8 in.) steel shapes for the composite beams, the system violates the maximum 80-mm (3.1-in.) steel deck height criteria of the current Eurocode 4 (EC4) (ECS, 2004). Two full-scale tests were conducted using simply supported beams with a 6-m (20-ft) span. The tentative results indicate that it may be possible to expand the EC4 criteria to include such deep decks (Thoendel and Studnicka, 2011). The project will complete by the end of 2012, at which time suitable design recommendations will be made.

Performance of Small-Diameter-Headed Stud Shear Connectors: Professor Josef Machacek is the director of this project.

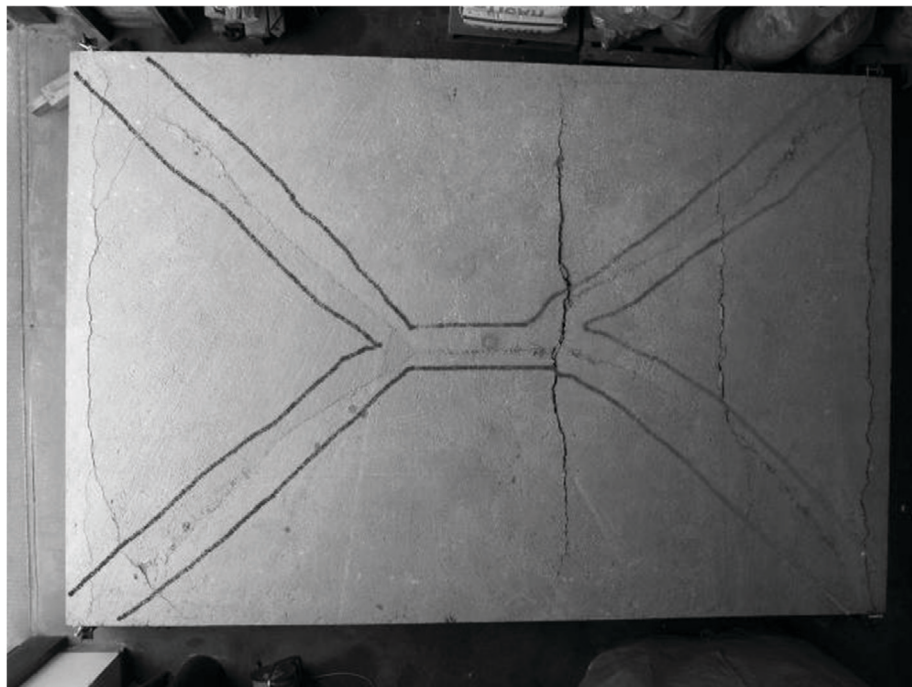


Fig. 1. Yield line failure mode of ambient temperature composite slab test. (Photograph courtesy of Professor Frantisek Wald)

Using pushout tests with 10- and 13-mm ($\frac{3}{8}$ - and $\frac{1}{2}$ -in.) shear studs, with concrete strengths of 20 and 30 MPa (nominally, 3 and 4 ksi), the representative strength parameters and variability characteristics were determined. Applied to partially encased composite members subjected to bending and axial force, as shown in Figure 3, the tests have demonstrated that the connectors behaved as ductile elements (Nguyen and Machacek, 2011). Nonlinear response of such beam-columns was evaluated using the ANSYS software. Overall, the results showed that the use of the Eurocode 4 criteria for the plastic distribution of the longitudinal shear force may be used.

Composite Beams with High-Performance Concrete and High-Strength Steel: Professors Jakub Dolejs and Ivan Tunega are the directors of this project.

Four composite beams have been tested, using 150-mm (6-in.) 70-MPa (10-ksi) concrete slabs with HE260A rolled steel shapes (250 mm or 10 in. high) in S460 steel (65-ksi yield stress). Pushout tests were also conducted to verify the behavior and performance of the shear connectors in the high-strength concrete. Finite element analyses and additional tests were also conducted to determine the capacity of the shear connection with its distribution along the length of the beam.

Overall, the aim of the project is to confirm or to modify the applicability of the Eurocode 4 criteria, if necessary, for shear connectors in high strength concrete. The final results will be available in late 2012.

Development of Innovative Steel-Glass Structures for Architectural and Structural Applications: This project has been funded by the Research Fund for Coal and Steel (RFCS), with Professors M. Netusil and M. Eliasova as the

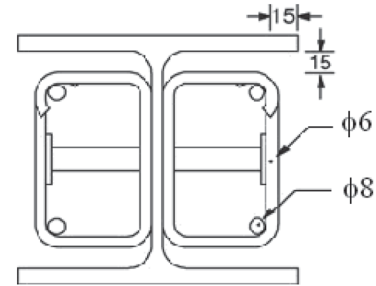


Fig. 3. Partially encased composite beam cross-section with small-diameter shear studs. (Drawing courtesy of Professor Josef Machacek)



Fig. 2. Collapsed composite slab assembly during fire test. (Photograph courtesy of Professor Frantisek Wald)

directors of the Czech component of the overall project. It is part of a larger-scale development of steel and glass structures and is operated as a joint effort among CTU, the German technical universities of Aachen and Dortmund, and the Steel Construction Institute of the United Kingdom. The lead research institution is the Technical University of Aachen.

Aiming for optimal interaction between glass and steel, various steel-glass structures have been examined. In particular, steel-supported glazing systems for use in façades, roofs and other parts of buildings have been explored, leading to the development of hybrid steel-glass beams, as illustrated in Figure 4. The web-to-flange connections are provided by polymer adhesive joints and the details of the joints may vary in accordance with the preferences of the architect and the structural engineer (Netusil and Eliasova, 2010).

At this time, analytical procedures have been used to develop practical design approaches, and a full-scale test has been conducted at CTU, as shown in Figure 5. Additional data will be available as the project progresses.

SOME CURRENT RESEARCH WORK AT THE UNIVERSITY OF LJUBLJANA IN LJUBLJANA, SLOVENIA

The University of Ljubljana is a premier European university with a broad program in all areas of civil engineering. Following the separation of the various regions of Yugoslavia, the western area became the country of Slovenia, with the city of Ljubljana as the capitol. The faculty of the university have been very aggressive in their efforts to join the



*Fig. 4. Hybrid steel-glass beam with adhesive web-to-flange connections.
(Figure courtesy of Professor Frantisek Wald)*

European research community, and the structural engineering efforts have been particularly successful under the leadership of Professor Darko Beg. The structural steel research program has featured a number of important projects that have been conducted as single studies and a number of efforts that are jointly pursued with other European schools.

Behavior and Strength of Bolted Connections in Bearing:

The director of this project has been Professor Darko Beg. The aim of the project is to clarify and expand the bearing criteria that are used in Eurocode 3 (ECS, 2005). Specifically, the design criteria are very conservative but also vague and impractical. Previous studies were focused on the strength and behavior of connections in high-strength steel, such as S690 (similar to ASTM A514); the current project addresses the performance of connections with up to 6 bolts in the mild S235 steel grade (for all practical purposes, the same as ASTM A36). The bolts are of the European 8.8 grade, which is comparable to A325.

Interestingly, the results to date show that the bearing criteria that were developed for connections in S690 steel are also suitable for mild steel (Može and Beg, 2011). Specifically, although the tests demonstrated that different limit states were observed for the connections that were tested, the bearing resistance was always the governing one. The final version of the design criteria will include suitable ductility considerations.

Longitudinally Stiffened Plate Girders Subjected to Moment and Shear Interaction:

Darko Beg is the director of this project, which is jointly operated with the University of Stuttgart in Germany. A series of large-scale tests were conducted in 2010, aiming to determine the behavior characteristics of plate girders subjected to high moment and shear. Figure 6 shows the test setup for the girders. A numerical model was developed for analysis using ABAQUS, and the results compared to within 5% of the test data. Once the numerical model has been fully verified, extensive parametric evaluations will be performed.

Further, the numerical results were compared to those predicted by the criteria of Eurocode 3, Part 1-5 (ECS, 2006). The largest difference was found for girders having one longitudinal stiffener in the compression zone, where the positive effect of the tensile stresses due to the bending moment is not considered in the computation of the shear capacity of the largest panel. Various resistance models have been developed, including two that are based on an interaction treatment and one that is based on the strength of the gross cross-section.

Extensive statistical analyses are now under way, correlating the physical and the numerical results. Among recent findings, higher “partial safety factors” must be applied for several cases. It is anticipated that a number of changes will



*Fig. 5. Full-scale test of a steel-glass beam.
(Photograph courtesy of Professor Frantisek Wald)*

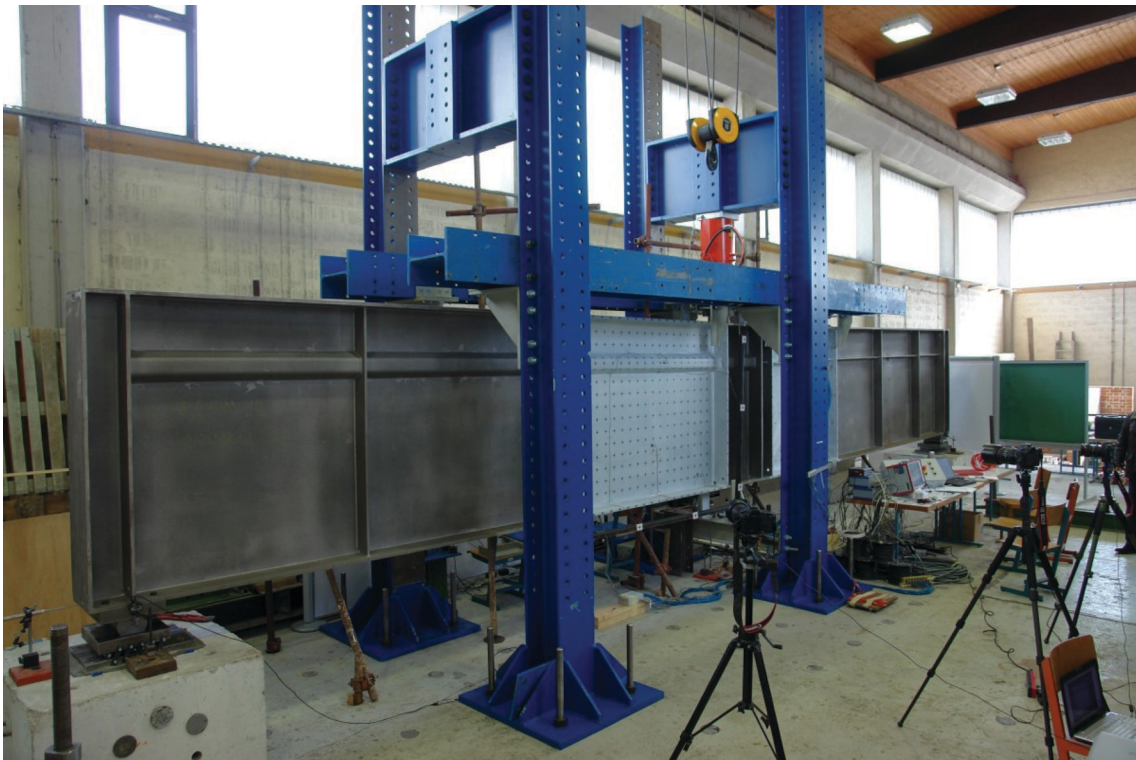


*Fig. 6. Test setup for a large-scale plate girder.
(Photograph courtesy of Professor Darko Beg)*

be proposed for Eurocode 3, once the results from Ljubljana and Stuttgart have been fully evaluated.

Intermediate Transverse Stiffeners in Plate Girders:

Darko Beg is the director of this project, which is also jointly operated with the University of Stuttgart.

Over the past several years, various authors have claimed that the influence of tension field action on the transverse stiffeners is much smaller than what is predicted by the EC3 design criteria. Two large, full-scale tests, as shown in Figure 7, were conducted to verify these results, if possible. The physical tests have now confirmed that the numerical findings are correct. On this basis, a new model has been developed, and an extensive parametric study has been performed. A simplified approach based on stiffness criteria has been developed for the design of the transverse stiffeners. The approach incorporates all relevant loading cases. The proposed approach has not yet been published, and it is anticipated that extensive discussions will be conducted by the EC3 technical committee.

Flame Straightening of Structural Steel Elements: This project has been sponsored by the Research Fund for Coal and Steel (RFCS), with Professor Darko Beg as the director



Fig. 7. Plate girder test to assess the influence of tension field action on the transverse stiffener. (Photograph courtesy of Professor Darko Beg)

of the study component that is being conducted at the University of Ljubljana.

The work to be conducted at Ljubljana focused on determining the residual stresses in steel plates of various grades of steel, as illustrated in Figure 8. Water-jet cutting was used for the traditional method of sectioning that provides the basis for the measurement of the strains associated with the residual stresses. It was also essential to evaluate the welding deformations in tee elements ahead of the flame straightening.

The primary effort of the research team was to provide numerical simulations of the flame-straightening process using the actual temperature field that was introduced. Further, an analytical method was developed to estimate the deflections of beams that had been straightened by heating in the usual V-shape. The principle of this approach is based on the fact that the heated area will yield in compression due to an external force, in the form of a strip across the flange and the V in the web. The neutral axis then forms in the apex of the V, and the tensile stresses in the unheated part of the shape will be in equilibrium with the heated part of the cross-section. Finally, the temperature that causes the yielding of the heated part is defined as the critical value. It has been determined that this temperature provides a good estimate of the rotation of the V that will occur under these conditions. This gives a realistic value of the contraction due to the cooling of the V.

SOME CURRENT RESEARCH WORK AT THE UNIVERSITY OF AUCKLAND IN AUCKLAND, NEW ZEALAND

The University of Auckland has had a prominent civil engineering program for many years, and the faculty members have enjoyed good relations with local designers and industry. The Heavy Engineering Research Association (HERA) of New Zealand effectively played the role of AISC for many years, and New Zealand has also benefited from close collaboration with the resources and market of Australia. In fact, design standards for the two countries are now developed and published jointly.

For several years, Dr. G. Charles Clifton worked as the chief technical officer of HERA. Upon joining the faculty of the University of Auckland, he started an aggressive research and development program for the Department of Civil Engineering, which is now the leading “steel university” in the country. It is particularly important to observe that seismic activity can be quite strong in New Zealand, as demonstrated by numerous larger and smaller earthquakes every year. Further, as examples of the steel research work at the university, it is interesting to note the following recently completed studies:

- Development and behavior of a new, long-span composite floor system.

- Development and behavior of a new, long-span composite floor system, with special emphasis on the use in a building with a riveted steel frame.
- Seismic assessment and retrofit of riveted steel-framed buildings, including beam-to-column connections with high deformation capacity but very low rotational strength.
- Composite slab strengthening solution with carbon fiber strips in the slab.
- Lightweight, low-cost buckling restrained braces for developing countries, with the potential of using bamboo tubes in lieu of an expensive solution with steel tubes.

Current research efforts are detailed in the following.

The Self-Centering Sliding Hinge Joint: The project is sponsored by the New Zealand Earthquake Commission. Professor G. Charles Clifton is the project director; the team researchers are H.H. Khoo and John Butterworth, as well as Greg MacRae from the University of Canterbury in New Zealand.

The sliding hinge joint (SHJ) is a New Zealand invention.

It is a beam-to-column connection intended for use in low-damage, steel moment-resisting frames. It has a pinned connection between the top flange of the beam and the column, with asymmetric friction connections in the bottom flange and web base. This allows for large inelastic rotations with limited connection and floor slab damage. Further, the SHJ decouples connection strength and stiffness, with significant advantages over conventional moment connections. The joint does lose strength during sliding, due to bolt tension losses in the asymmetric friction connections. It also does not always return the frame to the pre-earthquake position, delaying the immediate occupancy of the structure after the earthquake.

A self-centering sliding hinge joint (SCSHJ) with ring springs (RS) has also been developed to reduce strength losses and improve the dynamic recentering properties of the connection (Khoo et al., 2011). This will ensure that the frame residual drift is within post-construction tolerances. It involves connecting a ring spring to the beam bottom flange and the column flange of the SHJ, as shown in Figure 9a. Because the springs are only effective in compression, suitable detailing of same, as shown in Figure 9b, ensures that the spring will compress in both directions. Thus, the ring spring will:



*Fig. 8. Sectioning of the flange plate by water-jet cutting.
(Photograph courtesy of Professor Darko Beg)*

1. Develop moment resistance, reducing the number of bolts required in the asymmetric friction connection.
2. Store energy, which will contribute to recentering upon release.
3. Maintain the sliding joint strength due to limited degradation.

Five 10-story frames with different spring sizes were studied analytically, with up to 50% ring spring contribution to the moment resistance. This demonstrates that the dynamic recentering properties can be significantly improved, despite the absence of more favorable hysteretic curves in most self-centering systems. Finally, a full-scale subassembly test is currently under way, as shown in Figure 10.

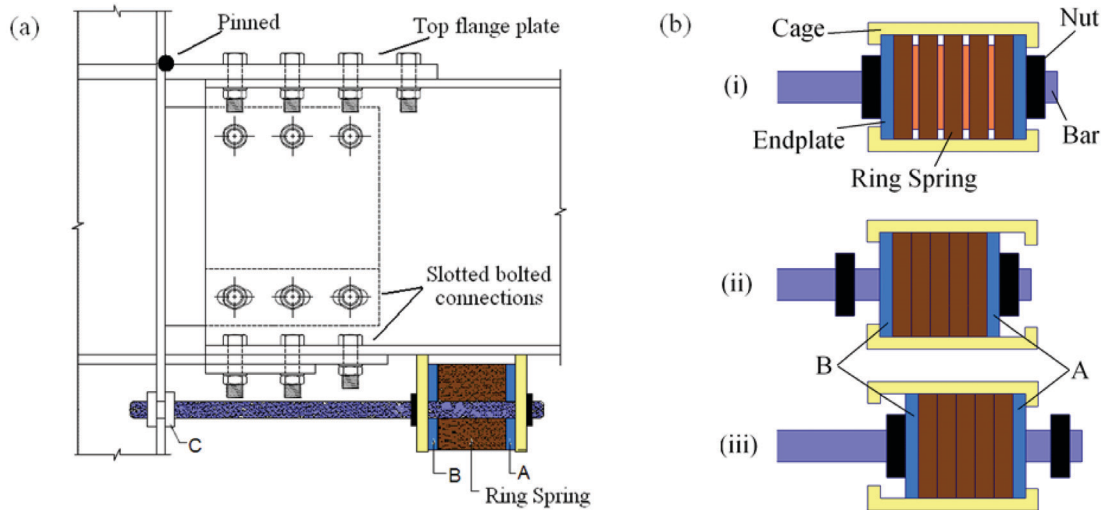


Fig. 9. (a) Self-centering sliding hinge joint; (b) ring spring layout. (Figure courtesy of Professor G. Charles Clifton)



Fig. 10. Full-scale frame subassembly test setup. (Photograph courtesy of Professor G. Charles Clifton)

Effects of Floor Slab Resistance on the Inelastic Behavior of Chevron-Type Eccentrically Braced Frames:

The director of this project is Professor G. Charles Clifton; the team researchers are D. Volynkin and C. Mathieson.

Following the February 2011 New Zealand earthquake, several examinations showed that eccentrically braced frames (EBFs) that were compositely connected to the floor slab experienced self-centering as well as less-than-expected active link yielding (Bruneau et al., 2011). A numerical model was created to study the effect of a floor slab on the out-of-plane resistance of the EBF structures. The deformation was modeled by a translational spring with a stiffness derived from yield line theory. Figure 11 shows the assumed yield line collapse mechanism formed under loading at the collector beam ends.

The analysis demonstrated that the floor slabs reduce the rotation of the active links. This caused additional forces to be distributed into the secondary elements of the EBF, leading to yielding in an increased number of elements. Following the earthquake, the structure exhibited self-centering as a result of the restoring force from the floor slabs. Without such a restoring force, EBFs have no inherent tendency to produce self centering. The researchers are now working to improve the floor slab model as well as to develop a design procedure that will take into account the out-of-plane resistance of the slab.

ACKNOWLEDGMENTS

Significant assistance has been provided by ISSRA members Professor Frantisek Wald of the Czech Technical University in Prague, Professor Darko Beg of the University of Ljubljana, and Professor G. Charles Clifton of the University of Auckland. Their efforts are sincerely appreciated.

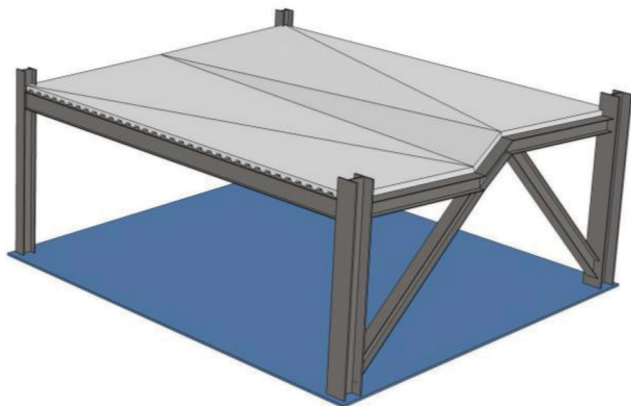


Fig. 11. Yield line model of structural system.
(Drawing courtesy of Professor G. Charles Clifton)

REFERENCES

- Bednar, J., Wald, F., Vodicka, J. and Kohoutkova, A. (2011), "Composite Fiber Concrete Slabs in Fire," *Proceedings Eurosteel Conference 2011*, Budapest, Hungary, pp. 1521–1526.
- Bruneau, M., Clifton, C.G., MacRae, G., Leon, R.T. and Fussell, A. (2011), "Steel Building Damage from the Christchurch Earthquake of February 22, 2011," Report of the New Zealand Society of Earthquake Engineering.
- European Committee for Standardization (2004), *Eurocode 4: Design of Composite Steel and Concrete Structures—Part 1-1: General Rules and Rules for Buildings*, Standard No. EN 1994-1-1, ECS, Brussels, Belgium.
- European Committee for Standardization (2005), *Eurocode 3: Design of Steel Structures—Part 1-1: General Rules and Rules for Buildings*, Standard No. EN 1993-1-1, ECS, Brussels, Belgium.
- European Committee for Standardization (2006), *Eurocode 3: Design of Steel Structures – Part 1-5: Plated Structural Elements*, Standard No. EN 1993-1-5, ECS, Brussels, Belgium.
- Khoo, H.H., Clifton, G.C., Butterworth, J., MacRae, G.A. and Mathieson, C.D. (2011), "Development of the Self-Centering Sliding Hinge Joint," *Ninth Pacific Conference of Earthquake Engineering*, Auckland, New Zealand.
- Može, P. and Beg, D. (2011), "Investigation of High Strength Steel Connections with Several Bolts in Double Shear," *Journal of Constructional Steel Research*, Vol. 67, No. 3, pp. 333–347.
- Netusil, M. and Eliasova, M. (2010), "Behavior of the Glued Joint in Hybrid Steel-Glass Beam," *Pollack Periodica: an International Journal for Engineering and Information Sciences*, Vol. 5, April, pp. 97–108.
- Nguyen, T.H.G. and Machacek, J. (2011), "Longitudinal Shear in Partially Encased Composite Steel and Concrete I-Member," *Proceedings Eurosteel Conference 2011*, Budapest, Hungary.
- Thoendel, S. and Studnicka, J. (2011), "Composite Steel and Concrete Beam with High Ribbed Deck," *Proceedings Eurosteel Conference 2011*, Budapest, Hungary, pp. 2139–2144.
- Ziemian, R.D., Editor (2010), *Guide to Stability Design Criteria for Metal Structures*, 6th ed., John Wiley & Sons, New York, NY.

GUIDE FOR AUTHORS

SCOPE: The ENGINEERING JOURNAL is dedicated to the improvement and advancement of steel construction. Its pages are open to all who wish to report on new developments or techniques in steel design, research, the design and/or construction of new projects, steel fabrication methods, or new products of significance to the uses of steel in construction. Only original papers should be submitted.

GENERAL: Papers intended for publication may be submitted by mail to the Editor, Keith Grubb, ENGINEERING JOURNAL, AMERICAN INSTITUTE OF STEEL CONSTRUCTION, One East Wacker Drive, Suite 700, Chicago, IL, 60601, or by email to grubb@aisc.org.

The articles published in the *Engineering Journal* undergo peer review before publication for (1) originality of contribution; (2) technical value to the steel construction community; (3) proper credit to others working in the same area; (4) prior publication of the material; and (5) justification of the conclusion based on the report.

All papers within the scope outlined above will be reviewed by engineers selected from among AISC, industry, design firms, and universities. The standard review process includes outside review by an average of three reviewers, who are experts in their respective technical area, and volunteers in the program. Papers not accepted will not be returned to the author. Published papers become the property of the American Institute of Steel Construction and are protected by appropriate copyrights. No proofs will be sent to authors. Each author receives three copies of the issue in which his contribution appears.

MANUSCRIPT PREPARATION: Manuscripts must be provided in Microsoft Word 2003 format. A laser-quality proof or high quality PDF must accompany your submittal. Download our complete author guidelines at www.aisc.org/ej.